PB81245672

Report No. FHWA/RD-81/090

ANALYTICAL STUDY FOR FATIGUE OF HIGHWAY BRIDGE CABLES

July 1981
Final Report

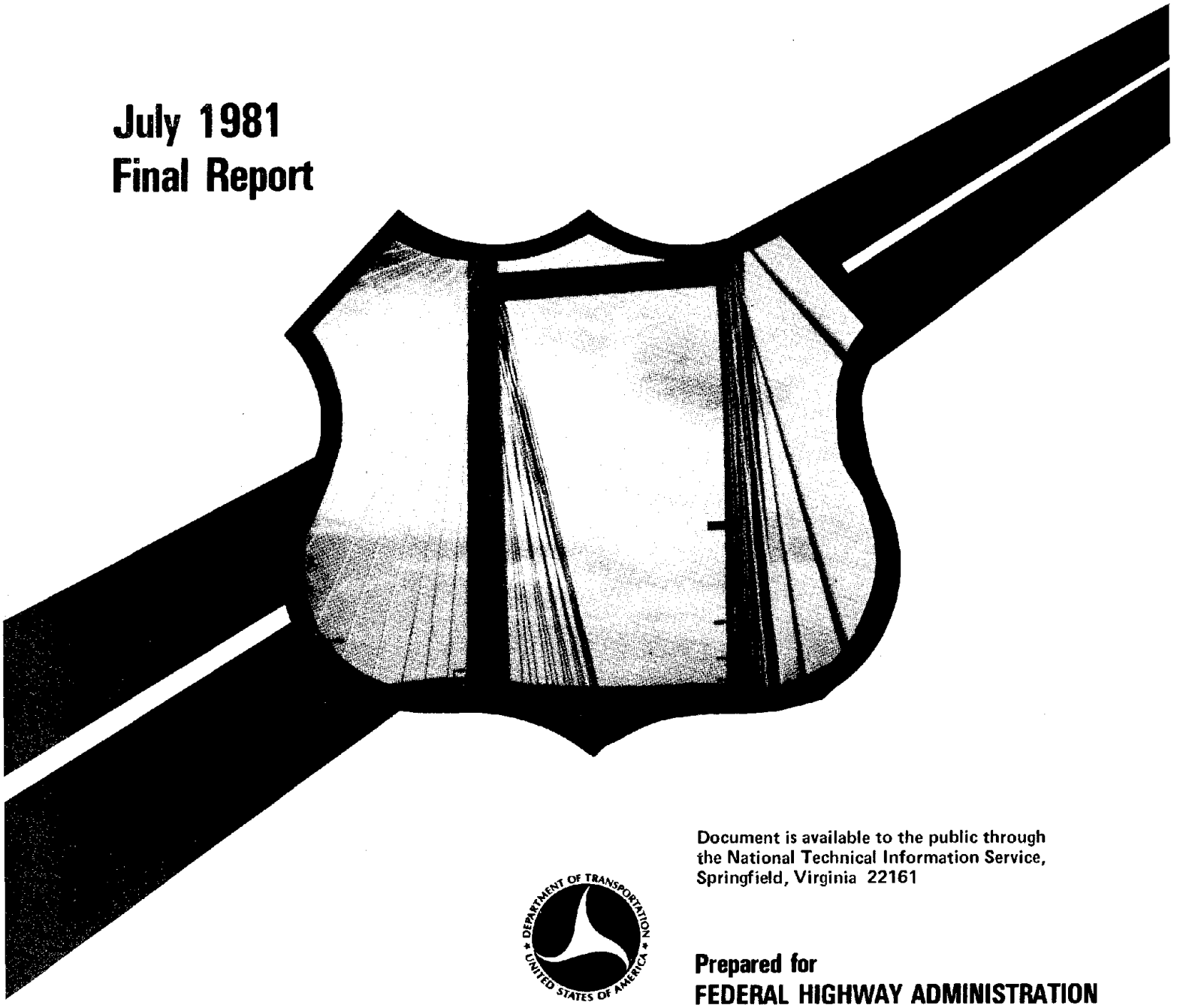

Document is available to the public through the National Technical Information Service, Springfield, Virginia 22161

Prepared for
FEDERAL HIGHWAY ADMINISTRATION
Offices of Research & Development
Structures and Applied Mechanics Division
Washington, D.C. 20590

REPRODUCED BY: NTIS
U.S. Department of Commerce
National Technical Information Service
Springfield, Virginia 22161

FOREWORD

Designers of major cable supported structures are well aware of the dangers of wind-induced vibrations. Also fatigue distress due to wind vibration of individual members could be a problem. This study was concerned with the individual stay cables of cable-stayed bridges and their vibration due to wind excitation.

Unlike most structural components, there exists no design specification for high strength bridge cable as used for suspended bridges. The fatigue problem caused by vibrations due to wind is not necessarily an axial-load fatigue problem but is one of cable bending close to the end of the cable where it is held by an attachment or socket of some type. The analysis presented in this report should give design engineers some insight into the problem as it applies to cable-stayed bridges.

Charles F. Scheffey
Director, Office of Research
Federal Highway Administration

NOTICE

This document is disseminated under the sponsorship of the Department of Transportation in the interest of information exchange. The United States Government assumes no liability for its contents or use thereof. The contents of this report reflect the views of the contractor, who is responsible for the accuracy of the data presented herein. The contents do not necessarily reflect the official views or policy of the Department of Transportation. This report does not constitute a standard, specification, or regulation.

The United States Government does not endorse products or manufacturers. Trade or manufacturers' names appear herein only because they are considered essential to the object of this document.

NOTICE

THIS DOCUMENT HAS BEEN REPRODUCED FROM THE BEST COPY FURNISHED US BY THE SPONSORING AGENCY. ALTHOUGH IT IS RECOGNIZED THAT CERTAIN PORTIONS ARE ILLEGIBLE, IT IS BEING RELEASED IN THE INTEREST OF MAKING AVAILABLE AS MUCH INFORMATION AS POSSIBLE.

Technical Report Documentation Page

1. Report No. FHWA/RD-81/090	2. Government Accession No.	3. Recipient's Catalog No. PB81 245672
4. Title and Subtitle Analytical Study for Fatigue of Highway Bridge Cables		5. Report Date July 1981
		6. Performing Organization Code
7. Author(s) S. Basu and M. Chi		8. Performing Organization Report No.
9. Performing Organization Name and Address Chi Associates, Inc. 956 North Monroe Street, Suite 200 Arlington, Virginia 22201		10. Work Unit No. (TRAIS) FCP 35L3-011
		11. Contract or Grant No. DOT-FH-11-9613
12. Sponsoring Agency Name and Address Office of Research and Development Federal Highway Administration U.S. Department of Transportation Washington, D.C. 20590		13. Type of Report and Period Covered Final Report
		14. Sponsoring Agency Code S01137

15. Supplementary Notes

FHWA Contract Manager: Lloyd Cayes (HRS-11)

16. Abstract

Fatigue behavior of highway bridge cables under wind loading is investigated in this report in a comprehensive analytical manner using methodologies of linear elastic fracture mechanics (LEFM). The report includes (1) the formulation of deflections and bending stresses of highway bridge cables under wind-induced and vortex shedding vibrations; and (2) the formulation of the fatigue behavior of bridge cables in terms of fatigue crack initiation and fatigue crack propagation in bridge cables and in constituent wires. The report further includes a discussion on the fatigue testing of wires and cables and an extensive outline of recommended research programs on the subject from both analytical and experimental standpoints.

17. Key Words Bridge cable, wind-induced vibration, vortex shedding, deflection, bending stress, fatigue life of wire and cable, fracture toughness, fatigue crack initiation and propagation, fatigue testing.		18. Distribution Statement No restrictions. This document is available to the public through the National Technical Information Service, Springfield, Virginia 22161.	
19. Security Classif. (of this report) Unclassified	20. Security Classif. (of this page) Unclassified	21. No. of Pages 180	22. Price

Form DOT F 1700.7 (8-72) Reproduction of completed page authorized

Metric Conversion

SELECTED CONVERSION FACTORS TO STANDARD INTERNATIONAL UNITS

To Convert From	To	Multiply By
inch	meter (m)	2.54×10^{-2}
inch^2	meter^2 (m^2)	6.452×10^{-4}
inch of mercury (32F)	pascal (Pa)	3.386×10^{3}
kilocalorie	joule (J)	4.184×10^{3}
kilogram-force	newton (N)	9.807
kilogram-force-meter	newton-meter (N-m)	9.807
kilogram-force/centimeter^2	pascal (Pa)	9.807×10^{4}
kilogram-force/meter^2	pascal (Pa)	9.807
kilogram-force/millimeter^2	pascal (Pa)	9.807×10^{6}
kip (1000 pounds)	newton (N)	4.448×10^{3}
kip/inch^2 (ksi)	pascal (Pa)	6.895×10^{6}
kip/inch$^2 \cdot \sqrt{\text{inch}}$ (ksi$\sqrt{\text{in.}}$)	pascal$\cdot\sqrt{\text{m}}$ (Pa$\sqrt{\text{m}}$)	1.099×10^{6}
mil	meter (m)	2.54×10^{-5}
millimeter of mercury (mm Hg)	pascal (Pa)	1.333×10^{2}
poise	pascal-second (Pa-s)	1×10^{-1}
pound-force	newton (N)	4.448
pound-force/inch^2(psi)	pascal (Pa)	6.895×10^{3}
pound-force/inch$^2 \cdot \sqrt{\text{inch}}$ (psi$\sqrt{\text{in.}}$)	pascal$\cdot\sqrt{\text{m}}$ (Pa$\sqrt{\text{m}}$)	1.099×10^{3}
torr [mm Hg, (0 C)]	pascal (Pa)	1.333×10^{2}
angstrom	meter (m)	1×10^{-10}
atmosphere (normal = 760 torr)	pascal (Pa)	1.013×10^{5}
bar	pascal (Pa)	1×10^{5}
calorie	joule (J)	4.184
degree Celsius	kelvin (K)	$t_K = t_C + 273.15$
degree Fahrenheit	degree Celsius	$t_C = (t_F - 32)/1.8$
degree Rankine	kelvin (K)	$t_K = t_R/1.8$
dyne	newton (N)	1×10^{-5}
dyne-centimeter	newton-meter (N-m)	1×10^{-7}
dyne/centimeter^2	pascal (Pa)	1×10^{-1}
electron volt	joule (J)	1.602×10^{-19}
erg	joule (J)	1×10^{-7}
ergs/centimeter^2	joule/meter^2 (J/m^2)	10^{-3}
foot	meter (m)	3.048×10^{-1}
foot-pound	joule (J)	1.356
gram-force/centimeter^2	pascal (Pa)	9.807×10^{1}

TABLE OF CONTENTS

Page

ABSTRACT i

METRIC CONVERSION ii

LIST OF FIGURES v

LIST OF TABLES viii

NOTATIONS ix

INTRODUCTION 1

CHAPTER 1. BACKGROUND 3

CHAPTER 2. AEOLIAN VIBRATION OF STAY CABLES 7
2.1 Nature of Aeolian Vibration 7
2.2 Vortex-Induced Excitation of Stay Cables. 7
2.2.1 Mechanism of vortex shedding 7
2.2.2 Analytical models of vortex excitation . . . 11
2.3 Wake and Other Effects 14

CHAPTER 3. GEOMETRICAL AND STRUCTURAL CHARACTERISTICS OF STAY CABLES15
3.1 Geometrical Characteristics 15
3.1.1 Lay configurations 15
3.1.2 Contact geometry 15
3.2 Structural Characteristics. 20
3.2.1 Flexural stiffness 21
3.2.2 Damping 25
3.3 End Anchorage 26

Page

CHAPTER 4. DYNAMIC ANALYSIS OF STAY CABLES 29
4.1 Natural Frequency and Normal Modes 29
4.2 Wind-Induced Vibration of Stay Cables 37
4.2.1 Deflections of cables 40
4.2.2 Bending stresses 47

CHAPTER 5. NUMBERICAL RESULTS OF DYNAMICS ANALYSIS 49

CHAPTER 6. FATIGUE LIFE ANALYSIS 59
6.1 An Overview 59
6.2 Fracture Mechanics Methodology 59
6.3 Fatigue Crack Initiation 60
6.3.1 Microstructural aspects 61
6.3.2 Engineering analysis 63
6.3.3 General discussion 68
6.4 Fatigue Crack Propagation 74
6.4.1 Steady state crack propagation 76
6.4.2 Fracture toughness and critical crack size . 79
6.4.3 Propagation life 87
6.5 Total Fatigue Life of Wires and Cables 87
6.5 Fatigue Testing of Wires and Cables 103

CHAPTER 7. DISCUSSION AND CONCLUSION 107
7.1 Discussion of Results 107
7.2 Concluding Remarks 110

CHAPTER 8. RECOMMENDED FUTURE RESEARCH 112

REFERENCES 124

APPENDIX A: DYNAMICS OF STAY CABLES 131

APPENDIX B. NATURAL FREQUENCIES OF PASCO-KENNEWICK AND LULING BRIDGE CABLES 137

LIST OF FIGURES

		Page
Figure 1.	Chain Cable Bridge	4
Figure 2.	Fan-shaped Cable-stayed Bridge	4
Figure 3.	Harp-shaped Cable-stayed Bridge	4
Figure 4.	Overall Flow Pattern Around a Circular Cylinder for Different Reynolds Number (Re)	8
Figure 5.	Hartlen-Currie Model for Vibrating Cylinder	11
Figure 6.	Cylinder System Response Under Vortex Induced Excitation	13
Figure 7.	Geometry of Parallel and Helical Wire Cables	16
Figure 8.	Contact Geometry of Wires in a Cable	18
Figure 9.	Improved High Strength Anchorages for Cable	27
Figure 10.	Nondimensional Frequency vs. Nondimensional Force (Symmetric Cable with Fixed Ends, n = 1 to 4)	32
Figure 11.	Nondimensional Frequency vs. Nondimensional Force (Symmetric Cable with Fixed Ends, n = 5 to 12)	33
Figure 12.	Nondimensional Frequency vs. Nondimensional Force (Symmetric Cable with Fixed Ends, n = 13 to 27)	34
Figure 13.	Nondimensional Frequency vs. Nondimensional Force (Symmetric Cable with Fixed Ends, n = 28 to 33)	35
Figure 14.	Nondimensional Frequency vs. Nondimensional Force (Symmetric Cable with Fixed Ends, n = 34 to 45)	36
Figure 15.	Pasco-Kennewick Group-IV Cables Mode Shapes (T = 400 kips [1.78×10^3 kN])	38
Figure 16.	Pasco-Kennewick Group-I Cables Mode Shapes (T = 1000 kips [4.45×10^3 kN])	39
Figure 17.	Nondimensional Deflection of Stay Cables (Z^2 = 0 to 0.10)	43
Figure 18.	Nondimensional Deflection of Stay Cables (Z^2 = 0.10 to 1.6)	44
Figure 19.	Nondimensional Curvature of Stay Cables (P = 66,000 to 80,000)	45
Figure 20.	Nondimensional Curvature of Stay Cables (P = 82,000 to 100,000)	46
Figure 21.	Nondimensional Curvature of Stay Cables (P = 102,000 to 120,000)	47

LIST OF FIGURES CONTINUED

		Page
Figure 22.	Cyclic Stress-Strain for Martensitic Structure	62
Figure 23.	Effect of Surface Condition on Fatigue Limit of Steel Alloys	62
Figure 24.	Schematic S-N Curve Showing Crack Limitation, Propagation and Total Life	64
Figure 25.	Fatigue Crack Initiation Data for HY-130 Steel Showing Dependence on Nominal Strees Fluctuations for Various Notch Geometries	65
Figure 26.	Relationship Between Yield Strength and $(K_I/\sqrt{\rho})th$ for High Strength Steels	67
Figure 27.	Dependence of Fatigue Crack Initiation Life of Various Steels on $\Delta K/\sqrt{\rho}$ at Stress Ratio +0.1	69
Figure 28.	Schematic Showing Fatigue Strength of Polished, Notched and Degreased Wire Specimen.	70
Figure 29.	Rotating Strut Fatigue Tests-Single Wires Improved Plow Steel	71
Figure 30.	Fatigue Tests om Improved Plow Wire	72
Figure 31.	Test Results of Prestressing Wires Showing a Wide Scatter	73
Figure 32.	Schematic of Fatigue Crack Growth Regions in Steel	75
Figure 33.	Fatigue Crack Propagation Data in Martensitic Steel	78
Figure 34.	Plane-strain Fracture Toughness of SAE 4340 Steel	80
Figure 35.	Circumferential Crack in a Cylindrical Shell	82
Figure 36.	Axial Crack in a Cylindrical Shell	82
Figure 37.	Approximate Geometry of Circumferential Cracking in a Wire	84
Figure 38.	Relationship Between Maximum Nominal Stress and Critical Crack Size for Different Toughness Values	86
Figure 39.	Crack Propagation Life of a Wire (K_{IC} = 60 ksi$\sqrt{in.}$ [65.94 MPa $\sqrt{m}$], σ = 90 ksi [620.55 MPa])	88
Figure 40.	Crack Propagation Life of a Wire (K_{IC} = 80 ksi $\sqrt{in.}$ [87.92 MPa $\sqrt{m}$], σ = 90 ksi [620.55 MPa])	89
Figure 41.	Crack Propagation Life of a Wire (K_{IC} = 100 ksi$\sqrt{in.}$ [109.9 MPa $\sqrt{m}$], σ = 90 ksi [620.55 MPa])	90
Figure 42.	Crack Propagation Life of a Wire (K_{IC} = 60 ksi$\sqrt{in.}$ [65.94 MPa $\sqrt{m}$], σ = 110 ksi [758.45 MPa])	91

LIST OF FIGURES CONTINUED

Page

Figure 43. Crack Propagation Life of a Wire (K_{IC} = 80 ksi $\sqrt{in.}$ [87.92 MPa $\sqrt{m}$], σ = 110 ksi [758.45 MPa]) 92

Figure 44. Crack Propagation Life of a Wire (K_{IC} = 100 ksi $\sqrt{in.}$ [109.9 MPa $\sqrt{m}$], σ = 110 ksi [758.45 MPa]) 93

Figure 45. Total Fatigue Life of a Wire Showing the Dominance of Initiation Life 94

Figure 46. Interference Between Probability Distributions of Applied Stress and Ultimate Tensile Strength 96

Figure 47. Representation of Cumulative Fatigue Damage Due to Various Stress Levels 98

Figure 48. Fatigue Representation Life of a Wire for Variable Load Range and Different K_{IC} Values 99

Figure 49. Comparison of Single Wire and Wire Rope Fatigue Strengths 101

Figure 50. Strand Nicking in a Helically Wound Cable 102

Figure 51. Specially Designed Stress Rig 118

Figure 52. Potentiometer Circuit for Crack Growth Measurements . . . 120

Figure 53. Schematic Relationship Between E_{R_0} and a 121

Figure 54. Schematic Relationship Between N and a 121

Figure 55. Schematic of Notched Specimen and Fixtures for Three-Points Bend Test 123

Figure B-1. Model of Intercity Bridge on Columbia River in Pasco-Kennewick, Washington 138

Figure B-2. Cable Stayed Span of Luling Bridge on Mississippi River, Louisiana 153

LIST OF TABLES

		Page
Table 1.	Comparison of Contact Geometry Parameters of Parallel and Twisted Cables	19
Table 2.	Mechanical Properties of Cable Materials	22
Table 3.	Properties of Cables Used in Examples	50
Table 4.	Comparison of Natural Frequencies	52
Table 5.	Computation of Deflection	56
Table 6.	Computation of Bending Stress	58
Table 7.	Correction Factors for a Single-Edge Notched Plate	85

Notations

A = Cross-sectional area of the cable

A_c = Area of cracking

A_n = Coefficient of solution $\Phi_n(X)$

B = Area of semi-circle

B_i = ith mode amplitude

B_n = Coefficient of solution $\Phi_n(X)$

C = A constant

C_L = Lift coefficient

C_n = Coefficient of solution $\Phi_n(X)$

C_1 = Coefficient of fatigue initiation equation

C_2 = Coefficient of fatigue propagation equation

D_n = Coefficient of solution $\Phi_n(X)$

E = Elastic modulus

E_{eff} = Effective elastic modulus of cable

E_o = Elastic modulus of straight cable

E_{R_o} = Potential difference across R_o

F = Total axial force

F_o = Amplitude of harmonic forcing function

$F(x,t)$, $F(t)$ = External or driving force

G = Bending moment of a wire

G' = Bending moment in deformed configuration

G_{1n} = Coefficient of solution $\psi_n(t)$

G_{2n} = Coefficient of solution $\psi_n(t)$

H = Twisting moment of a wire

H_s = Strain hardening correction term

I = Moment of inertia

K_I = Stress intensity factor

K_{IC} = Critical stress intensity factor

K_{ID} = Dynamic fracture toughness

K_{th} = Threshold stress intensity factor

$\overline{K}$ = Normalized stress intensity factor

L = Length of cable

M = Total twisting moment

$M(x)$ = Bending moment

$\mathcal{M}$ = Material properties

M_n = Generalized mass

N = Normal force in a single wire

N' = Normal force in deformed configuration

N_i = Number of cycles to crack initiation

N_j = Fatigue life at jth loading

N_p = Number of cycles to crack propagation

N_T = Total fatigue life

N_1, N_2,...= Fatigue life at loading 1, 2, ... etc.

P = Nondimensional force

$P(\sigma)$ = Probability distribution of applied stress

$P(\sigma_u)$ = Probability distribution of ultimate strength

Q = Nondimensional frequency

R = Radius of wire

Re = Reynolds number

R_o = A variable resistance

R_s = Specimen resistance

R_{sh} = Shunt resistance

St = Strouhal number

T = Axial force in cable

T_n = Generalized force vector

T_{on} = Magnitude of generalized force vector

V = Wind velocity

V_{cr} = Critical wind velocity

X = Nondimensional independent variable

Y = Nondimensional deflection

Y_n = Maximum nondimensional deflection of nth mode

Z = A nondimensional function of P and Q

a = Crack length

a_c = Critical crack length

a_i = Initial crack length

b_1 = Interaction constant in Van der Pol's equation

b_2 = Another interaction constant

c = Damping coefficient

c_n = Damping coefficient corresponding to nth mode

c_z = Maximum fiber distance

d = Diameter of cable

f_n = Natural frequency of nth mode

f_s = Strouhal frequency

$f(P,Z)$ = A function of P and Z

g = A function of crack geometry

$g(P,Z)$ = A function of P and Z

h = Thickness of cylindrical shell

ℓ = Horizontal length of cable

m = Number of wires in cable

m_0, m_1, m_2, ... = Number of wires in layers 0, 1, 2 ... etc.

n = Strain hardening exponent

r, r_h = Helix radius

r' = Helix radius in deformed configurations

r_0 = Resistance of plotter circuit

$r_0(r_{h_0})$, $r_1(r_{h_1})$, $r_2(r_{h_2})$ = Helix radii in layers 0, 1, 2, ... etc.

s_ξ = Standard deviation of variable ξ

s_σ = Standard deviation of applied stress

$s_{\sigma u}$ = Standard deviation of ultimate strength

t = Time parameter

x = An independent variable denoting position

y, $y(x,t)$ = Deflection of cable

$y_n(x,t)$ = Deflection of cable at nth mode

α = Helix angle

α' = Helix angle in deformed configuration

α_n = Root of the frequency equation

β = Contact angle

β_n = Root of the frequency equation

Γ = Specific weight of cable

γ = Exponent of the fatigue equation

Δ = A symbol indicating range

δ = Logarithmic decrement of damping

δ_c = Crack tip opening displacement

δ_{mn} = Kröneker delta

δ_0 = Mean free ferrite path

ε = Van der Pol constant

$\overline{\varepsilon}_p$ = Plastic strain at crack tip

π = A mathematic constant

Φ_n, $\Phi_n(X)$ = nth mode shape corresponding to $Y(X)$

ϕ = Angle of twist

$\phi_m(X)$ = mth mode shape of $y(x,t)$

$\phi_n(X)$ = nth mode shape of $y(x,t)$

$\psi_n(t)$ = nth generalized coordinate

ζ = Van der Pol constant

ζ_n = Structural damping factor of nth mode

η = Nondimensional damping coefficient

χ_n = Maximum nondimensional curvature of nth mode

ξ = A stress variable

λ = A function of crack geometry

μ = Coefficient of fatigue equation

ν = Poisson's ratio

ρ = Mass density of cable material

ρ_a = Mass density of air

ρ_c = Radius of curvature

ρ'_c = Radius of curvature in deformed configuration

τ = A nondimensional time parameter

σ = Applied stress, tensile stress

σ_b = Bending stress

σ_j = Applied stress at jth loading

σ_u = Ultimate tensile strength

σ_y = Yield strength

Ω_o = Ratio between Strouhal frequency and natural frequency

ω = Circular natural frequency

ω_{fb} = Bending frequency factor

ω_n = Circular natural frequency of nth mode

ω_s = Circular Strouhal frequency

θ = Crack orientation angle

INTRODUCTION

This report is the outcome of an analytical investigation on the fatigue behavior of cables used in cable-stayed and suspension type highway bridges. The investigation deals with the analytical formulation of the deflection and bending stress caused by the wind-induced vibration, as well as the fatigue behavior of bridge cables due to such vibration.

The main results of the present investigation are conveniently divided into two categories. The first category includes the analysis of deflection and bending stress and is presented in Chapters 4 and 5 of the report. The analysis is preceeded by necessary background materials presented in the first three chapters. Mathematical formulations are kept to a minimum in these chapters and care is exercised to reduce the results in graphical and tabular forms. This is so done, in our opinion, to provide useful guidelines to design engineers without necessarily confusing them by mathematical complexities. For the sake of completeness, however, the detailed mathematical derivations are included in Appendix A.

The second category of main results includes the analysis of the fatigue behavior of bridge cables in terms of the methodologies of linear elastic fracture mechanics (LEFM). It is not intended in this report to justify the applicability of LEFM methodologies in describing the fatigue behavior of bridge cables. It is our understanding that the existing work on the fatigue behavior of bridge cables is insufficient to either substantiate or refute the results obtained during the course of this investigation, and presented systematically in Chapter 6. We do not wish to suggest that the results in this chapter be used by design engineers without discretion. It is our opinion, however, that in the absence of any design guidelines, the present report is at least able to provide some directions at which further research should be aimed.

In line with the above statements, we draw some concluding remarks in Chapter 7 of the report and recommend future research programs in this area in Chapter 8. The remarks are mostly concerned with the applicability of the results herein to a practical design situation. We note that a design engineer can apply the results in Chapters 4 and 5 directly to a design situation provided all criteria and assumptions underlying the analysis are properly met. We also note that a design engineer can use the results in Chapter 6 to obtain an order of magnitude estimate for the fatigue behavior of bridge cables. However, much research is needed, as outlined in Chapter 8, to arrive at a stage whereby all pertinent analytical results can be translated to design tools for the fatigue design of bridge cables.

CHAPTER 1
BACKGROUND

The concept of using stay cables in bridge design dates back to early seventeenth century, as we find sketches by Faustus Verantius in Italian books showing several parallel inclined chain cables holding a bridge deck between two piers (Figure 1). In 1821, the French architect Poyet suggested a bridge design (Figure 2) which is conceptually identical to modern-day fan-shaped cable stayed bridges. The other type of stay arrangement with parallel stays, called harp-shaped (Figure 3), was suggested by Hatley as early as 1840.

In the United States, however, the cable stayed bridge is a relatively new concept in bridge design and construction. Between the latter part of the nineteenth and the early part of the twentieth centuries the use of cable stayed bridge design lost popularity in most parts of the world including Europe. One reason for its disuse was the collapse of some cable stayed bridges during the nineteenth century and subsequent comments concerning these failures by the famous French engineer, Navier. Therefore, the recent resurgence of the cable stayed bridge design makes an accounting of previous experience in design practice essential. This is particularly so because of the dramatic failure of the first Tacoma Narrows suspension bridge in the State of Washington almost 40 years ago.

Designers of modern cable stayed bridges have taken into consideration special design requirements for the stability of structures. One of the most important is the wind-induced vibration. Existing literature on this subject suggests that a significant amount of work has been done to establish methods of design to insure aerodynamic stability of bridge structures. In many cases, wind tunnel tests of prototype models of the proposed designs are involved. However, the complete analysis of the fatigue behavior of individual cables caused by wind vibration has not been resolved. When a cable is subjected to wind forces, the air flow divides and recombines about the nearly circular cross-section of the cable. While we shall explain this phenomenon in greater detail in Chapter 2 of this report, it is sufficient to briefly remark at this point that such a phenomenon gives rise to formation and shedding of vortices. When the wind speed is such that the vortex shedding frequency is equal to one of

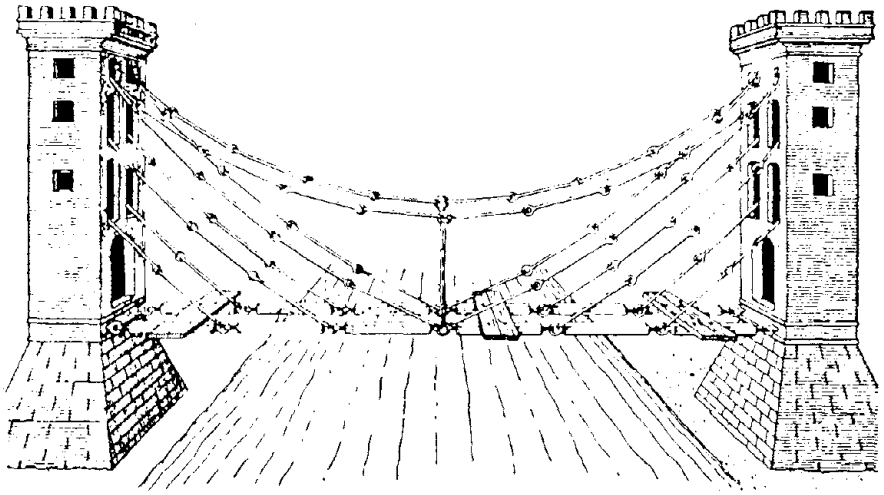

Figure 1. Chain Cable Bridge (Leonhardt[1])

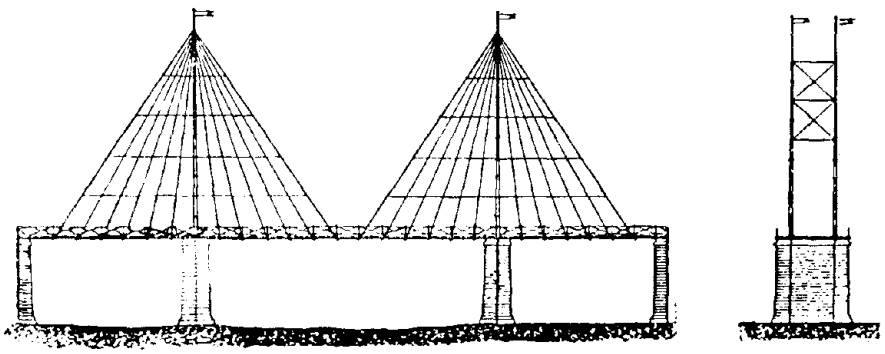

Figure 2. Fan-shaped Cable-Stayed Bridge (Leonhardt[1])

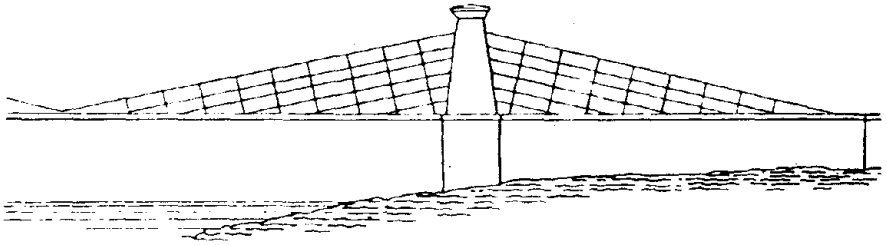

Figure 3. Harp-shaped Cable-stayed Bridge (Leonhardt[1])

the natural frequencies of the cable, a resonant condition can occur. In this case, if the structural damping is low, the wind force can cause large amplitude vibration of the cable, and hence large bending stress. Moreover, due to the harmonic nature of wind force, the bending stress becomes cyclic and repeated. This gives rise to fatigue loading of the cable.

In the case of cable stayed bridge, the problem of cable fatigue is further aggravated by a large change of stresses at the fixed ends of a cable. For this reason, special considerations must be given to the design of end anchorages which are used to join a cable with other fixed structural components. It is also necessary for cable materials to have a high fatigue strength.

At the present time, there exists no fatigue design specification for high strength bridge cables used in suspension and cable stayed bridges. The available axial-load fatigue data are not sufficient to establish either a criterion for defining fatigue failure or for establishing general guidelines for designing cables to withstand high fatigue-load applications.

The lack of design specifications or design guidelines are, by no means, without reason. The foremost difficulty lies in analytically describing the fatigue behavior of a cable by using conventional fracture mechanics methodologies. A second, but related, problem arises in attempts to relate the fatigue life of a cable to a wire. Yet, a third problem is related to the experimental determination of fatigue characteristics of cables and wires. On the other hand, there is a growing trend to construct stayed structures in the United States, as well as elsewhere in the world. In keeping with this trend, and to guarantee the integrity of these structures, it is essential to look into the above difficulties in some detail.

Evidently, the problem of cable fatigue is fairly involved, and a unique solution to the problem is not feasible within the scope of the present contract. With this in mind, we shall attempt to address those particular aspects of the problem which are responsive to the contract objectives. In short, we shall analytically determine the range of natural frequencies of bridge cables and their susceptibility to aeolian vibration. Further, we shall analytically determine the induced bending stresses and fatigue characteristics of bridge

cables. No attempt will be made in this report to develop a new theory of fatigue characteristics of wires and cables. Nor will an attempt be made in this report to validate the application of a particular fracture mechanics methodology in the fatigue design of bridge cables. Such a claim will have to await an extensive amount of experimental investigation. However, we intend to develop in this report some guidelines for bridge engineers to determine frequency ranges that may be crucial to particular cable designs and configurations. We also intend to provide in this report some guidelines which will enable bridge engineers to perform an order of magnitude studies of fatigue life of particular cable designs.

CHAPTER 2

AEOLIAN VIBRATION OF STAY CABLES

2.1 Nature of Aeolian Vibration

The wind-induced vibration of flexible structural members such as wires and cables has been recognized since antiquity. The fact that a taut wire can be induced into vibration by a wind stream was experienced by the Greeks as early as 300 BC. The concept of using wire ropes and cables as structural members in bridges can be traced back to the early seventeenth century. However, a systematic study of the wind-induced vibration of the above structural members did not begin until recently.

As stated before, a long slender elastic structure near resonance conditions can develop flow-induced oscillations by extracting energy from the flow around them. The oscillations, coupled with the flow, give rise to a fluid-structure interaction resulting in a nonlinear response. The fluid-structure interaction is widely covered by four general classes of phenomena: 1) Vortex-induced oscillation; 2) Flutter; 3) Galloping; and 4) Buffeting. For a given structural member and a given flow condition, all these phenomena may be equally important. On the other hand, in dealing with the wind-induced vibration of stay cables, we shall consider vortex-induced oscillation to be the most important fluid-structure interaction. A detailed description of the mechanism of vortex shedding and analysis of the vortex-induced excitation of stay cables will be given in the next section. For the sake of completeness, a brief description of other classes of interaction phenomena will also be provided in Section 2.3 of this Chapter.

2.2 Vortex-Induced Excitation of Stay Cables

2.2.1 Mechanism of vortex shedding:

Without any loss of generality, we shall consider a stay cable to be a long slender elastic structure of circular cross-section. The mechanism of vortex shedding from a stay cable can then be illustrated in terms of the overall flow pattern around a circular cylinder with increasing Reynolds numbers as shown in Figure 4. The Reynolds number (Re), a dimensionless parameter characterizing the flow regime, is a function of the flow velocity, the diameter or the

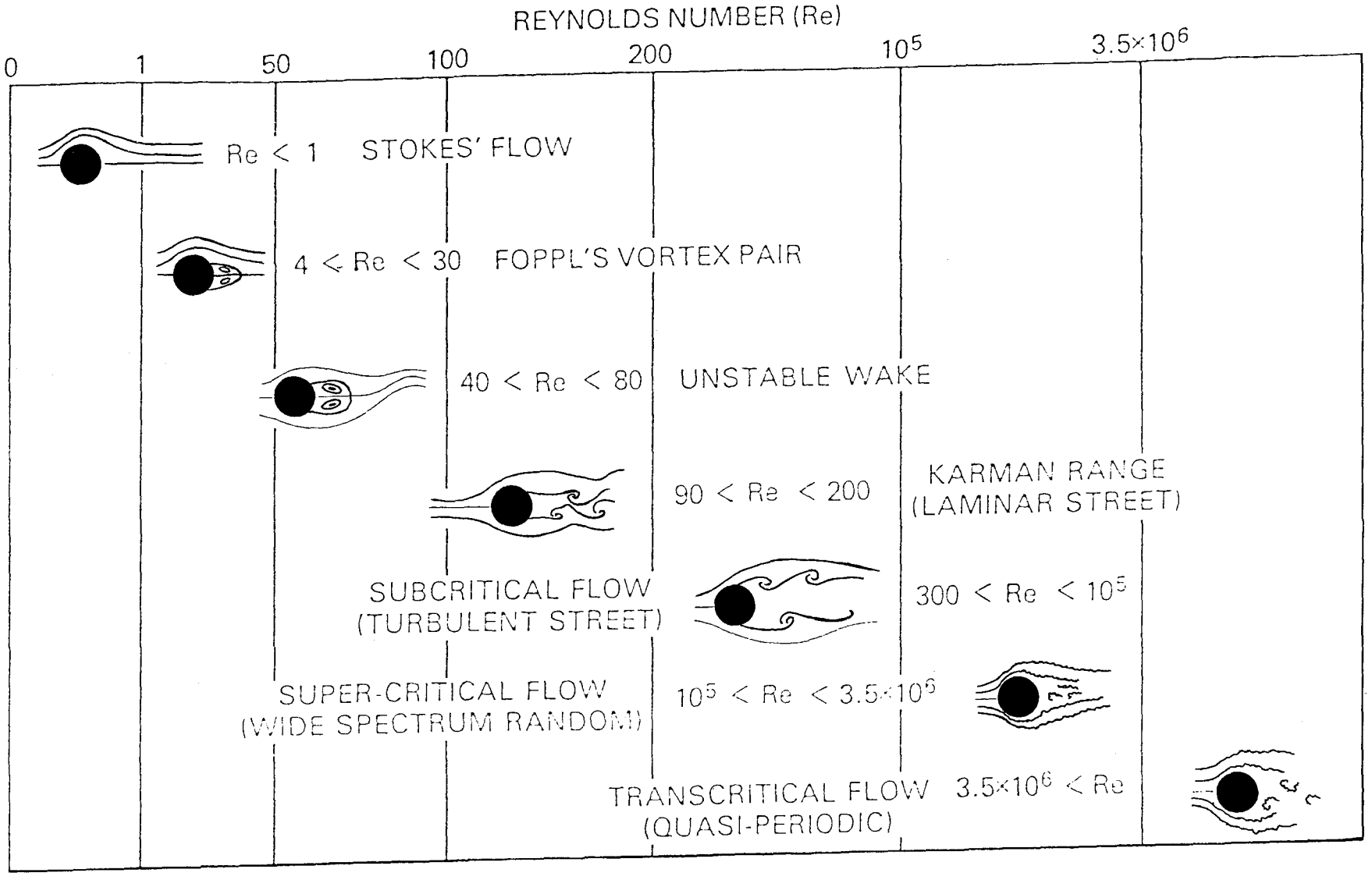

Figure 4. Overall Flow Pattern Around a Circular Cylinder for Different Reynolds Number (Re)

characteristic depth of the body in flow, and the kinematic viscosity of the fluid. For a given fluid medium and a given depth of body in consideration, the Reynolds number is directly related to the flow velocity. The higher the Reynolds number, the higher the flow velocity, and correspondingly, the more turbulent is the flow.

We will now briefly review the wake formulations in various flow regimes. At extremely low Reynolds numbers, the flow is similar to a small particle settling in a colloidal solution. In this range there is no wake formation. At Reynolds numbers between 5 and 10, the boundary layer over the cylinder begins to separate in a more or less symmetrical fashion, forming a Foppl vortex pair downstream. The pattern remains stable up to a Reynolds number of about 40, beyond which the vortex starts shedding because of wake instability. At about Reynolds number 90, the detached shear layer starts to fold up after its separation and forms concentrated vortices. The fluid in the vortices, however, is still laminar, and the vortex street persists downstream for many diameters. At Reynolds numbers above 300, the shear layer becomes turbulent. Its separation point moves further around, and the wake width becomes narrower. Beyond this, the flow pattern remains essentially unchanged, presumably up to Reynolds number 2×10^5. For Reynolds numbers in the range of 2×10^5 and 3×10^6, the boundary layer undergoes a transition and the wake is disorganized. At Reynolds numbers beyond 3×10^6, a boundary layer becomes fully turbulent.

The subcritical and the supercritical flow regimes shown in Figure 4 are important to bridge designers. In the subcritical flow, the wake consists of easily recognizable and regularly spaced alternating vortices similar to the Karman street, although the fluid inside the vortices may be turbulent. In the supercritical flow, there is no well organized vortex street and the energy in the wake is diffused into a wide spectrum of frequencies, rather than in a single dominating frequency.

The vortex shedding phenomenon of stay cables described above is associated with a frequency f_s (Strouhal frequency) given by $f_s = \frac{St \cdot V}{d}$ where St is the Strouhal number, V is the wind velocity and d is the diameter of the stay cable. The Strouhal number St in honor of V. Strouhal[2] is one of the most significant parameters that accounts for the vortex shedding phenomenon.

A considerable amount of research has been done to determine the Strouhal numbers for various structural shapes and to establish relationships between Strouhal numbers and Reynolds numbers. For design purposes, the Strouhal number of a cylinder can be considered constant over a broad range of Reynolds numbers and this constant is equal to 0.2.

If the Strouhal frequency, f_s, is close to any of the natural frequencies f_n of the structure, a nonlinear phenomenon known as synchronization or lock-in occurs, and in unfavorable conditions, the structure can undergo large amplitude vibrations. For a structural member of circular cross-section and large slenderness ratio, such as stay cable, it has been found [3] that $f_n < f_s < 1.4\ f_n$. The maximum amplitude of excursion occurs presumably at the middle of the range. It should be noted here that the vortex shedding does not necessarily result in an alternating transverse force. This is created only when there is a suitable afterbody and hence, an alternating lift force. Besides, while the lock-in of Strouhal frequency with the natural frequency of the structure will give rise to sustained oscillations, the transverse force exerted by the vortex shedding is not strong enough to cause a large amplitude oscillation [4]. Therefore, the magnitude of sustained oscillations depends strongly upon the lift coefficient of the structure. Structural damping is another parameter, besides the Strouhal frequency f_s (or Strouhal number St) and the lift coefficient, which is of major importance in determining the amplitude of oscillations and the range of synchronization.

2.2.2 Analytical models of vortex excitation:

The response of structural members under vortex-induced excitation is conveniently formulated in terms of various analytical models [5-7], the most noteworthy of which is the one proposed by Hartlen and Currie [5]. The latter model employs a Van der Pol-type soft nonlinear oscillator (see Figure 5) where the fluctuating lift force associated with vortex shedding is coupled to the body motion. The model is based on the wake-oscillator concept introduced by Birkhoff and Zarantonello [8], and on the experimental results of Bishop and Hassan [4].

This concept may be applied to a stay cable when the latter is considered as a circular cylinder vibrating in a direction transverse to the flow. The

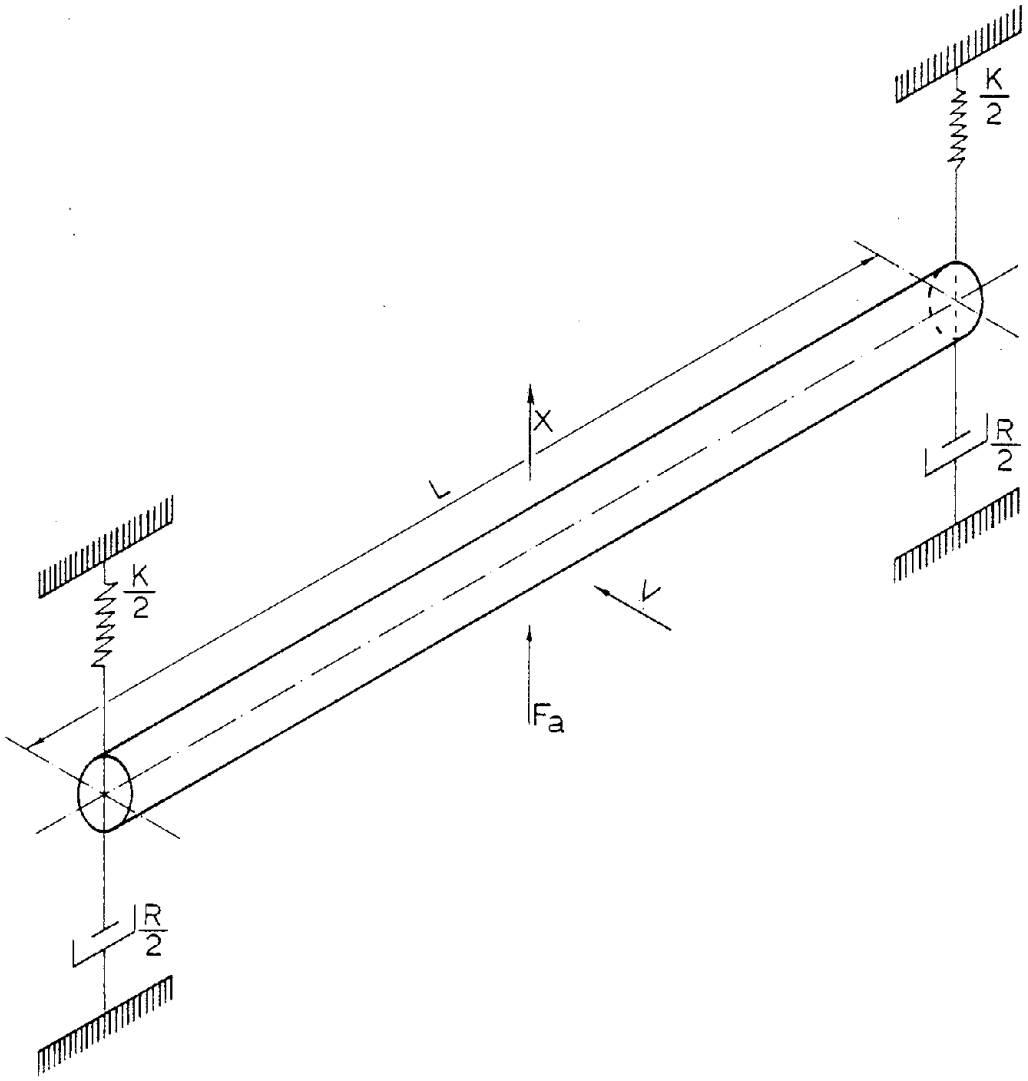

Figure 5. Hartlen-Currie Model for Vibrating Cylinder

pair of equations which result from this type of consideration are second order differential equations of the Van der Pol type. The equations contain a member of nondimensional parameters including nondimensional damping coefficient, ν, Van der Pol constants, ε and ζ, interaction constants, b_1 and b_2, and finally, the ratio, Ω_o, between Strouhal frequency defined earlier and the natural frequency.

Of the above parameters, ν, b_1, and Ω_o can be determined for a given geometry and for given material properties of a stay cable. The other three parameters, ε, ζ, and b must be chosen to provide the best fit for experimental data. Such experiments have been conducted, among others, by Jones [9] for the elastically mounted circular cylinders forced externally by fluctuating lift components. When the Hartlen-Currie model for the vibrating circular cylinder was fitted to experimental data, it was found that the dimensionless amplitude $Y(t)$, and the lift coefficient $C_L(t)$ are related to the dimensionless wind speed and the dimensionless damping as indicated in Figure 6.

In the past various attempts have been made to improve some inherent discrepancies of the original Hartlen-Currie model. Griffin, et al., [10] considered additional empirical parameters in the equation for lift coefficient. Landl [11] introduced a nonlinearity of fifth order in the damping term in the lift equation. Szechenyi [12] assumed a fictitious symmetric aerofoil attached to the cylinder and examined its oscillation under the action of a periodic lift force. Iwan and Blevins [7] arrived at the Hartlen-Currie model through considerations based on the vortex street. All these models basically result in a relationship between the dimensionless amplitude and the dimensionless damping factor.

It is not apparent whether these models are readily applicable to flexible structures such as a stay cable. One serious objection arises because the measurement of vortex-induced effects in flow past a rigid oscillating cylinder [3] clearly indicates that the cylinder continues to vibrate in resonance outside the lock-in range. For a flexible cylinder, this effect will be more pronounced. A fundamental objection is often raised concerning the validity of the Van der Pol oscillator to describe the fluid-structure interaction, regardless of whether the structure is rigid or flexible. To

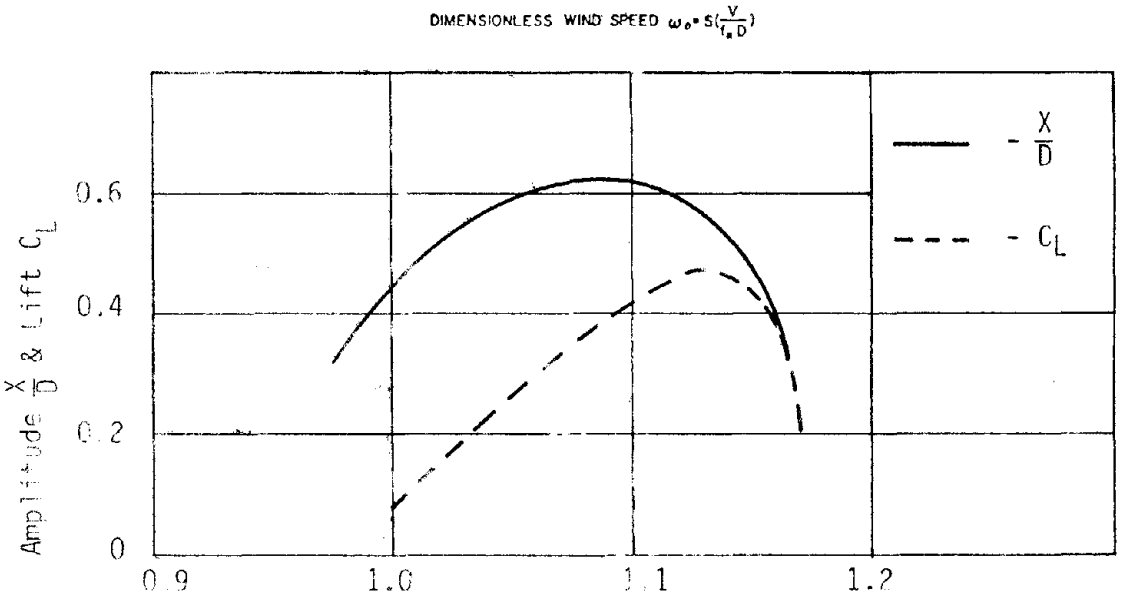

a. Lift Coefficient and Cylinder Amplitude vs. Wind Speed (Hartlen and Currie[5])

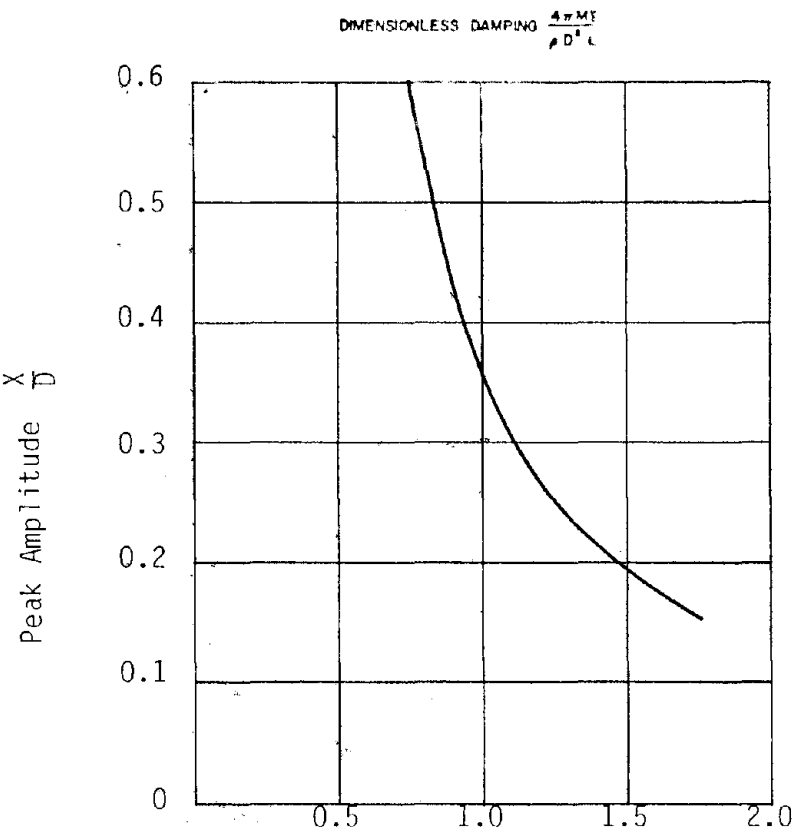

b. Cylinder Amplitude vs. Damping (Hartlen and Currie[5])

Figure 6. Cylinder System Response Under Vortex Induced Excitation

circumvent these problems and to achieve the main objectives of the present investigation, we shall consider, for subsequent analysis, a simplified wind force model whereby the driving force F(t), has the following form:

$$F(t) = \frac{1}{2} \rho d V^2 C_L \cos\omega_s t \tag{1}$$

The term ω_s in the above expression is the circular Strouhal frequency and is equal to $2\pi f_s$. Further discussion of this model concerning the dynamic analysis of stay cables will be presented in Chapter 4.

2.3 Wake and Other Effects

In general, the wake effect is concerned with the vibration of structural members located in the wake of other members. For example, if the stay cables are arranged in a square pattern, a situation can occur wherein an individual cable lies downwind in the wake of another. In this case, the leeward cable is subjected to unsteady loading resulting from velocity fluctuations in the downstream flow. In particular, if the leeward cable is in the proximity of a high shear gradient of the wake, it may experience a large amplitude oscillation. This is called wake-induced galloping. Buffeting, on the other hand, is a wake-induced random oscillation produced by turbulent wind or gust.

Flutter is a self-excited oscillation caused by the interaction of structural, inertial, and aerodynamic forces. It is usually a high speed phenomenon in which aerodynamic forces augment the oscillatory deflections. Flutter of a flexible bridge member consists predominantly of a torsional type although in some cases, the torsional vibration may be coupled with a secondary motion due to transverse vibration. It is important to note that although a stay cable is not flutter-prone, it may still be subject to buffeting or galloping oscillations.

As mentioned earlier, the scope of the present investigation does not cover an analytical formulation of the latter classes of fluid-structure interaction phenomena. For this reason, the discussion of these phenomena will be limited only to this section. The readers are, however, referred to Scanlan and Tomko [13], Davenport, et al., [14], Irwin [15], and Scanlan and Gade [16] for some excellent expositions on this subject.

CHAPTER 3

GEOMETRICAL AND STRUCTURAL CHARACTERISTICS OF STAY CABLES

3.1 Geometrical Characteristics

The structural properties of stay cables and their operating characteristics depend, to a large extent, on the geometry of cable configurations. It is, therefore, important to investigate the geometrical characteristics of a stay cable for further analysis of its structural properties. In this section, we present the results of CHI ASSOCIATES, INC's investigation to this effect which includes a study of wire geometry in a cable, the determination of contact points and contact surfaces between wires, and the effect of clearance between wires on the overall geometrical and structural properties of a cable.

3.1.1 Lay Configurations

The two different cable or lay configurations which have been investigated under this task are: parallel wire configuration and helically wound configuration. These two configurations for a two-layer cable are shown in Figure 7 .

Under the category of helically wound configuration, several constructions which include single strand operation, and multiple strand operation, are possible. For the purpose of this report, we shall consider a cable to be made of a number of layers of individual wires either wound helically or bunched in parallel by a single strand operation. Each construction procedure produces a unique contact geometry, and different contact geometries give rise to different amounts of contact stress between the wires. Foregoing this differentiation at present, let us consider the transverse cross-section of a cable in general. The cross-section of individual wires are approximately elliptical (see Figure 7a). In the case of the parallel wire configuration (Figure 7b), the circular cross-section may be considered as a limiting case of elliptic cross-section whereby the semi-major axis is equal to the semi-minor axis. Hence, for the sake of brevity, we will address ourselves to the general case of an elliptic cross-section.

3.1.2 Contact Geometry

If two wires in the same layer are contacting each other, as is shown in Figure 8 , the line of contact between these two wires is a helix with radius r_h. The latter is a function of the radius, R, of the wire, the

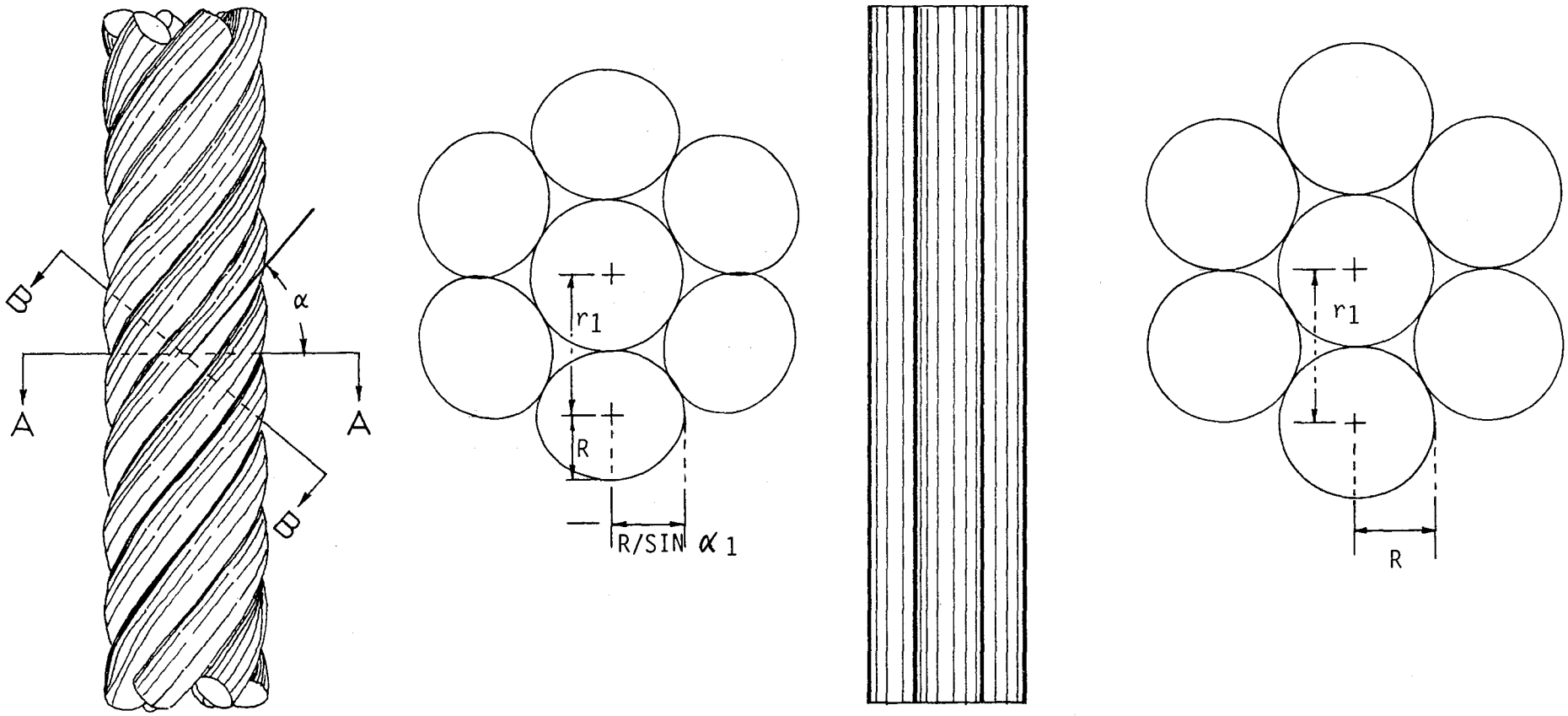

a. Helical Wire Cable

b. Parallel Wire Cable

Figure 7. Geometry of Parallel and Helical Wire Cables

helix angle or lay angle, α, of the particular layer in question, and the number of wires, m, in the layer. Also, the angle, β, between the line of circumferential contact and that of radial contact as shown in Figure 8, is a function of the above parameters.

Noting the following representations of different layers in a cable, namely,

Layer 0 (core)	$r_0 = 0 = r_{h_0}$, $\alpha_0 = \frac{\pi}{2}$, $m_0 = 1$
Layer 1	r_1, r_{h_1}, α_1, m_1
Layer 2	r_2, r_{h_2}, α_2, m_2
⋮	⋮

the geometrical characteristics of different cable configurations may be determined and compared. We have done this for a 3-layered case (both parallel and helical) for a given wire radius, R, and for given values of α_1, m_1, α_2, ... etc. The results are shown in Table 1. It is important to note in this Table that, as the number of layers in a cable increases, so does the helix radius, r_h. Furthermore, the contact angle, β, approaches a limiting value 90^0 indicating that the contact points of the wires are on their semi-major axes. This will create clearance between wires in successive layers of a helically wound cable.

The study of geometrical characteristics of cables reported herein essentially follows the work of Chi[17], Karamchetty[18], and Phillips and Costello[19]. The detail derivations of complex functional relationships between r_h, β, and other geometrical parameters mentioned earlier are omitted here since they may be found in the references above as well as in the monthly Progress Reports on this project submitted by CHI ASSOCIATES, INC. to the Federal Highway Administration.

The other geometric parameter of importance is the radius of the curvature of a wire both in the stressed and unstressed state. For elliptic cross-section, the radius of curvature ρ_c at the contact point in the unstressed state is given by:

$$\rho_c = \frac{r}{\sin^2\alpha} \qquad (2)$$

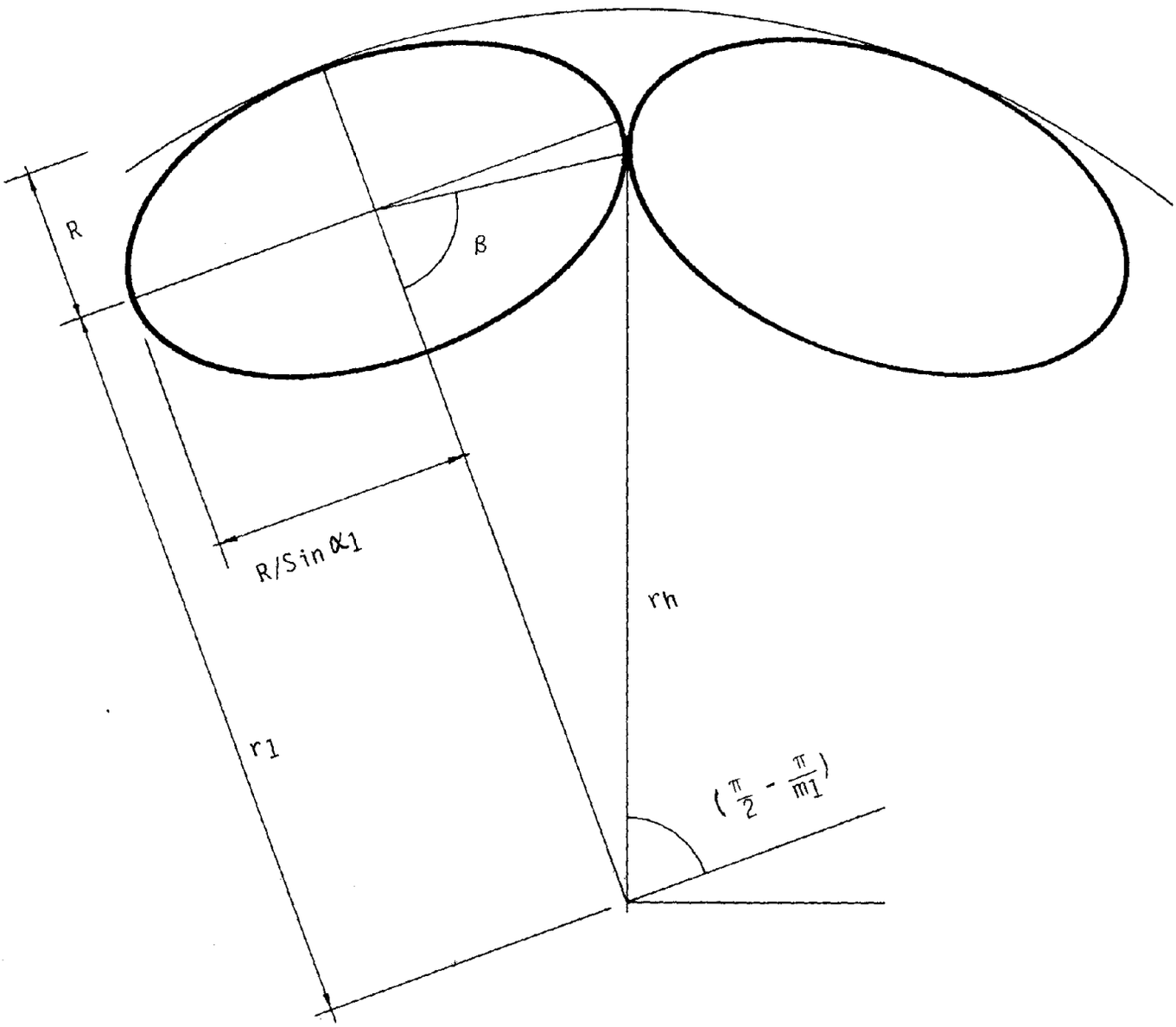

Figure 8. Contact Geometry of Wires in a Cable

TABLE 1.

Comparison of Contact Geometry Parameters of Parallel and Twisted Cables

	r_o (cm)		r_h (cm)		α		β	
	Parallel	Twisted	Parallel	Twisted	Parallel	Twisted	Parallel	Twisted
Layer 0 (core) R = 0.635 cm. m = 1	0.0	0.0	----	----	90°	90°	----	-----
Layer 1 R= 0.635 cm m = 6	0.635	0.635	1.10	1.12	90°	80°	----	48°
Layer 2 R=0.635 cm m= 12	1.270	1.270	2.35	2.50	90°	70°	----	70°
Layer 3 R=0.635 cm. m=18	1.905	1.905	3.62	4.20	90°	60°	----	85°

where r and α have been defined before. In the stressed state, the radius of curvature is transformed to ρ_c'. The determination of ρ_c' involves the evaluation of elliptic integrals of the type mentioned in Seely and Smith [20].

So far we have confined our discussion to cable geometry and contact geometry. The knowledge of contact geometry enables us to determine the location of contact points or more precisely, contact surfaces across which wires transmit forces and motion. It is also at these contact surfaces that contact stresses are generated. For some cable configurations, especially helical, contact stresses may be significant enough to cause strand nicking which then acts as a source of fatigue crack initiation. We have, therefore, considered it relevant to study contact stresses in a cable.

Hruska [21], Leissa [22], Starkey and Cress [23], Stein and Bert [24] are some of the early workers who analyzed the stresses in wire ropes. A rope consists of a number of strands and its stress analysis is fairly complex. However, the analysis of a strand is relatively simple. Phillips and Costello [19] analyzed strands by the method of separating the strand into thin wires and solving the general nonlinear equations. Since a cable is known as strands among manufacturers, the method used by Phillips and Costello to determine the contact stresses is applicable. The result of preliminary analysis using the above method shows that the effect of helix angle on the contact stress is relatively small. In particular, for parallel wire cables (helix angle of 90 degree) the contact stress approaches a zero value. In view of this and in view of the fact that in modern cable-stayed bridges, cables consist mostly of parallel wire configuration, the contact stress will not be considered as a dominant factor in the dynamic analysis. On the other hand, it should be remembered that in the case of helical configuration, the contact stress may be responsible for strand nicking and subsequent initiation of fatigue crack. For such cases, therefore, the contribution of the contact stress in determining the total fatigue life of a cable must be taken into account.

3.2 Structural Characteristics

The structural characteristics of a cable which influence its dynamic response are flexural stiffness and damping. The end anchorage is another

important factor that influences the deflections and stresses at the ends of a cable. We shall discuss this latter factor in detail in Section 3.3 of this report.

Both the flexural stiffness and the damping depend, among other things, upon the wire material. Parallel wire cables are made from uncoated stress-relieved wires which have ASTM Designation A421-77BA. These cables are manufactured by the PRESCON Corporation of San Antonio, Texas, INTYCO, Inc., Melrose, Illinois, and Bureau BBR, Ltd., Zurich, Switzerland. Helical wire structural strand with zinc-coated steel wires has ASTM specification A586-68. Helically wound structural wire ropes are manufactured according to ASTM specification A603-70. The mechanical properties of these materials are shown in Table 2.

3.2.1 Flexural Stiffness:

The flexural stiffness of a single wire is easily derived from the knowledge of its elastic modulus and the moment of inertia. The determination of the stiffness of a cable, on the other hand, is a little more involved. For example, the stiffness of a bridge stay cable depends not only upon its elastic modulus and the moment of inertia, but also upon its length and axial stress. Ernst[25] showed that the effective elastic modulus, E_{eff}, of a cable reduced considerably along its length according to the following formula:

$$E_{eff} = E_o \left(1 + \frac{\Gamma^2 \ell^2 E_o}{12\sigma^3}\right)^{-1}$$

in which

Γ = specific weight of cable

ℓ = horizontal length of cable

E_o = elastic modulus of straight cable

σ = tensile stress of cable

The above expression indicates that for the given length of a cable, the reduction in elastic modulus is inversely proportional to the third power of the tensile stress. In other words, for minimum reduction in elastic modulus, high stresses and consequently, high-strength steel, must be used for stay-cables. Since the cable materials under consideration (ASTM A421-77BA and A586-68) are indeed high strength steel, we shall assume, without further recourse to the above formualation, that the effective elastic modulus is equal to that of a straight

Table 2 - Mechanical Properties of Cable Materials

Material	Zinc Coating Class	Nominal Diameter		Minimum Stress at 1% Extension		Tensile Strength, min	
		in.	mm.	psi.	MPa.	psi.	MPa.
A 586-68	A	0.040-0.110	1.016-2.794	214,286	1477	220,000	1517
		0.110	2.820	228,571	1576	220,000	1517
	B	0.090	2.286	214,286	1477	210,000	1448
	C	0.090	2.286	200,000	1379	200,000	1379
A 603-70	A	0.040-0.110	1.016-2.794	214,286	1477	220,000	1517
		0.111	2.820	228,571	1576	220,000	1517
	B	0.040	1.016	214,286	1477	210,000	1448
	C	0.040	1.016	200,000	1379	200,000	1379
A 421-77		0.196	4.978	204,000	1407	240,000	1655
(Type BA)		0.250	6.350	204,000	1407	240,000	1655
		0.276	7.010	199,750	1377	235,000	1620

cable. This assumption means that the only other source of variation in flexural stiffness along the length of a cable is its moment of inertia.

Consider, for example, a cable made from a number of single wires placed in several layers. When this cable is anchored at two ends in a cable-stayed bridge, and is acted upon by an external force or moment system, its curvature changes along the length. Moreover, a certain geometrical grouping of wires in a definite pattern occurs along the length. Inside the end-anchorage, all wires seem to act monolithically as a single elastic body. However, a few diameters away from the fixed ends the outer wires start to act separately, leaving only the core wires which tend to group together. Scanlan and Swart [26] reported a case in which the effective stiffness value of a Pheasent conductor cable was only 50 percent of its maximum theoretical value. The latter value corresponds to the case where all wires in the cable are considered to be "welded" together to form one unit.

Flexural stiffness of a cable can be determined semi-empirically by using either quasi-static or vibration tests. Specifically, the quasi-static test consists of applying a sinusoidally distributed transverse loading on a suitably supported cable segment. The vibration test determines the stiffness from information on loop length, frequency or strain and displacement. Flexural stress of a cable can also be determined analytically. The methods differ according to the cable configuration. Within the scope of this report, we shall briefly outline two methods, one each for the parallel wire configuration and the helical wire configuration.

The first method is based on the work of Scanlan and Swart [26] and is applicable to parallel wire configuration. In this method, the flexural stiffness, EI, is estimated from the knowledge of displacement and curvature using the following equation:

$$EI = \frac{Ty + M(x)}{y''} \tag{3}$$

where T = axial force

$M(x)$ = bending moment

y = cable displacement in tranverse direction

y'' = curvature of the cable

The displacement, y, is normally obtained from quasi-static tests and the curvature, y", is determined by numerical integration. In the absence of any experimental result, however, the alternate approach to determine the flexural stiffness involves an iteration procedure to solve the equation.

The second method is based on the work of Phillips and Costello [19] and is applicable to helical wire configuration. In this method, the total axial force, F, and the total twisting moment, M, on a cable are expressed in terms of forces and moments acting on individual wires as follows:

$$F = m\,(T\sin\alpha' + N'\cos\alpha') \tag{4a}$$

$$M = m\,(H\sin\alpha' + G'\cos\alpha' + Tr'\cos\alpha' - N'r'\sin\alpha') \tag{4b}$$

where T is the axial force in a single wire, N is the normal force, G and H are bending and twisting moments respectively, and where r and α are helix radius and helix angle respectively. The term m in the above expressions denotes the number of wires in a cable. The terms N', G', r' and α' are the corresponding values of N, G, r, and α in the deformed configuration. The flexural stiffness can now be defined as the partial derivative of the total moment, M, with respect to the angle of twist, ϕ, i.e.

$$EI = \frac{\partial M}{\partial \phi} \tag{5}$$

The procedure, therefore, involves computation of partial derivatives of T, N, G, H, etc. with respect to ϕ. The detail computation is shown in reference (27).

We have used the above methods to compute the flexural stiffness of a sample 1x7-wires cable of both parallel and helical configurations. For the purpose of illustration, we have selected a wire radius of 0.0825 inch (0.21 cm). The cable has been assumed to be subjected to a varying axial force in the range between 5000 lbf (22.24 kN) and 25,000 lbf (111.20kN). These values are representative of the axial cable stress normally encountered in design practices. For helical configuration, five different helix angles ranging from 74 degrees to 78 degrees have been chosen.

The results of our calculation show that the flexural stiffness of a cable is a function of its configuration or, more precisely, of its helix angle. In this particular example, we have assumed that the wires in the cable are not

"welded" or grouped together. Hence, in both parallel configuration and helical configuration, the respective minimum values of moment of inertia at any section of the cable have been considered for computational purpose. Such consideration has led to a variation of nearly five percent in the effective flexural stiffness value. It is, therefore, expected that as the cable diameter becomes larger, and as the wires in the cable tend to group together, the variation in effective flexural stiffness may increase considerably. This is in agreement with Scanlan's findings reported earlier. More important to note at this point, however, is the fact that the wide variation of the flexural stiffness of a cable has little effect on its natural frequencies. In the next chapter in dealing with the dynamic analysis of a cable, we shall present some supporting evidence to this effect.

3.2.2 Damping:

The damping of a stay cable is due to viscous and friction forces which always oppose the excitation of the cable. The damping is usually expressed in terms of the logarithmic decrement, δ, defined to be the natural logarithm of the ratio of two successive peak amplitudes in a free, decreasing oscillation. If B_i and B_{i+1} are the ith and (i+1)th amplitudes, respectively, the damping is given by:

$$\delta = \mathrm{Log}_e \frac{B_i}{B_{i+1}} \tag{6}$$

For cables, in general, the value of δ is usually on the order of 0.04 to 0.08.

The above definition of damping is particularly applicable for a single degree of freedom system. For a continuous structure, such as a cable, it is often advantageous to consider another definition of damping coefficient, namely, the viscous damping coefficient. The latter, denoted by c_n, is proportional to mass per unit length, ρA, and the natural frequency, ω_n, of the nth mode (n= 1, 2, . . .). The relationship is given by:

$$c_n = 2\zeta_n \omega_n \rho A \tag{7}$$

where ζ_n is the structural damping factor. This factor is approximately equal to $\delta/2\pi$. Noting that, for higher modes δ and hence ζ_n decreases as ω_n increases, one can assume for design purposes that the product $\zeta_n \omega_n$ is constant. This

effectively means c_n is constant. Denoting this constant by c, one can write:

$$c = \frac{\delta}{\pi} \omega_1 \rho A \tag{8}$$

where ω_1 is the fundamental frequency of the cable. In the dynamic analysis of a stay cable, we are going to make use of the above approximation for the viscous damping.

3.3 End Anchorage

When cables are used as structural members, several considerations must be taken into account to determine their load bearing capacities and performance characteristics. One of these considerations is the end anchorage which connects a cable to other supporting structural members. The end anchorages vary widely in their design and manufacturing techniques depending on the size and properties of the cable to which they are attached. However, they have one basic function in common, that is, they transfer load from the cable to other structural members. Consequently, the dynamic response and the fatigue life of a cable depend much on the type of end anchorage.

Early versions of end anchorage design for large diameter cables used the molten zinc type sockets. However, the pouring temperature of zinc alloy was found [28] to considerably affect the fatigue strength of wires in the socket. An excellent solution to overcome this problem was devised in Germany[29, 30]. The so-called "HiAm-anchorage" was subsequently developed by the Bureau BBR-Zurich, and it was reported that the fracture of wires in a cable was almost equally distributed over the length of the cable so that the anchorage was not any weaker than the cable itself. The schematic of a typical HiAm-anchor is shown in Figure 9a. Another end anchorage widely used in the United States has been developed by Prescon Corporation of Texas. A schematic of this anchorage is shown in Figure 9b.

The HiAm-anchorage system consists of button heads bearing on a stressing ring which is threaded both internally and externally. The ring is recessed in the end of the member before stressing. The Prescon system is similar to the HiAm system, but rather than using a stressing ring which is recessed before stressing, the button heads bear directly on a round plate which is threaded into the socket. An overview of different cable constructions with partirular

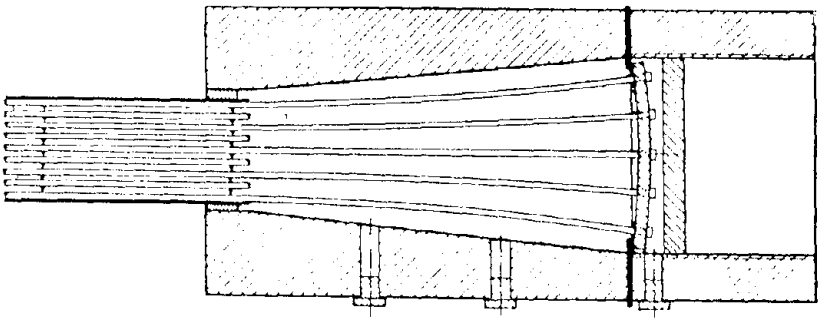

a. The Schematic of a Typical Hi-Am Anchor

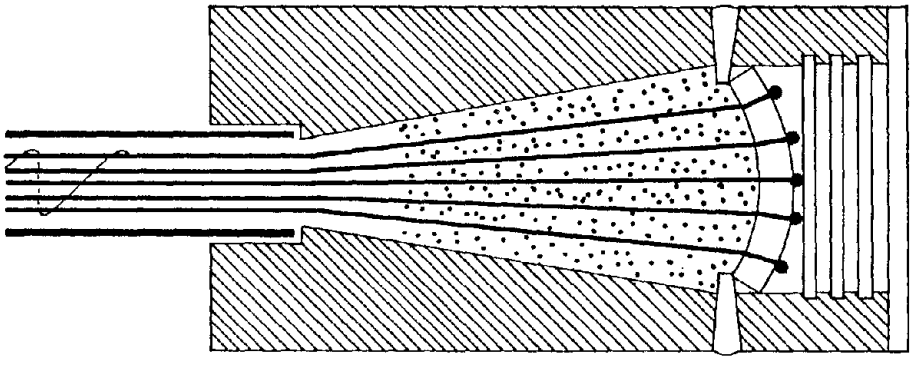

b. The Schematic of a Prescon Anchor

Figure 9. Improved High Strength Anchorages for Cable

note on various end anchorages may be found in reference (31). The reader is also referred to a recent paper on fatigue resistant tendons for cable-stayed construction by Birkenmaier[32].

The effect of end anchorage on the dynamic response and the fatigue behavior of a cable system can be studied analytically by considering proper boundary conditions in solving the dynamic equation. The choice of boundary conditions, however, depends on the nature of load transfer between the cable and the socket. The existing literature on stay cables does not provide sufficient information on the latter subject. We, therefore, consider this to be an area of possible future research.

Within the scope of this project, we have made an attempt to address this problem in two different ways. In the first method, the dynamic equation of a cable is solved for the most general case of arbitrarily specified elastically constrained end conditions. The detailed solution procedure is given in Appendix I. In the second method, the solution of the dynamic equation of a cable for the case of fixed end conditions is found. The deflections and bending stresses at the ends of a cable can also be evaluated by substituting the elastic constants with proper viscoelastic parameters. Such consideration is based on the assumption that the end anchorage is viscoelastic rather than elastic in nature.

In concluding this section, we note that the end anchorages currently used in cable design reduce the theoretical bending stress at the wire ends of a cable by as much as 50 percent. Moreover, the use of HiAm and Prescon type anchorages insure that the bending stress is uniformly distributed over the entire length of the cable rather than having a large magnitude at the ends. Based on these facts, it seems that the dynamic response and the fatigue behavior of cable ends under the commonly occurring wind forces are not significantly different than those pertaining to any other cross sections of the cable. On the other hand, for gusts, random wind loading and other cases, the fatigue behavior of cable ends may cause serious concern even in the presence of high fatigue resistant type anchorages. In these cases, special care should be taken to design cable ends as well as in attaching them to other structural members.

CHAPTER 4

DYNAMIC ANALYSES OF STAY CABLES

The governing differential equation of the motion of a stay cable has the following general form:

$$\rho A \frac{\partial^2 y}{\partial t^2} + c \frac{\partial y}{\partial t} + \frac{\partial^2}{\partial x^2} \left(EI \frac{\partial^2 y}{\partial x^2} - T\right) = F(x,t) \tag{9}$$

where $y = y(x,t)$ = displacement in transverse direction

ρ = mass density

A = cross sectional area

c = damping coefficient

$F(x,t)$ = external force in transverse direction

EI = flexural stiffness

T = axial force

Assuming that the flexural stiffness is constant along the length of the cable, the above equation can be rewritten as:

$$\rho A \frac{\partial^2 y}{\partial t^2} + c \frac{\partial y}{\partial t} + EI \frac{\partial^4 y}{\partial x^4} - T \frac{\partial^2 y}{\partial x^2} = F(x,t) \tag{10}$$

The solution of the above equation is given by:

$$y(x,t) = \sum_n \phi_n(x) \phi_n(t) \tag{11}$$

where $\phi_n(x)$ = nth natural mode of the cable

$\phi_n(t)$ = nth time-domain solution of the equation

The detail solution of equation (10) can be found in Appendix A. In the following section of this chapter, the expressions for natural frequencies and normal modes of a stay cable will be derived.

4.1 Natural Frequency and Normal Modes

The natural frequencies and mode shapes of a cable are obtained from the governing equation for the small amplitude, free, transverse vibration as follows:

$$EI \frac{d^4 y}{dx^4} - T \frac{d^2 y}{dx^2} - \rho A \omega^2 y = 0 \tag{12}$$

This equation can be derived from equation (10) by a separation of variables technique and by neglecting the damping and the external forcing terms.

Nondimensionalizing equation (12) by setting

$$Y = \frac{y}{L} \text{ and } X = \frac{x}{L} \tag{13}$$

where L is the length of the cable, and dividing through by EI/L^3 , we obtain:

$$\frac{d^4Y}{dX^4} - P\frac{d^2Y}{dX^2} - QY = 0 \tag{14}$$

in which $$P = \frac{TL^2}{EI} = \text{nondimensional force} \tag{15a}$$

$$Q = \frac{\rho A\omega^2 L^4}{EI} = \text{nondimensional frequency} \tag{15b}$$

The nondimensional parameter Y in the above equation is related to the mode shape as follows:

$$Y(X) = \sum_n \Phi_n(X) \tag{16}$$

where $\Phi_n(X)$ = nth natural mode of the cable in terms of nondimensional parameter X.

Equation (14) has been solved previously by Chi [33] for the most general case of elastically constrained end conditions. In Appendix A of this report, the detailed derivation of frequency equation and the solution of equation (14) are given. For the purpose of computing natural frequencies, we shall, however, make use of the relationship between the nondimensional force, P, and another nondimensional quantity denoted by Z^2. The latter is actually a function of P and Q ($Z^2 = 4Q/P^2$) defined earlier; however, it has been found that the use of nondimensional parameter Z^2 instead of Q simplifies the formulation of deflection and bending stress considerably. For this reason, in the subsequent nondimensional analysis, we shall consistently use P and Z^2 being the two most important nondimensional parameters.

The relationship between P and Z^2 is obtained from the frequency equation of small amplitude, free, transverse, vibration of a cable. The analytical method is outlined in detail in Appendix A. In this section, a graphical representation of the relationship between P and Z^2 is shown in Figures 10 through 14 for certain practical ranges of such parameters as the cable size, cable length, axial tension, etc. The ranges are given below:

Cable size: 1 layer cable - 7 wires (smallest section)
15 layer cable - 631 wires (largest section)

Wire radius: 0.125 inch (0.318 cm)

Cable length: $50 \leq L \leq 600$ [ft]
$15.2 \leq L \leq 182.9$ [m]

Axial tension: $60 < \sigma < 120$ [ksi]

$413.7 < \sigma < 827.4$ [MPa]

It should be noted that Figures 10 through 14 correspond to the cable configuration with both ends fixed. This particular end condition adequately represents the dynamics of cable in a cable-stayed bridge. The figures also correspond to the first 45 natural modes of vibration. The computation of natural frequencies for this somewhat high mode value is essential since flexible slender structures are also often known to vibrate in resonance at higher modes.

Substituting the values of P and Q from equations (15a) and (15b) in the expression for Z^2, it is seen that:

$$Z^2 = \frac{4Q}{P^2} = \frac{4\rho\omega^2 EI}{\sigma^2 A} \tag{17}$$

From the knowledge of axial tension, cable length, elastic modulus, and moment of inertia, one can determine the nondimensional force, P. The nondimensional parameter, Z^2 can then be determined from the graphs in Figures 10 through 14. It is further seen from the expression for Z^2 that the natural frequency, ω, is given by:

$$\omega = \sqrt{\frac{\sigma^2 A}{4\rho EI}}\, Z = \omega_{fb} Z \tag{18}$$

where ω_{fb} is defined as a bending frequency factor given by:

$$\omega_{fb} = \sqrt{\frac{\sigma^2 A}{4\rho EI}} \tag{19}$$

For a cable of given length, diameter, and tension, the bending frequency factor is a constant, and can be easily computed. The natural frequency, ω_n, of any mode n can therefore be found from equation (18) by substituting proper values of Z from the graphs. The use of graphs and the computation of natural frequencies will be illustrated for specific numerical examples in Chapter 5 of this report.

The normal modes Φ_n (X) are determined from the solution of equation (14) upon substitution of the relationship shown in equation (16). The general form

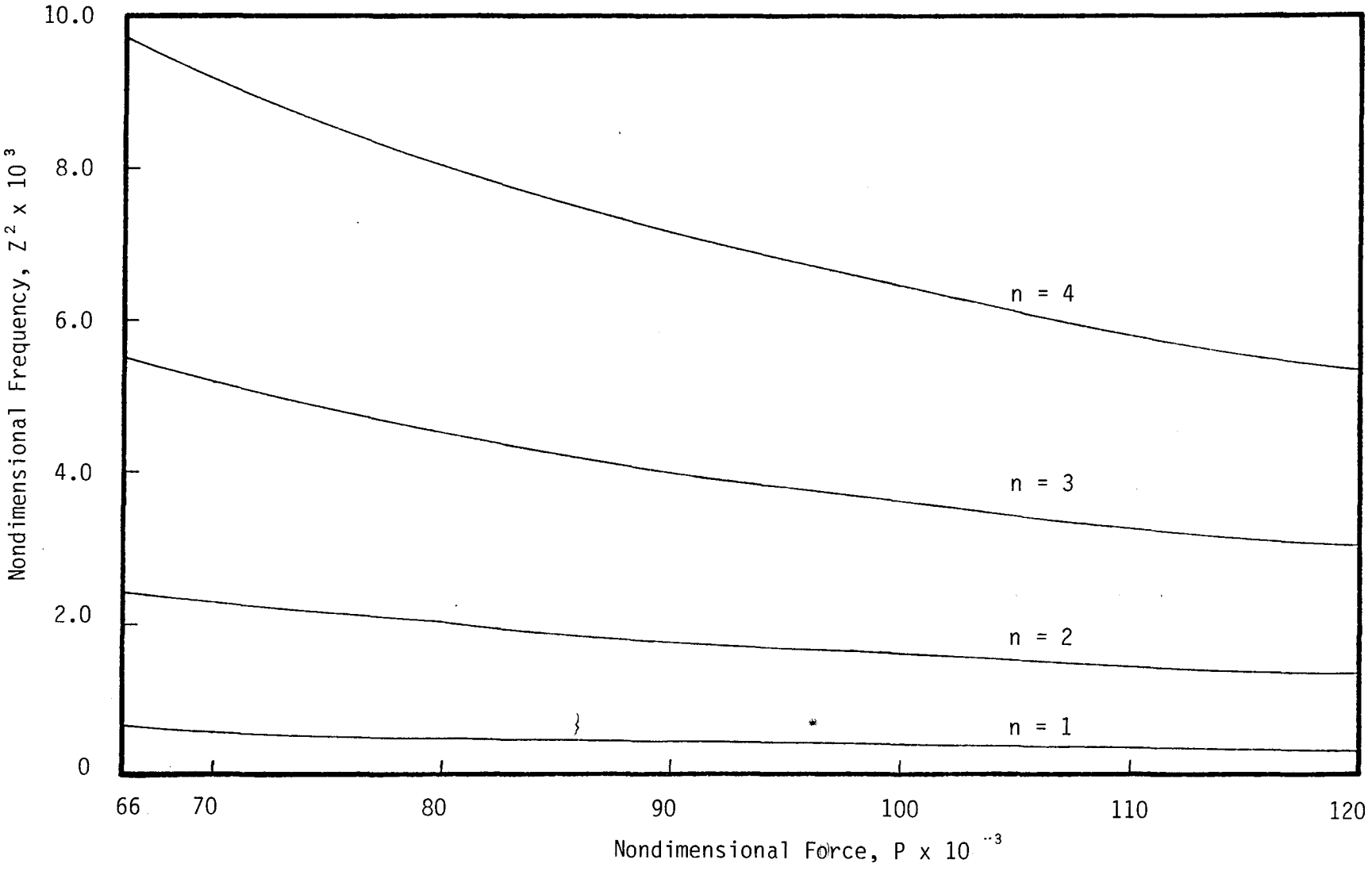

Figure 10. Nondimensinoal Frequency vs. Nondimensional Force

(Symmetric Cable with Fixed Ends)

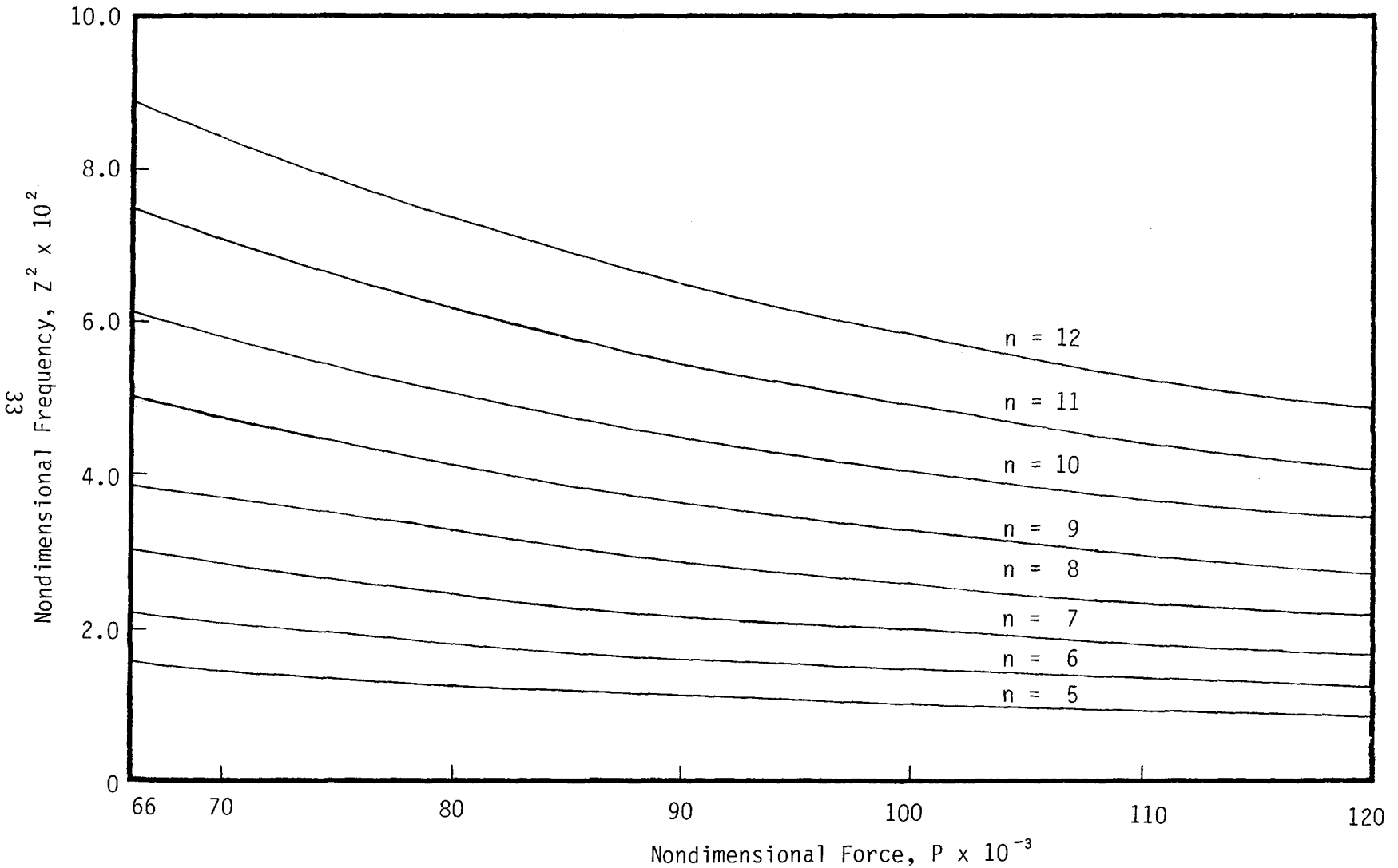

Figure 11. Nondimensional Frequency vs. Nondimensional Force

(Symmetric Cable with Fixed Ends)

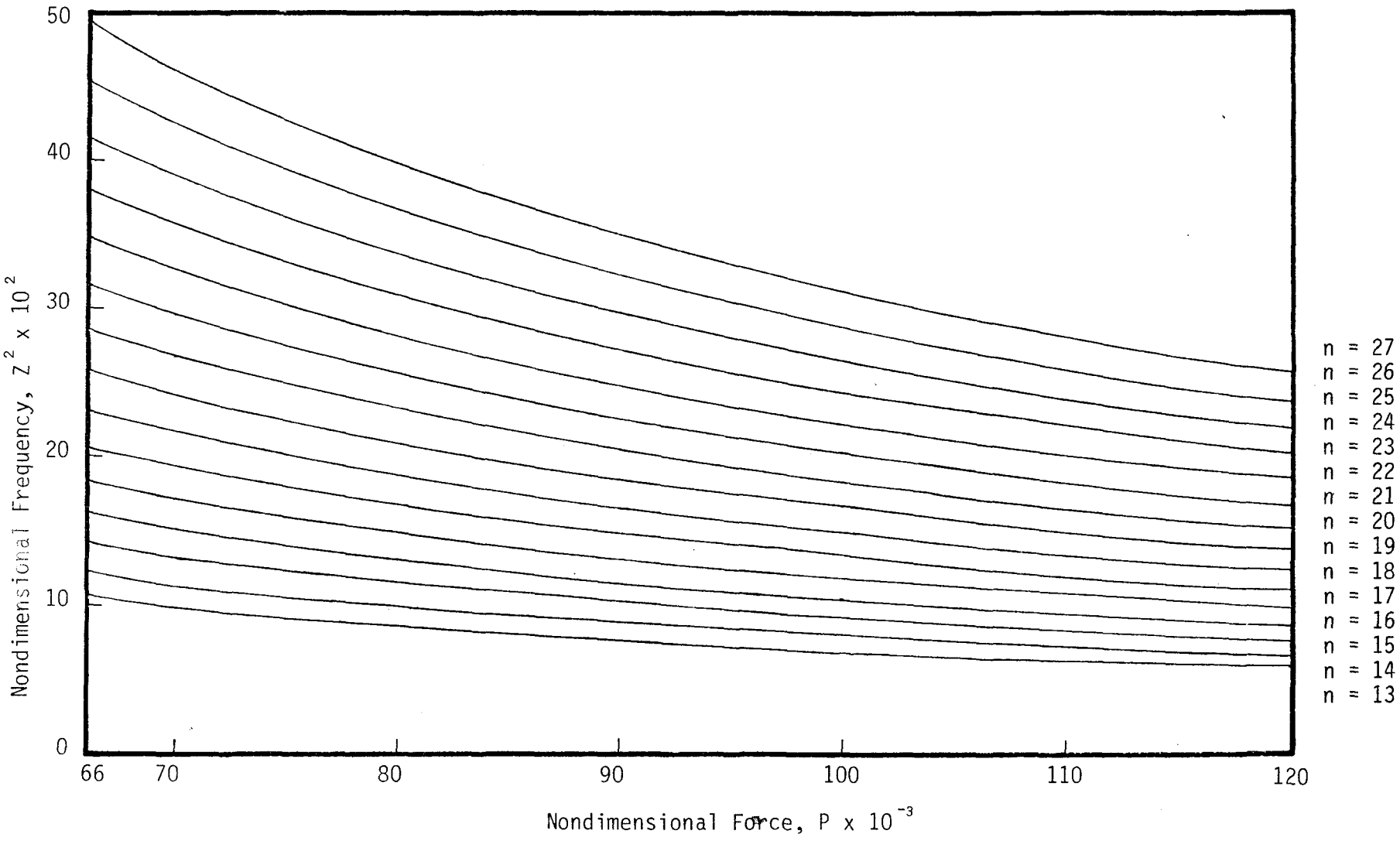

Figure 12. Nondimensional Frequency vs. Nondimensional Force
(Symmetric Cable with Fixed Ends)

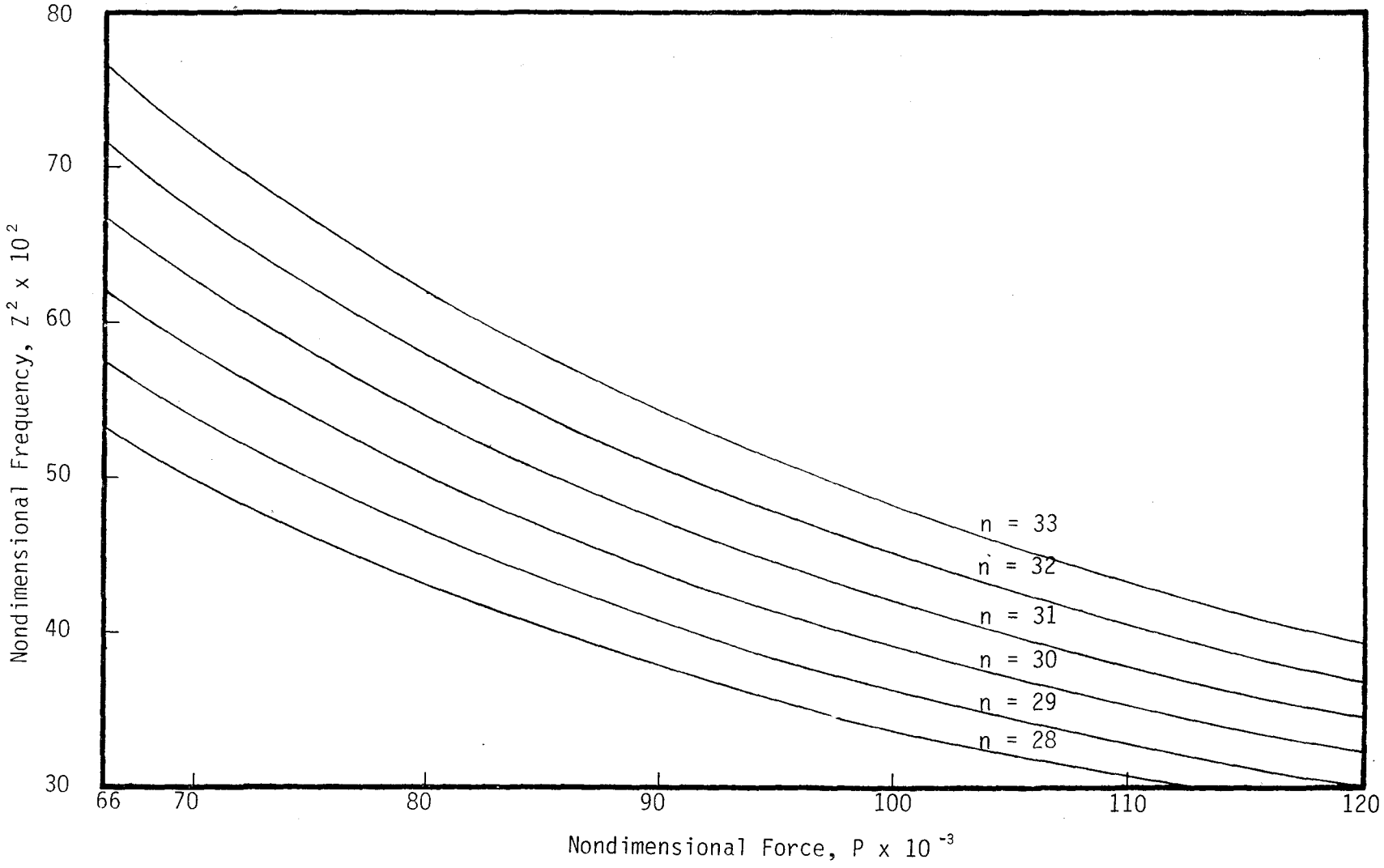

Figure 13. Nondimensional Frequency vs. Nondimensional Force

(Symmetric Cable with Fixed Ends)

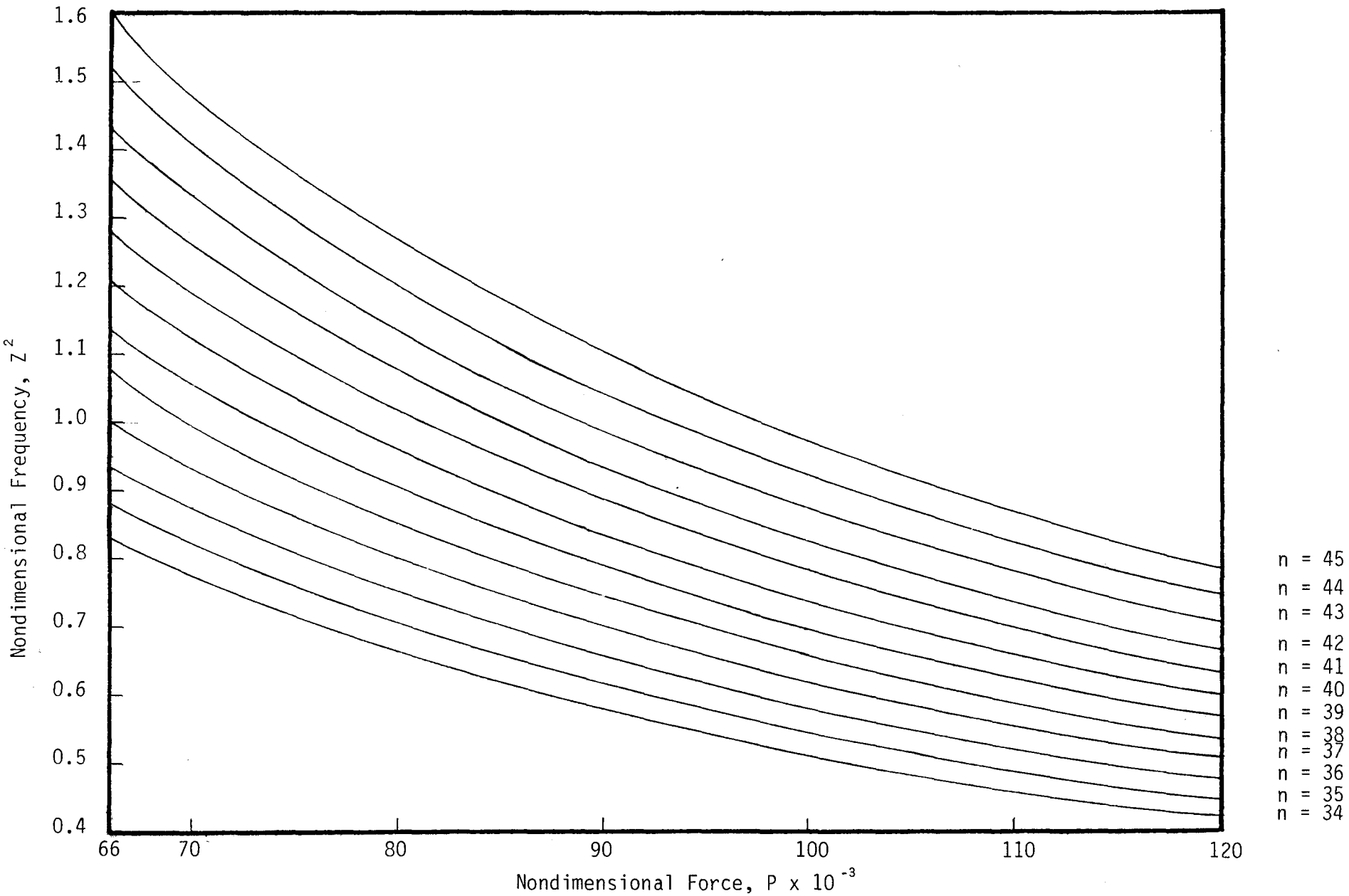

Figure 14. Nondimensional Frequency vs. Nondimensional Force (Symmetric Cable with Fixed Ends)

of the solution is given by:

$$\Phi_n(X) = A_n \sin\alpha_n X + B_n \cos\alpha_n X + C_n \sinh\beta_n X + D_n \cosh\beta_n X \tag{20}$$

where A_n, B_n, C_n, D_n are constants to be determined from the given boundary conditions and where α_n, β_n, are the roots of the frequency equation. The derivation of the expression for normal mode is discussed in detail in Appendix A.

We mention here that a long slender flexible cable with both ends fixed has a response which is very similar to that of a string. This is also evident from the fact that the root, β_n, of the frequency equation in Appendix A is large (usually > 10) for long cables. Under this circumstance, the mode shape expression in equation (20) reduces to the following form:

$$\Phi_n(X) = \sin\alpha_n X - \frac{\alpha_n}{\beta_n} \cos\alpha_n X \tag{21}$$

It is now easy to determine the mode shape from the above equation. As an example, we have computed the mode shapes of a Group IV Pasco-Kennewick bridge cable up to 10 modes for two different values of axial tension. The results are shown in Figures 15 and 16.

4.2 Wind-Induced Vibration of Stay Cables

Having obtained the natural frequencies and mode shapes of small amplitude, free, transverse vibration of a stay cable, we now proceed to analyze the wind-induced vibration of the cable as a forced vibration problem. It was earlier assumed in Section 2.2.2 that wind force is spatially independent and harmonic in nature. Further, it was assumed in Section 3.2.2 that the structural damping, c, is proportional to the mass per unit length of the cable. Under these two assumptions, equation (10) can be solved to determine the response of the cable to wind loading. The detailed solution is given in Appendix A. In this section, we shall discuss the physical basis of the analytical derivation presented in Appendix A, as well as the results obtained therein in relation to the vortex-induced vibration of stay cables.

In Section 2.2.1 of Chapter 2 dealing with the vortex shedding mechanism

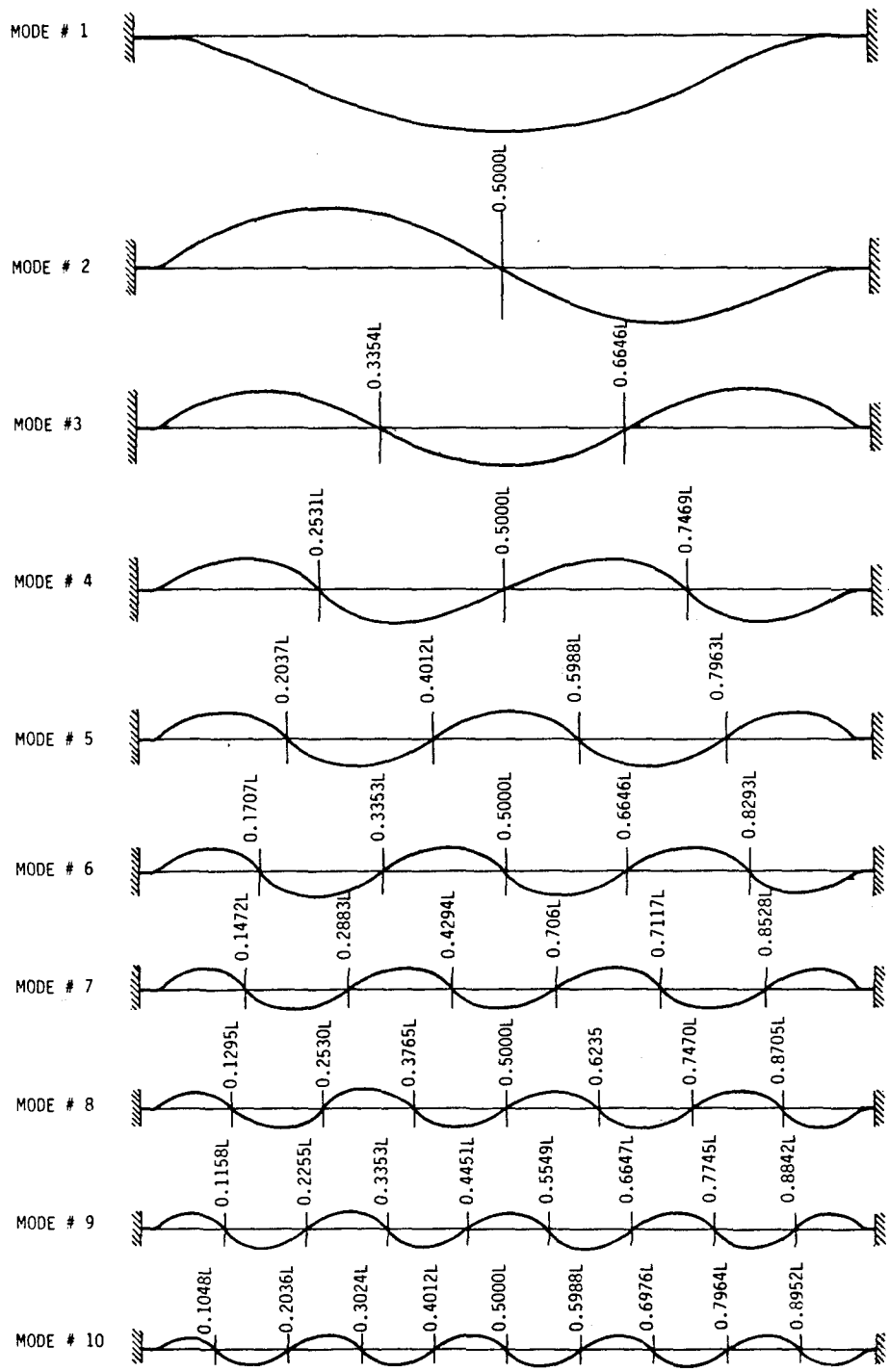

Figure 15. Pasco-Kennewick Bridge - Group IV Cable Mode Shapes (F = 400 kips)

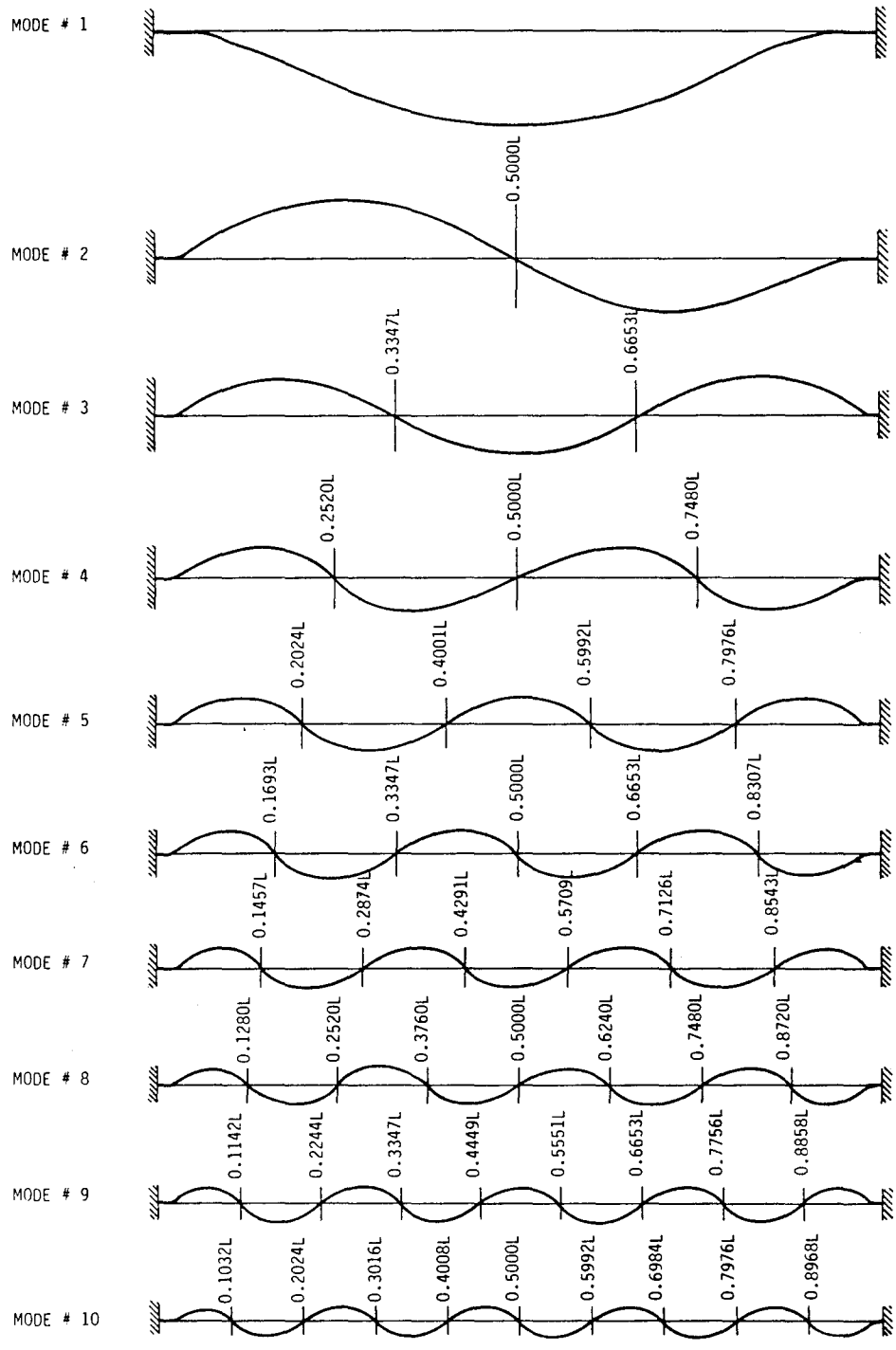

Figure 16. Pasco-Kennewick Bridge - Group I Cables Mode Shapes (F = 1000 kips)

of circular cylinders, we have given an expression for the Strouhal relation, namely,

$$f_s = \frac{St \cdot V}{d} \tag{22}$$

where f_s is the Strouhal frequency. This relationship can be used to determine f_s if the wind velocity, V, is known. Conversely, if one assumes that f_s is known from the vortex-induced resonance condition (for example, $f_n < f_s < 1.4\ f_n$ for resonance), one can find the critical wind velocity, V_{cr}, simply by transposing the equation (22) in the following form:

$$V_{cr} = \frac{f_n \cdot d}{St} = \frac{\omega_n d}{2\pi St} \tag{23}$$

where, for simplicity, f_s has been equated to the natural frequency f_n.

The rationale for the above type argument is based on the consideration that we are addressing the subject of wind-induced vibration of stay cables caused only by the vortex shedding phenomenon. Recalling now the expression for the wind force model given by equation (1), it is seen that:

$$F(t) = F_o \cos\omega_s t = \frac{1}{2}\rho d V_{cr}^2 C_L \cos\omega_s t \tag{24}$$

in which the magnitude of wind force, F_o, can be determined from the knowledge of V_{cr} and the lift coefficient, C_L. The governing differential equation of cable vibration (equation (10)) can now be solved with the above assumptions and the most general solution is given as:

$$y(x,t) = F_o \sum_n \phi_n(x)\ [G_{1n} \sin\omega_s t + G_{2n} \cos\omega_s t] \tag{25}$$

where G_{1n} and G_{2n} are the coefficients of a particular temporal solution of equation (10) and where $\phi_n(x)$, as before, denotes the mode shape. The detail derivation of the solution, as well as the derivation of expressions for G_{1n} and G_{2n} are given in Appendix A.

4.2.1 Deflections of cables:

The most general expression for the deflection of a cable with fixed ends is given by equation (25) above. The expression contains a number of variables all of which are functions of some basic parameters such as the geometrical and structural properties of a cable, the applied tension, and the wind velocity Therefore, it is reasonable to perform a parametric study of the deflection.

On the other hand, the number of parameters is too large to deal with for a meaningful parametric study. The compromise lies in grouping the parameters in some nondimensional forms. We have already shown in Section 4.1 of this chapter how various parameters are grouped together in two nondimensional quantities, P and Z^2, and how the relationship between these two quantities are used to determine the natural frequencies of a cable. In what follows, we shall consider such an approach to determine the deflection. In particular, we shall determine a relationship between the maximum nondimensional deflection and the nondimensional frequency. It should be noted that this is an alternative to the analysis cited in Section 2.2.2 in connection with the analytical models of vortex excitation of circular cylinder.

Equation (25) can be greatly simplified in practical applications, due to the following considerations. At least in subcritical flow regime, there is only one dominating driving frequency in the wake. This frequency would principally excite a single natural mode closest to it, according to the synchronization theory of nonlinear resonance. Suppose that the frequency associated with the resonant mode be ω_n then the deflection expression, (equation (25)), is simplified to:

$$y(x,t) = F_o \, \phi_n(x) \, [G_{1n} \sin \omega_n t + G_{2n} \cos \omega_n t] \tag{26}$$

It should be noted that G_{2n} vanishes at resonant conditions. In order to obtain the maximum deflection, we assume that the mode shape, $\phi_n(x)$, is normalized. Hence,

$$y_{max} = F_o \, G_{1n} \tag{27}$$

since the maximum values of $\phi_n(x)$ and $\sin \omega_n t$ are both one.

It is seen that the maximum deflection is simply the product of the magnitude of wind force, F_o, and the coefficient, G_{1n}, whose expression is given in Appendix A. The evaluation of G_{1n}, however, is fairly involved since the expression contains generalized mass, generalized force vector, lift coefficient, damping coefficient, and others. While the detailed analysis is given in Appendix A, we find it convenient at this point to define a nondimensional maximum deflection, Y_n, as follows:

$$Y_n = \frac{\sqrt{\sigma} \; \sqrt{\sigma} \, \delta A}{\rho_a \; V d^2 L} \quad y_{max}$$

where ρ_a denotes the density of air. All other symbols in the above expression are defined elsewhere in the text. As shown in Appendix A, the nondimensional deflection, Y_n, in the above form can be expressed as a function of the nondimensional parameter, Z^2. This relationship is shown in graphical form in Figures 17 and 18 for various values of nondimensional force, P.

4.2.2 Bending Stress:

The bending stress at any point in a cable is related to its curvature at that point. The general expression for the curvature is obtained by differentiating equation (25) with respect to x and this gives:

$$y''(x,t) = F_o \sum_n \phi_n''(x) \; [G_{1n}\sin\omega_n t + G_{2n}\cos\omega_n t] \tag{29}$$

where y" and ϕ_n'' denote the second derivatives with regard to x of y(x,t) and $\phi_n(x)$, respectively. Once again, a progressive simplification similar to the one described for deflection analysis will lead to:

$$y''(x,t) = F_o\phi_n''(x)G_{1n}\sin\omega_n t$$

The maximum curvature at end-fixity is now obtained by evaluating $\phi_n''(x)$ at x=0 and by equating $\sin\omega_n t$ to 1. This gives:

$$y''_{max} = F_o G_{1n} \frac{\alpha_n}{\beta_n} (\alpha_n^2 + \beta_n^2) \tag{31}$$

where α and β are, as before, the roots of the frequency equation. The detailed derivations of the above expression is given in Appendix II.

Defining a nondimensional maximum curvature by

$$\chi_n = \frac{\sqrt{\rho}\, EI\delta}{\rho_a V d^2 \sqrt{\sigma}\, L} \; y''_{max} \tag{32}$$

One can compute χ_n in terms of the nondimensional parameter, Z^2, in a similar manner to that shown in the previous section. The detail derivation of the above relationship is given in Appendix A. The relationship between χ_n and Z^2 is shown graphically in Figures 19 through 21 for the purpose of evaluating bending stress. The maximum value of the latter can be evaluated by means of the following equation:

$$(\sigma_b)_{max} = E c_z y''_{max} \tag{33}$$

where c_z is the maximum fiber distance in the cable.

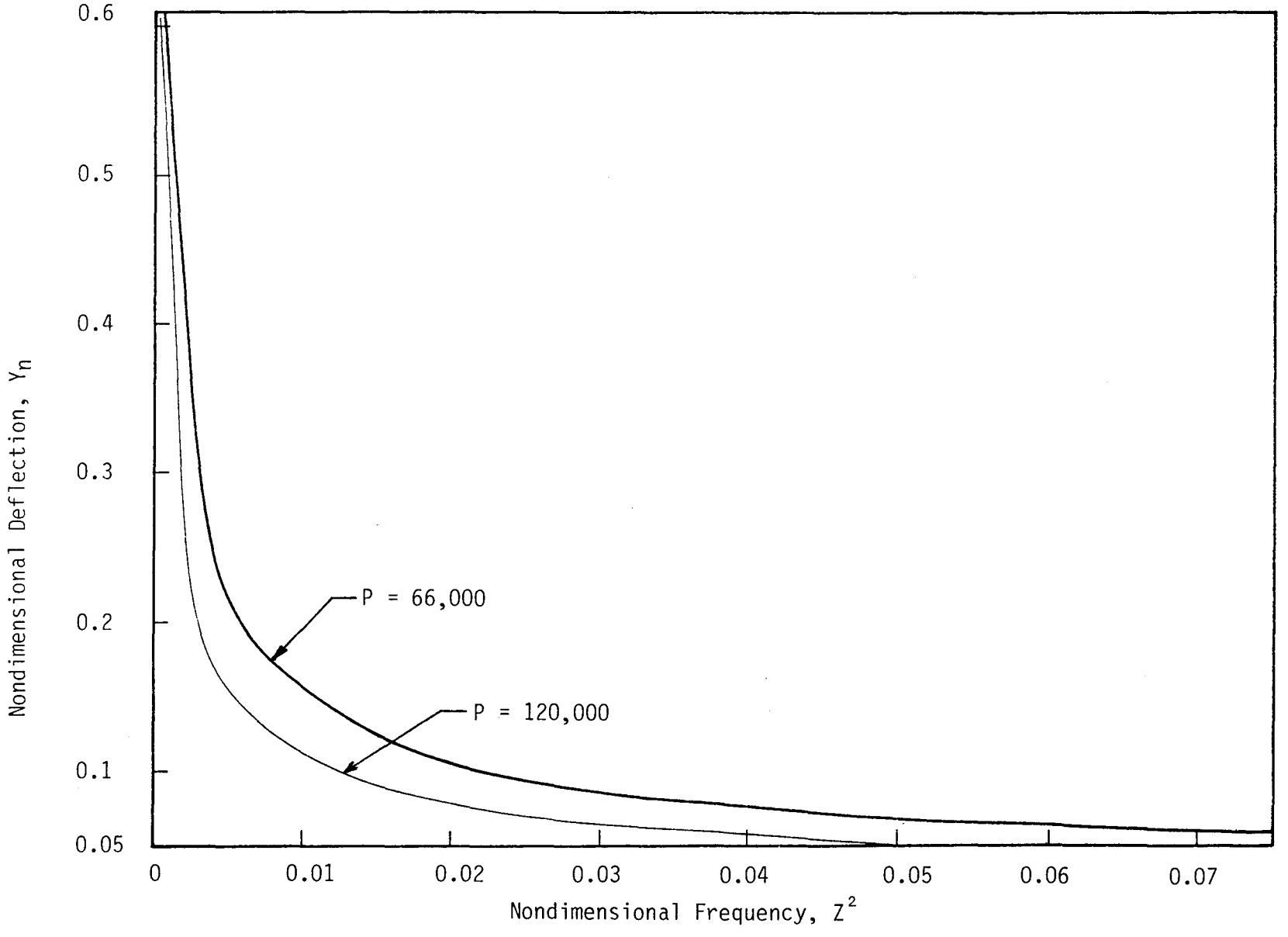

Figure 17. Nondimensional Deflection of Stay Cables

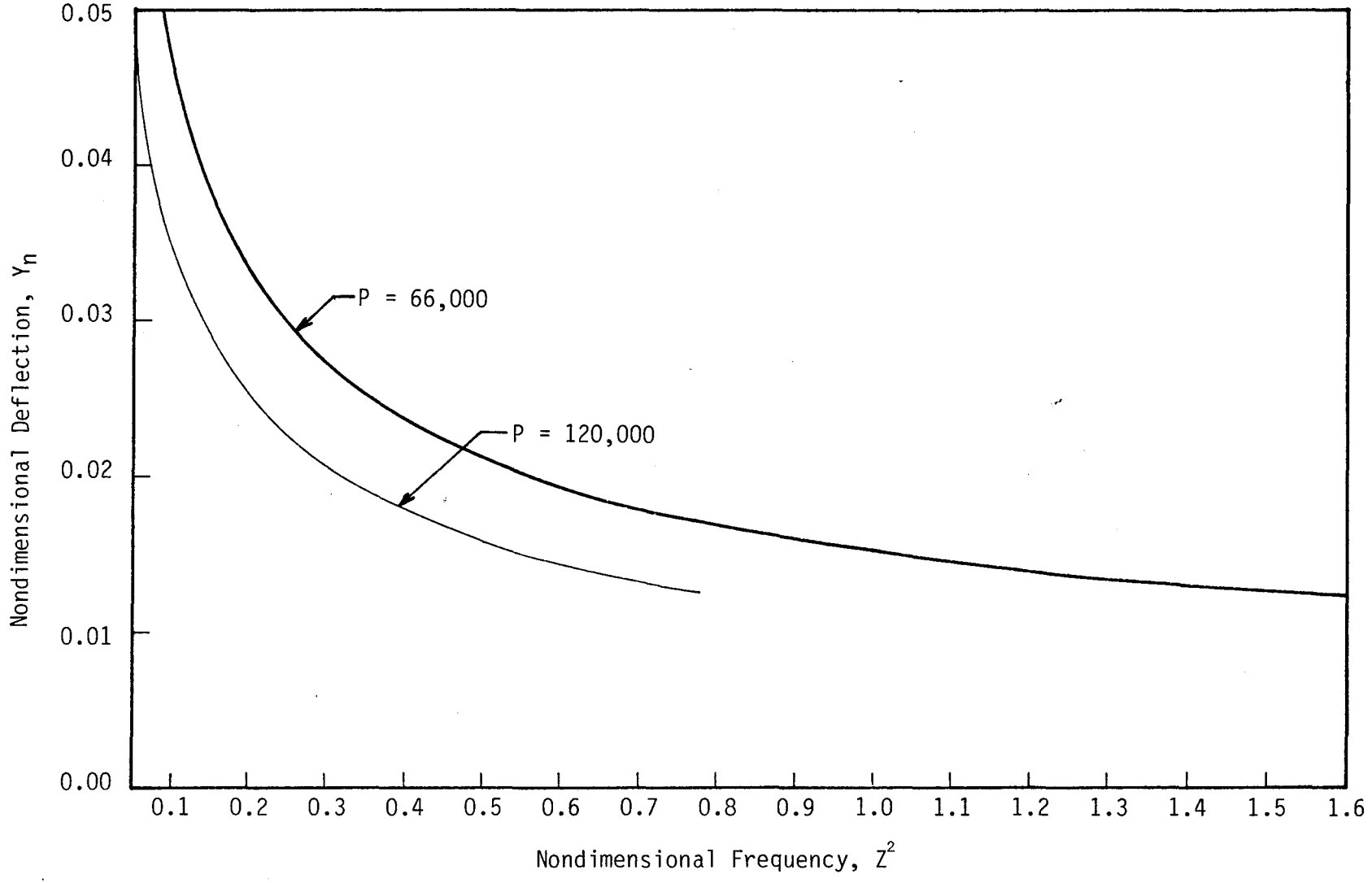

Figure 18. Nondimensional Deflection of Stay Cables

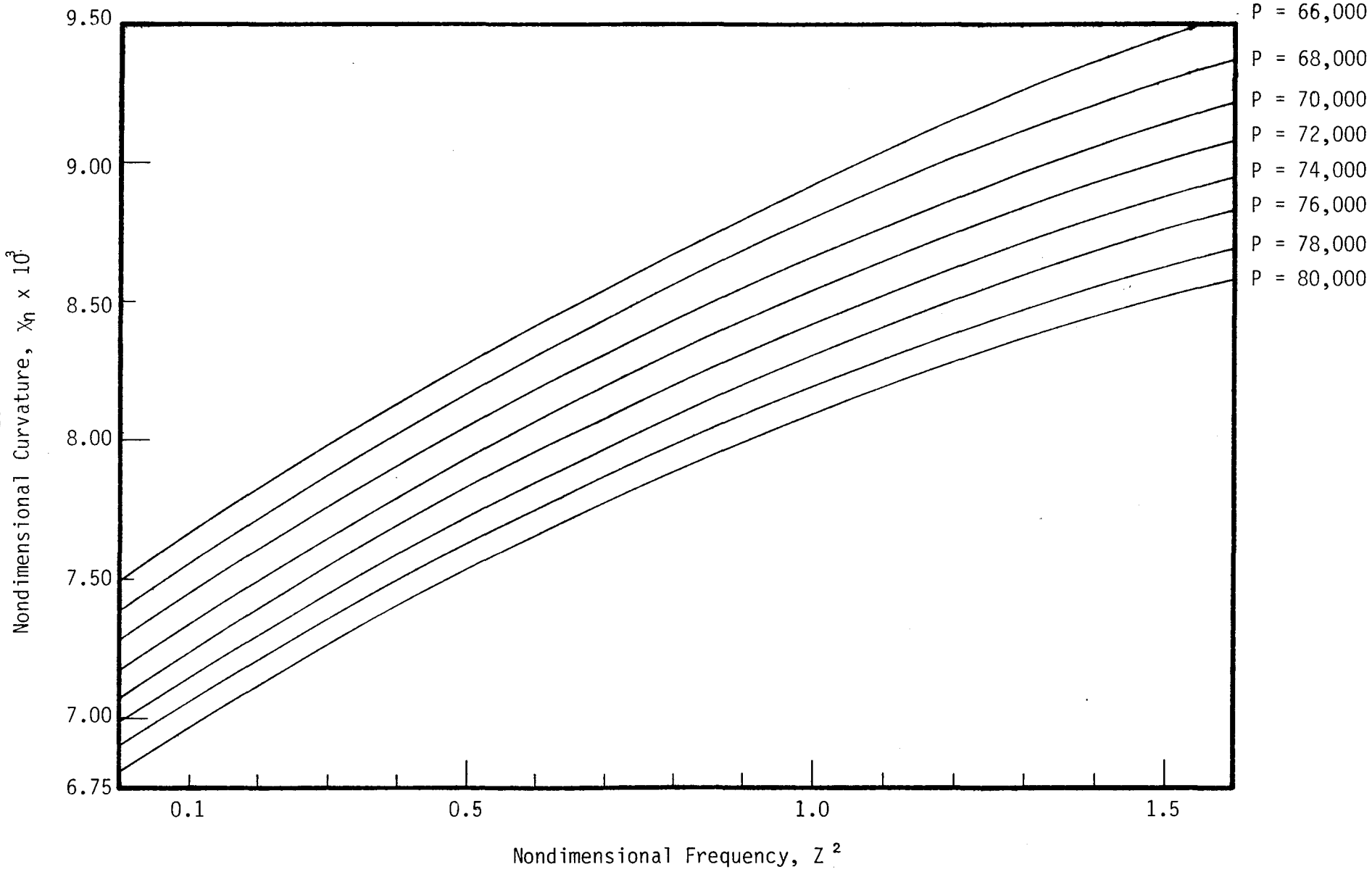

Figure 19. Nondimensional Curvature of Stay Cables

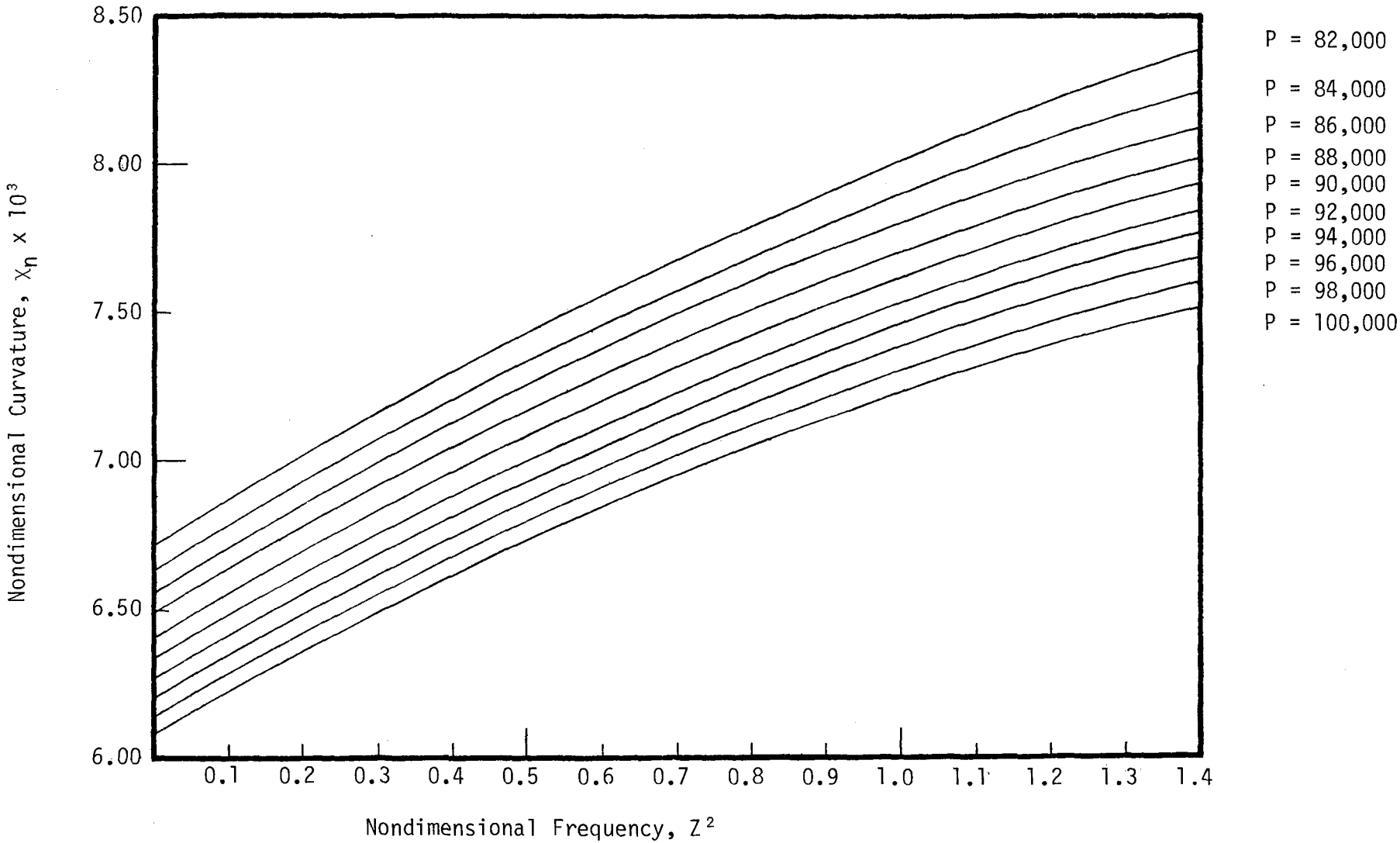

Figure 20. Nondimensional Curvature of Stay Cables

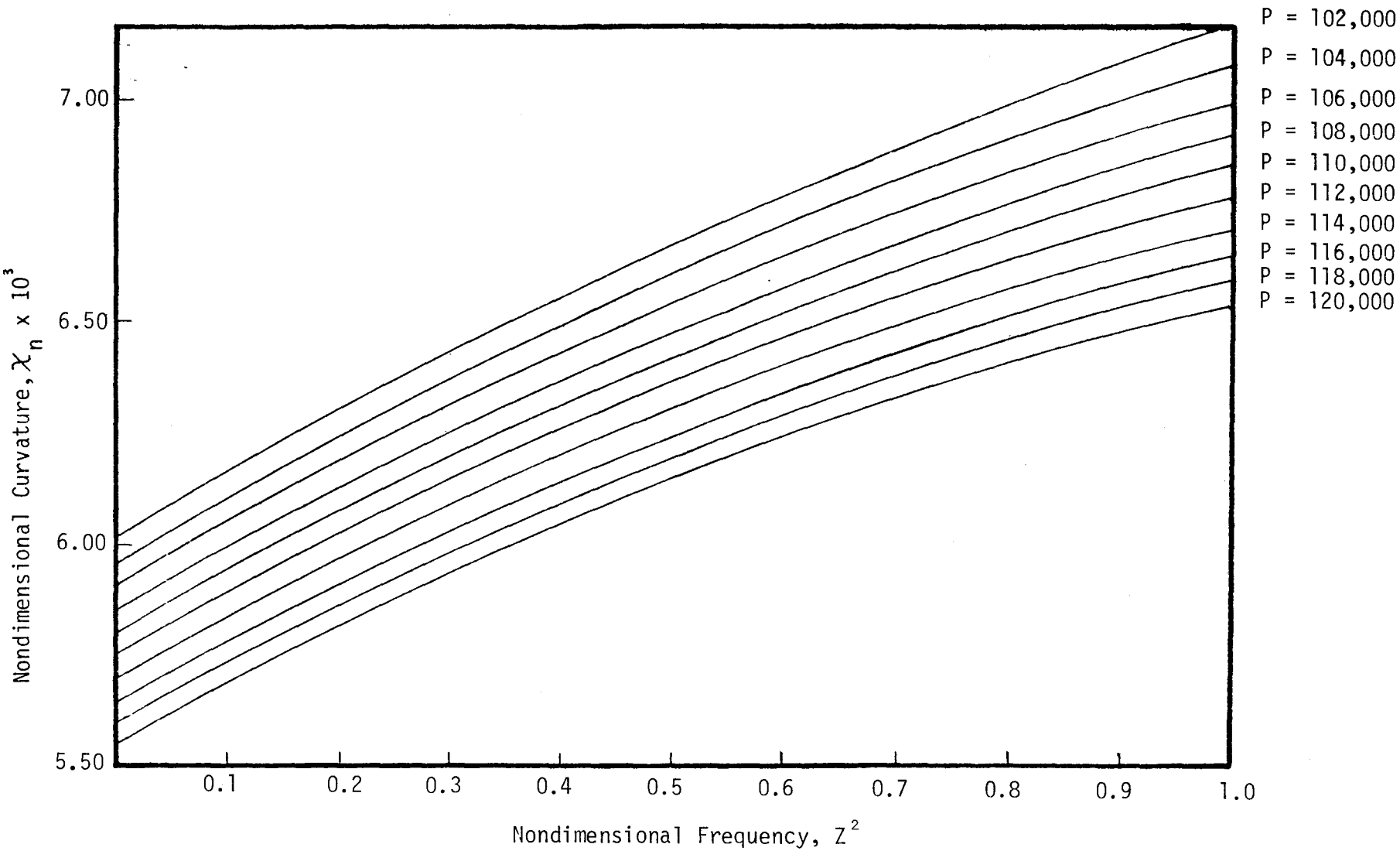

Figure 21. Nondimensional Curvature of Stay Cables

It should be noted in passing that in the derivation of relationships between Y_n and Z^2, and between χ_n and Z^2, the values of Strouhal number, St, and lift coefficient, C_L, are assumed to be 1.2 and 1.4, respectively. These two parameters appear explicitly in the expressions for Y_n and χ_n as shown in Appendix A. We also mention in passing that the dynamic analysis of stay cables developed in this chapter will be illustrated in detail in Chapter 5 of the report.

CHAPTER 5

NUMERICAL RESULTS OF DYNAMIC ANALYSIS

In Chapter 4, expressions for natural frequencies, maximum nondimensional deflections, and curvatures have been derived for stay cables in general. Further, the graphical relationships between these quantities and the nondimensional parameters P and Q have been developed in Chapter 4.
In this chapter, we will demonstrate the use of results derived in the previous two chapters for specific bridge cables. To this end, the following bridge cables have been chosen for further studies:

1. Pasco-Kennewick Bridge Group I and Group IV cables;
2. Luling Bridge Group I and Group IV cables.

Some of the geometrical properties of these cables are shown in Table 3. The cross-sectional areas of the cables have been computed on the basis of information on wire diameter, number of wires, and number of layers. Outer diameters of cables indicated in the Table correspond to those of polyethylene pipes which are jacketed on the cables. The minimum and maximum moment of inertia of these cables are shown; the minimum value corresponds to the case in which all wires are considered separately, and the maximum value corresponds to the case in which all wires are grouped or "welded" together to form one unit. Table 3 also indicates two different levels of applied tension and corresponding values of axial force to four different cable diameters.

The exact natural frequencies of these cables have been calculated by using both beam vibration and string vibration theories. For reference purposes, the results are shown in Appendix B. For long (Group I) cables, frequencies are given up to the 30th mode. For short (Group IV) cables frequencies are given up to the 20th mode. The reason for this is that the nominal wind velocities corresponding to the higher frequencies of short cables are outside the range of design interest for this study. The frequency values corresponding to the beam theory have been calculated using a value of $E = 29 \times 10^6$ psi (200×10^3 MPa) and using a maximum value of the moment of inertia, while those corresponding to the string theory have been calculated by neglecting the stiffness.

Table 3. Properties of Cables Used in Examples

Cable		No. Wires	No. Layers	Length (ft) (m)	Diam. of a Wire (in) (cm)	Area (in^2) (cm^2)	Outer Diam. Cable (in) (cm)	Min. I (in^4) (cm^4)	Max. I (in^4) (cm^4)	Axial force at 59 ksi (K) (MN)	Axial force at 108 ksi (K) (MN)
Pasco-Kennewick Bridge	Group I	283	10	506 (154.23)	0.25 (0.63)	13.89 (89.61)	6 (15.24)	0.054 (2.25)	20.53 (854.52)	820 (2.65)	1500 (6.67)
	Group IV	73	6	180 (54.86)	0.25 (0.63)	4.76 (30.71)	4 (10.16)	0.019 (0.79)	2.42 (100.73)	280 (1.25)	520 (2.31)
Luling Bridge	Group I	307	10	580 (176.78)	0.25 (0.63)	15.07 (97.23)	6 (15.24)	0.059 (2.46)	24.22 (1008.11)	890 (3.96)	1650 (7.34)
	Group IV	108	6	200 (60.96)	0.25 (0.63)	5.30 (34.19)	4 (10.16)	0.021 (0.87)	3.03 (126.12)	315 (1.40)	580 (2.58)

Example 1

In this example, we are going to compute the natural frequencies of a Pasco-Kennewick Group I cable using the graphs and formulas developed in Chapter 4. The geometrical and mechanical properties of the cable are:

$$L = 506 \text{ ft. } (154.23 \text{ m})$$
$$O.D. = 6 \text{ in. } (15.24 \text{ cm})$$
$$A = 13.89 \text{ in.}^2 \ (89.61 \text{ cm}^2)$$
$$I_{max} = 20.53 \text{ in.}^4 \ (854.52 \text{ cm}^4)$$
$$E = 29\text{x}10^6 \text{psi } (200\text{x}10^3 \text{ MPa})$$
$$\rho = 0.000734 \ \frac{\text{lb-sec}^2}{\text{in.}^4} \ (7.85 \text{ gm/cm}^3)$$

The cable is subjected to a tensile stress of 108 ksi (744.66 MPa).

Step 1

In this step, the nondimensional force, P, is computed using given data and using equation (15a). Thus,

$$P = \frac{(\sigma_x A)L^2}{EI} = \frac{108\text{x}10^3\text{x}13.89\text{x}(506\text{x}12)^2}{29\text{x}10^6\text{x}20.53}$$
$$\cong 92{,}895$$

The nondimensional parameter, Z^2, is determined next using Figure 10. For the first four modes of vibration, the values of Z^2 are given below:

$$Z_1^2 = 0.464\text{x}10^{-3} \qquad \text{for } n = 1$$
$$Z_2^2 = 1.680\text{x}10^{-3} \qquad n = 2$$
$$Z_3^2 = 3.920\text{x}10^{-3} \qquad n = 3$$
$$Z_4^2 = 7.040\text{x}10^{-3} \qquad n = 4$$

Step 2

In this step, the bending frequency factor, ω_{fb}, defined in equation (19) is computed. Thus,

$$\omega_{fb} = \sqrt{\frac{\sigma^2 A}{4\rho EI}}$$

$$= \sqrt{\frac{(108\text{x}10^3)^2 \text{x}13.89}{4\text{x}0.000734\text{x}29\text{x}10^6\text{x}20.53}} \quad \text{rad/sec.}$$

$$\simeq \quad 304.44 \text{ rad/sec.}$$

The circular natural frequencies of the first four modes of vibration are now computed using equation (18). Thus,

$$\omega_1 = \omega_{fb} \cdot Z_1 = 304.44 \text{ x } \sqrt{0.464\text{x}10^{-3}} \quad \text{rad/sec.}$$
$$\simeq 6.5578 \text{ rad/sec.}$$

and similarly,

$$\omega_2 = 12.4783 \quad \text{rad/sec.}$$

$$\omega_3 = 19.0608 \quad \text{rad/sec.}$$

$$\omega_4 = 25.5438 \quad \text{rad/sec.}$$

When these values are compared with the exact values (Appendix B) in the following Table, one can see that the largest error in the computation of frequencies using graphs is about 4%, and that this error corresponds to the fundamental mode. For higher modes, the error is often much less (e.g., for third mode, the error is 0.5%).

Table 4. Comparison of Natural Frequencies

Mode No.	Natural Frequency (rad/sec.) Exact Solution	From Graph	Error %
1	6.3180	6.5578	3.8
2	12.6380	12.4783	1.3
3	18.9621	19.0608	0.5
4	25.2917	25.5438	1.0

It should be noted that for the number of even modes the error percentage is usually slightly higher than it is for the odd number of modes. For all practical purposes, the computation of frequencies by means of graphs gives fairly accurate estimates.

Example 2

This example will demonstrate the use of nondimensional maximum deflection and maximum curvature curves as developed in Chapter 4. The cable is the same as in Example 1. In addition to the parameters provided in Example 1, the following are assumed.

$$\rho_a = 1.123\times10^{-7} \quad \frac{\text{lb-sec}^2}{\text{in}^4} \quad (1.201\times10^{-3}\text{gm/cm}^3)$$

$$\delta = 0.08$$

$$St = 0.2$$

$$C_L = 1.2$$

Step 1

In this step, we shall compute the critical wind velocities that will put the cable in resonance in various modes. Thus, using equation (23), we find, for the first mode:

$$V_{cr} = \frac{\omega_1 d}{2\pi St} = \frac{6.5578\times6}{2\pi\times0.2} \simeq 30.17 \text{ in./sec.}$$

$$= 1.71 \text{ mph } [2.74 \text{ km/hr}]$$

Similarly, for the second, third, and fourth modes, the critical wind velocities for resonance are:

$$V_{cr} = 3.38 \text{ mph } [5.41 \text{ km/hr}] \quad \text{for } n = 2$$

$$= 5.17 \text{ mph } [8.27 \text{ km/hr}] \quad n = 3$$

$$= 6.93 \text{ mph } [11.09 \text{ km/hr}] \quad n = 4$$

The result indicates that the critical wind velocities corresponding to the fundamental and lower mode resonance are relatively small. While the prevailing wind velocity at a particular site of "cabled" structure may conceivably be as low as 7 mph [11.2 km/hr], it is equally probable that higher wind velocities may prevail. In this case, higher modes will be in resonance. For this reason, we have decided to compute a few more higher modes.

For example, consider the 15th, 29th, and 43rd modes. The frequencies of these modes as computed according to the steps given in Example 1 are:

$$\omega_{15} = 96.2724 \text{ rad/sec.}$$
$$\omega_{29} = 190.1227 \text{ rad/sec.}$$
$$\omega_{43} = 296.7314 \text{ rad/sec.}$$

The corresponding values of critical wind velocity are:

$$V_{cr} = 26.12 \text{ mph } [41.79 \text{ km/hr}] \quad \text{for } n = 15$$
$$= 51.58 \text{ mph } [82.52 \text{ km/hr}] \quad n = 29$$
$$= 80.50 \text{ mph } [128.80 \text{ km/hr}] \quad n = 43$$

It seems that 26 mph [41.6 km/hr] wind velocity is likely to occur in a particular site and therefore, the cable in this example is likely to resonate in 15th mode. For this case, it will be necessary to determine the deflection and bending stress corresponding to this mode.

Step 2

In this step, we will compute the amplitude of forcing function using equation (1). Thus,

$$F_o = \frac{1}{2}\rho_a d C_L V_{cr}^2$$
$$= \frac{1}{2}(1.123\text{x}10^{-7})\text{x}6\text{x}1.2V_{cr}^2$$
$$= 4.0428\text{x}10^{-7}V_{cr}^2$$

This is, of course, the magnitude of forcing function per unit length of the cable and hence, has the unit of lb/ft (N/m). Knowing the V_{cr} for different modes, it is now possible to find F_o which would cause the cable to vibrate in particular modes. We now compute F_o for the modes shown above.

$$F_o = 4.0428\text{x}10^{-7}\ V_{cr}^2$$
$$= 0.00037 \text{ lb/in.} = 0.00442 \text{ lb/ft } [0.0648 \text{ N/m}]$$
$$\text{for } n = 1$$

and similarly,

$$F_o = 0.01717 \text{ lb/ft } [0.2505 \text{ N/m}] \quad \text{for } n = 2$$
$$= 0.04017 \text{ lb/ft } [0.5862 \text{ N/m}] \quad n = 3$$
$$= 0.07217 \text{ lb/ft } [1.0532 \text{ N/m}] \quad n = 4$$
$$= 1.02526 \text{ lb/ft } [14.9618 \text{ N/m}] \quad n = 15$$

$= 3.99808$ lb/ft [58.3447 N/m] $\quad n = 29$

$= 9.73824$ lb/ft [142.1119 N/m] $\quad n = 43$

If the resonance mode of a cable, (for instance, the 15th mode) in a particular structure and at a particular site is known, the above computation will give the magnitude of the forcing function that needs to be used in the calculation of the maximum deflection and bending stress. Alternatively, if the nominal wind velocity at a particular site is known, the magnitude of the forcing function can be computed by substituting for V_{cr} in the expression for F_0, the value of the wind velocity. In a similar manner, using the Strouhal relation and the value of nominal wind velocity, the resonant frequency, and hence, the mode number can be determined. This information is then utilized to evaluate the maximum deflection and bending stress. The methods of computation are shown in Steps 3 and 4 below.

Step 3

In this step, the maximum nondimensional deflection will be computed by using graphs in Figures 17 and 18. For example, consider the first mode for which $Z^2 = 0.464 \times 10^{-3}$. We also know that the nondimensional force P is 92,895. Corresponding to these two values, the maximum nondimensional deflection can be read from Figure 17, and the value is approximately 0.569. Note that in Figure 17, there are only two graphs which correspond to P = 66,000 and P = 120,000. For reasons of clarity, the deflection curves for all other intermediate values of P have not been drawn. In computing the maximum nondimensional deflection, Y_n, the interpolation method has been used.

In order to verify the accuracy of the graphical method, the maximum nondimensional deflections are calculated using exact analysis and using a computer program developed to perform model superposition analysis. The output from the computer program is shown in Appendix B. One can note that, for the first mode resonance, Y_n is equal to 0.607, and hence the error is less than 7 percent.

Knowing Y_n, the maximum deflection may be calculated by using equation (27). Thus,

$$y_{max} = \frac{\rho_a V d^2 L}{\sqrt{\sigma}\ \sqrt{\rho}\ \delta A}\ Y_n$$

$$= \frac{1.123\text{x}10^{-7}\text{x}(6)^2\text{x}(506\text{x}12)}{(\sqrt{108\text{x}10}^3)(\sqrt{0.000734})(0.08)(13.8917)}\ VY_n$$

$$= 2.48\text{x}10^{-3} VY_n$$

This means for the first mode resonance that:

$$y_{max} = 2.48\text{x}10^{-3}\text{x}30.17\text{x}0.569 \text{ in.}$$
$$= 0.0426 \text{ in. } (0.1082 \text{ cm})$$

The completion has been repeated for other modes of vibration with results summarized in the following Table.

Table 5. Computation of Deflection

Mode No.	Y_n	y_{max} (in. [cm])
1	0.569	0.0426 [0.1082]
2	0.382	0.0563 [0.1431]
3	0.212	0.0478 [0.1215]
4	0.164	0.0496 [0.1260]
15	0.042	0.0479 [0.1216]
29	0.021	0.0478 [0.1215]

Step 4

We are now going to compute the bending stress. For this, we shall determine first the nondimensional curvature using Figures 19 through 21. Consider again the first mode for which $Z^2 = 0.464\text{x}10^{-3}$. Corresponding to this value and the value of P = 92,000, the nondimensional curvature χ_1, can be obtained from the graphs in Figure 20. The value is approximately equal to $6.306\text{x}10^{-3}$.

The value of y''_{max} may now be calculated using equation (32). Thus,

$$y''_{max} = \frac{\rho_a \, d^2 \sqrt{\sigma} \, L}{\sqrt{\rho} \, \delta \, EI} \quad V_n \, X_n$$

$$= \frac{1.123\text{x}10^{-7}\text{x}(6)^2 \text{ x}\sqrt{108\text{x}10^3} \text{ x } (506\text{x}12)}{\sqrt{0.000734} \text{ x}(0.08) \text{ x } (29\text{x}10^6)\text{x}(20.5329)} \quad V_n X_n$$

$$\simeq 6.25 \text{ x } 10^{-6} \; V_n X_n$$

This means for the first mode resonance that

$$y''_{max} = 6.25\text{x}10^{-6}\text{x}30.17\text{x}6.306\text{x}10^{-3} \quad (\text{ in.}^{-1})$$

$$\simeq 1.1892\text{x}10^{-6} \text{ in.}^{-1} \; (3.0206\text{x}10^{-6}\text{cm}^{-1})$$

The bending stress is now calculated using the standard strength of materials formulation, namely:

$$(\sigma_b)_{max} = E \; c_z y''_{max}$$

For a 10-layer cable, there are 19 wires along any diametrical axis. Hence, the maximum fiber distance, c_z, may be considered as 19 times the radius of a wire. Therefore, in this case, c_z becomes equal to 2.375 in. (6.033 cm). Finally, the maximum bending stress becomes equal to:

$$(\sigma_b)_{max} = 29\text{x}10^6 \text{ x } 2.375 \text{ x } 1.1892 \text{ x } 10^{-6} \quad \text{psi}$$

$$\simeq 81.906 \text{ psi } (564.742 \text{ MPa})$$

The above computation has been repeated in a manner similar to the previous steps for the 2nd, 3rd, 4th, 15th, and 29th modes. The results obtained are summarized in the Table 6 below. It should be noted that these results, when compared with the exact values obtained from computer printout, indicate the accuracy of the graphical procedure developed in this report.

Table 6. Computation of Bending Stress

Mode No.	χ_n	y''_{max} (in.$^{-1}$ [cm^{-1}])	$(\sigma_b)_{max}$ (ksi [MPa])
1	6.306×10^{-3}	1.1892×10^{-6} [3.0206×10^{-6}]	0.0819 [0.5647]
2	6.34×10^{-3}	2.357×10^{-6} [5.987×10^{-6}]	0.1624 [1.1194]
3	6.35×10^{-3}	3.611×10^{-6} [9.172×10^{-6}]	0.2487 [1.7149]
4	6.355×10^{-3}	4.844×10^{-6} [12.305×10^{-6}]	0.3336 [2.3006]
15	6.5×10^{-3}	18.676×10^{-6} [47.437×10^{-6}]	1.2863 [8.8690]
29	6.870×10^{-3}	38.979×10^{-6} [99.0×10^{-6}]	2.685 [18.511]

CHAPTER 6
FATIGUE LIFE ANALYSIS

6.1 An Overview

The general engineering practice for design, specifications and fabrication of any structure is based on correlations of the latter with service experience. Normally, service experience leads to identifying weak links in a structure, and reliability is obtained by improving these weak links. In the case of a cable-stayed bridge, lack of the above information at this stage imposes a severe limitation on a comprehensive fatigue life analysis. However, within the framework of fracture mechanics methodology, a preliminary approach to the problem may well be conceived. This preliminary approach will be described in detail in this chapter.

6.2 Fracture Mechanics Methodology

Fracture mechanics is basically a study of the fracture or discontinuity in terms of such commonly used engineering parameters as applied stress, specimen and crack geometry, and material properties. In linear elastic fracture mechanics (LEFM), this is equivalent to describing the stress field in the vicinity of a crack tip or a surface of discontinuity in terms of the above parameters. The magnitude of this stress field is higher than one obtained in the absence of any discontinuity. This relative increase in magnitude is described by a term K_I called the stress-intensity factor. The subject of LEFM deals with the relationship between K_I, nominal stress σ, crack or flaw size a, and material properties, such as M. In functional form, the relationship can be written as:

$$K_I = f(\sigma, a, M) \tag{34}$$

One of the principles of fracture mechanics is that unstable fracture occurs when K_I reaches a critical value K_{IC}. One can note from the above relationship that for a given σ and a given set of material properties, the change in a is directly associated with a change in K_I. Thus, if the value of the crack size corresponding to K_{IC} is denoted by a_c, one can write:

$$a_c = f_1 (\sigma, K_{IC}, M) \tag{35}$$

The parameter a_c represents the terminal conditions in the life of a structural component and the parameter K_{IC} represents the inherent ability of a material to resist progressive tensile crack extension. For this reason K_{IC} is more commonly called the fracture toughness of the material.

At the outset, the fatigue life analysis of a structural component is seemingly unrelated to the field of fracture mechanics, since it deals with the life of the component under repeated cyclic loading in terms of the total number of load cycles elapsed. Moreover, the component is believed to be free of any discontinuity or crack, at least macroscopically and, therefore, the concept of stress concentration seems to lose its meaning. On the other hand, more often than not, a structural component contains initial defects. This is largely the result of manufacturing processes. Even if these defects are microscopic in nature, at one stage of repeated loading they give rise to localized stress concentration which causes fatigue crack initiation. While these cracks are of subcritical dimensions, they nevertheless act as sources of discontinuity, thereby raising the values of K_I the terminal condition a_c is reached. This, then, is the stage of fatigue crack propagation prior to the stage of macroscopic failure associated with the unstable crack growth.

The above description serves as a link between the fatigue life analysis of a structural component and the conventional LEFM methodology. More precisely, it indicates how the fatigue behavior of a structural component can be described in terms of fracture mechanics parameters K_I (K_{IC}), a_c, σ, the material properties M, and the number of load cycles. A complete description of the fatigue life of a structural component involves three distinct stages. These are:

Fatigue crack initiation
Fatigue crack propagation
Crack instability or final fracture

These stages will be dealt with in more detail in the specific case of bridge cables.

6.3 Fatigue Crack Initiation

A complete knowledge of fatigue crack initiation in bridge cables requires the understanding of the basic mechanism of fatigue in high strength materials.

Very little work has been done in this area partly because it is extremely difficult to observe microstructural changes caused by the fatigue process in such materials. With this limitation in mind, we shall attempt to describe the microscopic aspects of fatigue crack nucleation in bridge cables.

6.3.1 Microstructural Aspects

The chemical composition and mechanical properties of bridge cable materials presently under investigation indicates that the material is a multi-phase system and has martensitic structure. During constant strain-amplitude cycling of such structures, the stress range generally decreases within the first 20% of its life as shown schematically in Figure 22, whereupon it remains relatively constant until the final fracture of component occurs.

The hystersis loop in Figure 22 represents the case of strain-softening, a phenomenon which takes place only if $\sigma_u/\sigma_y \leq 1.2$ where σ_u is the ultimate tensile strength and σ_y, the 0.2% offset yield strength. This is indeed the case of the cable material presently under investigation. The implication of strain-softening high strength materials is that they produce dislocation slips which are very small and highly localized and hence, within the nominal elastic range. Therefore, large stress concentration in these materials arises from the structural imperfection in the form of inclusions or voids induced by the manufacturing technology.

During the load application and stress reversals, the microvoids tend to coalesce, thereby forming the site of crack nucleation. In high strength materials, the void coalescence, rather than cleavage, is the microscopic phenomenon contributing to crack initiation.

Considering the case of bridge cables, it can be noted that the crack initiation in a single, polished and unnotched wire is likely to be caused by the above void coalescence mechanism. A cable, on the other hand, is composed of several single wires tied together in parallel or in some helical combination. During external cyclic loading of the cable by wind or other forces, individual wires undergo different amounts of bending which cause contact surface and hence, contact stress to be generated between the wires. If repeated contact due to cyclic loading occurs, it will produce mechanical notches in an otherwise unnotched wire. It is, therefore, important

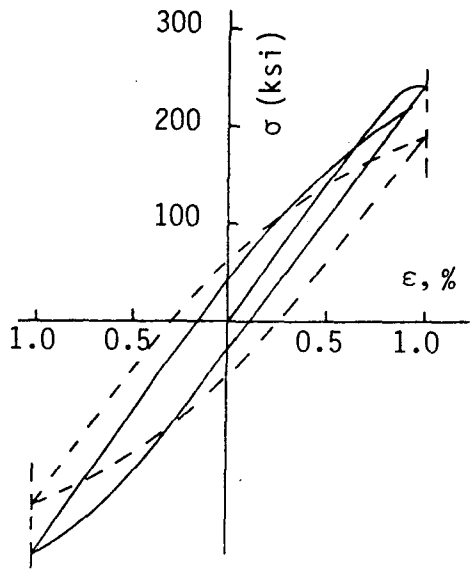

Figure 22. Cyclic Stress-Strain for Martensitic Structure (Landgraf, et al [34])

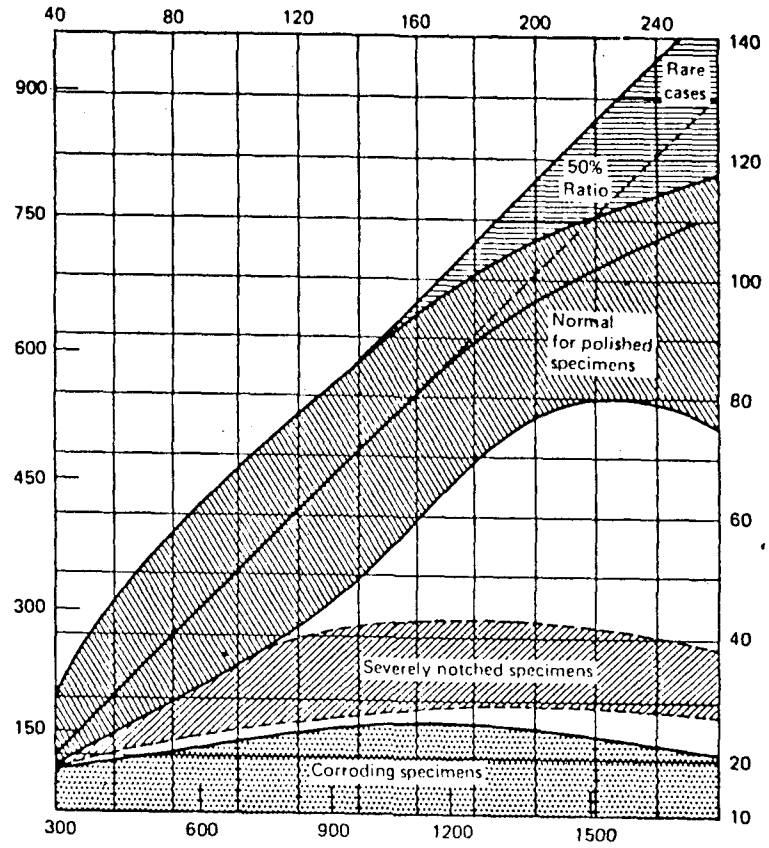

Figure 23. Effect of Surface Condition on Fatigue Limit of Steel Alloys (Bullens[35])

to note the following:

1. Crack initiation in a single, unnotched and polished wire is brought about by the void coalescence mechanism.

2. Crack initiation in an unnotched and polished wire within a wire bundle (cable) is brought about by a combination of void coalescence and mechanical notching due to contacts between the wires.

3. Crack initiates faster in initially notched specimens.

6.3.2 Engineering Analysis

The brief description of microstructural aspects of the fatigue crack nucleation sheds some light in understanding the basic fatigue mechanism in bridge cables. It also leads to two important observations, namely:

1. The crack initiation mechanism in bridge cables or wires is correlated to strain-softening or strain-hardening parameter of the cable material, whichever the case may be.

2. The fatigue strength of a wire, which is a measure of its resistivity to crack growth, depends on the surface texture of the wire as indicated in the schematic shown in Figure 23.

Based on these observations, we will now develop a framework for the analytical study of fatigue crack initiation in bridge cables. Thus consider a single wire subjected to cyclic loading. The conventional procedure for describing the fatigue behavior of the wire is to generate a design fatigue curve (S-N curve) based on the experimental data on nominal stress or stress range and the number of cycles elapsed before failure. The schematic of a S-N curve is shown in Figure 24. Note that the total S-N curve indicated by a solid line is an assymptotic combination of the crack initiation curve and crack propagation curve both indicated by broken lines. The shape of the crack initiation curve suggests that an empirical relationship of the following form exists between the number of cycles to crack initiation, N_i, and the nominal stress range, $\Delta\sigma$.

$$N_i = C_1(\Delta\sigma)^{-\gamma} \tag{36}$$

where C_1 and γ are two constants which depend, in general, on the material properties M stated earlier and on the strain hardening exponent, n. Yokobori[37] has found a similar relationship for the crack initiation in aluminum. When the crack initiation data (See Figure 25) of Barsom and McNicol[38] for HY-130 steel were curved-fitted to the above expression, we obtained:

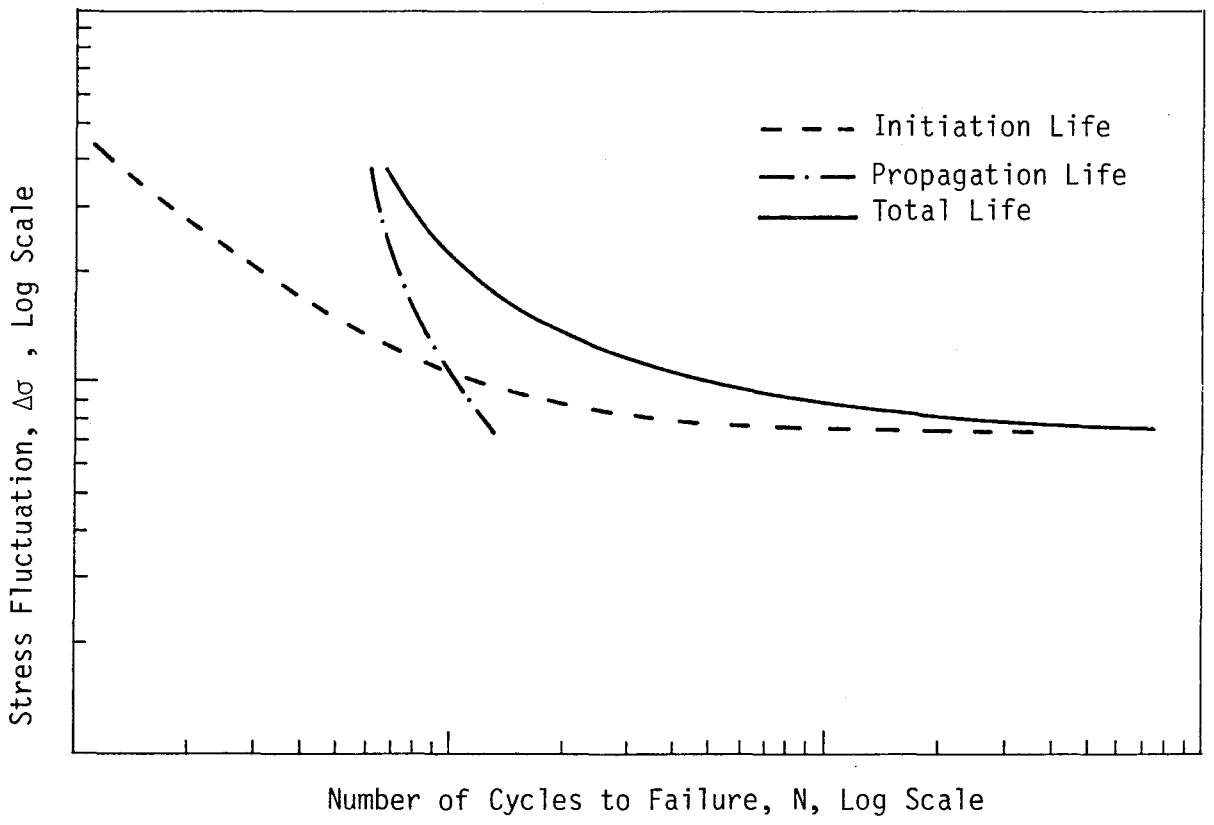

Figure 24. Schematic S-N Curve Showing Crack Initiation, Propagation and Total Life (Rolfe and Barsom[36])

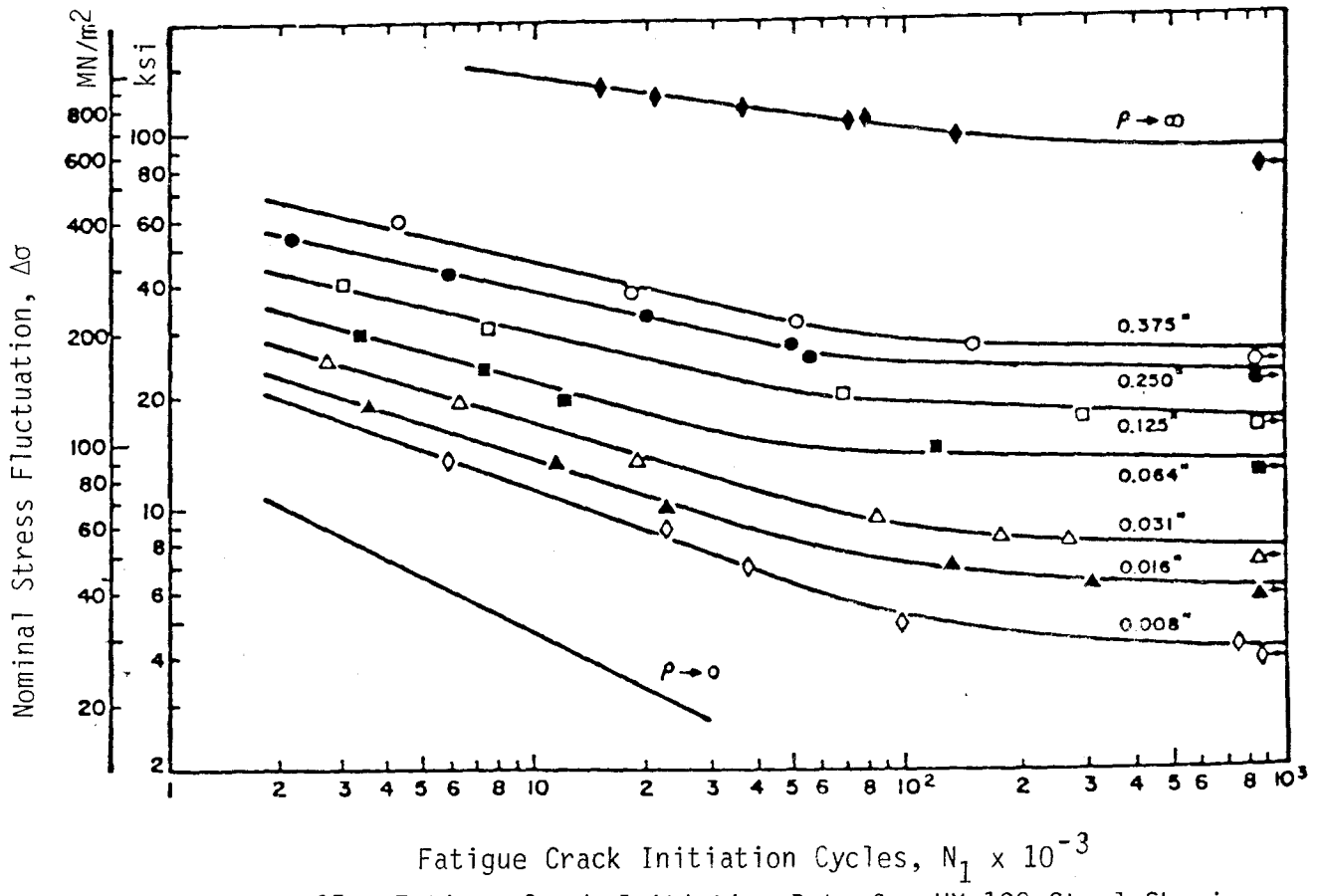

Figure 25. Fatigue Crack Initiation Data for HY-130 Steel Showing Dependence on Nominal Stress Fluctuation for Various Notch Geometries (Barsom and McNicol [38])

$$C_1 = 3.06 \times 10^7, \ \gamma = 3.3$$

It should be recalled that the objective of the empirical formalism is to obtain expressions for the constants C_1 and γ in terms of measurable mechanical properties such as ultimate tensile strength, yield strength, etc., as well as in terms of a strain hardening exponent. However, this requires a large set of statistical data from identical experiments with specimens having the same geometry but a varying degree of mechanical properties. This is not available in current literature and should, therefore, constitute the forefront of further research.

The above analysis of crack initiation does not reflect directly the effect of notches. From an engineering standpoint, it is of considerable interest to study this latter case. This is conventionally done by establishing a relationship between the number of cycles to crack initiation and the quantity $\Delta K_I/\sqrt{\rho}$ where the term K_I is explained before and ρ is the notch radius. The usual experiment involves testing specimen with different notch radius. In the case of a wire of .25 in. (6 mm) diameter, such experiment is not likely to produce reliable results. However, it is analytically possible to obtain a threshold value of $\Delta K_I/\sqrt{\rho}$ denoted by $(\Delta K_I/\sqrt{\rho})_{th}$ below which crack will not initiate. For this, the following relationship is used. (See also Figure 26.)

$$\left(\frac{\Delta K_I}{\sqrt{\rho}}\right)_{th} = 10\sqrt{\sigma_y} \tag{37}$$

where σ_y is the yield strength. Thus, for the wire material (σ_y = 204 ksi [1407 MPa]), the threshold value becomes 142.83 ksi (949 MPa). On the other hand, the threshold value of $\Delta K_I/\sqrt{\rho}$ is related to the maximum applied stress. The exact functional relationship between these two quantities depends on the nature of crack, i.e., whether the crack is circumferential, axial, single-edged, double-edged, elliptical or otherwise. This requires extensive analytical investigation. At present, we assume that the maximum elastic stress at the root of the notch, σ_{max}, is the one due to an elliptical crack [40] and is given by:

$$\sigma_{max} = \frac{2K_I}{\sqrt{\pi\rho}} \tag{38}$$

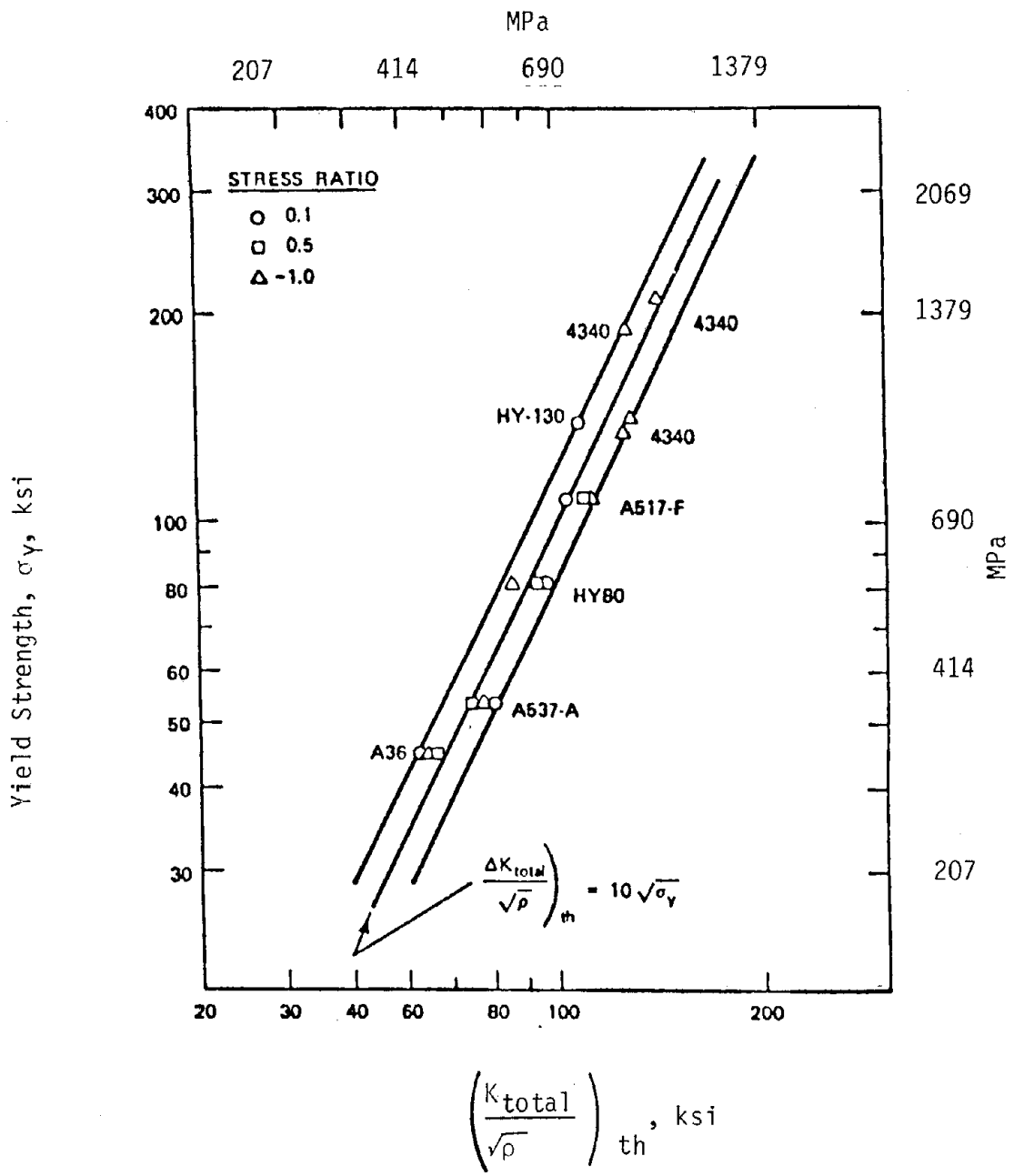

Figure 26. Relationship Between Yield Strength and $(K_I/\sqrt{\rho})_{th}$ for High Strength Steels (Roberts, et al.[39])

This means that the maximum stress fluctuation corresponding to the threshold value of $\Delta K_I/\sqrt{\rho}$ is 161.17 ksi (1111 MPa). It represents the case of $\rho \to \infty$ or in other words, an unnotched specimen. There is no data to substantiate the value; however, two results of Barsom and McNicol [37] are worth noting in this regard. First, the value of $(\Delta K_I/\sqrt{\rho})_{th}$ (142.83 ksi) [949 MPa]) is close to the one obtained for ASTM 4340 steel (σ_y = 212 ksi [1462 MPa]) shown in Figure 27. Second, the value of σ_{max} (161.17 ksi [1111 MPa]) is consistent with the one experimentally obtained for HY-130 steel.

The above analysis gives us some information on the fatigue crack initiation life of the wire. More specifically, the analysis determines the fatigue limit or the endurance limit of the wire material. The number of cycles corresponding to this endurance limit is primarily the fatigue initiation life. For higher values of applied stress range, the number of cycles to crack initiation rapidly decreases. Figure 28 shows schematically the fatiuge limit of polished, notched and degreased single wires of the type that is frequently used in cable-stayed bridge construction. Assuming a stress threshold value of 160 ksi (1103 MPa) for the wire material under investigation, and assuming a value of $\gamma = 3.3$, an empirical fatigue crack initiation curve may be obtained in a manner similar to the ones shown in Figure 27.

6.3.3 General Discussion

The analysis presented in the preceding section demonstrates that the fatigue initiation life of a wire is correlated to its yield strength and strain hardening exponent. In addition, the initiation life of a notched wire depends on the notch geometry. Therefore, a complete understanding of crack initiation in a wire remains an unresolved issue. Limited experimental efforts have previously been directed in this area, most notably by Reemsnyder [42] who tested single wires for fatigue life in a rotating strut machine. The results of his experiments are shown in Figures 29 and 30. Since the yield strengths of the wire materials in his experiments are of the same order of magnitude, the results serve to verify the analytical framework discussed in previous sections. More recently, Fisher and Viest [43] have performed experiments with single wires (as well as strands made from such wires) which have different yield strengths and tensile properties. However, their results (See Figure 31) are too scattered to form any homogeneous statistical groups.

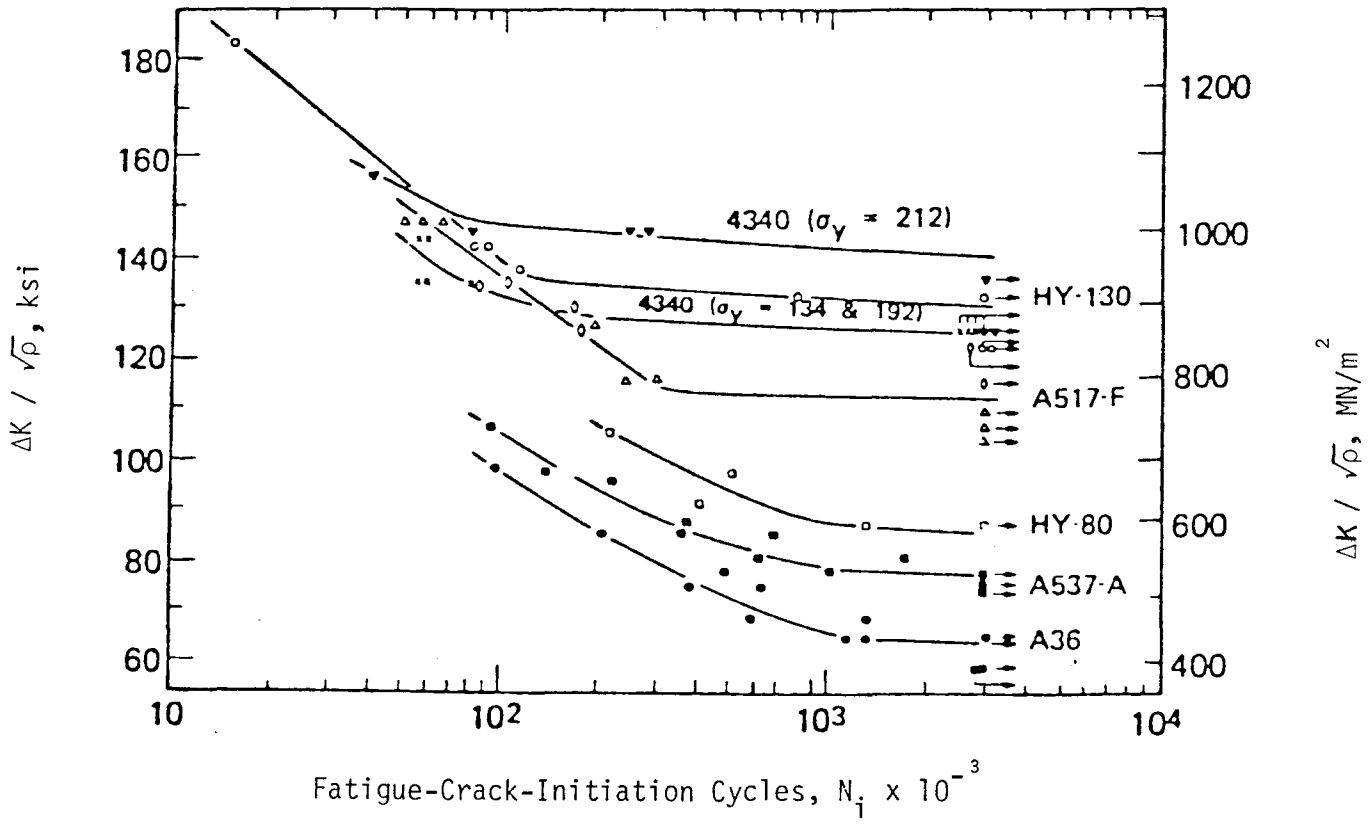

Figure 27. Dependence of Fatigue Crack Initiation Life of Various Steels on $\Delta K/\sqrt{\rho}$ at Stress Ratio +0.1 (Barsom and McNicol [41]).

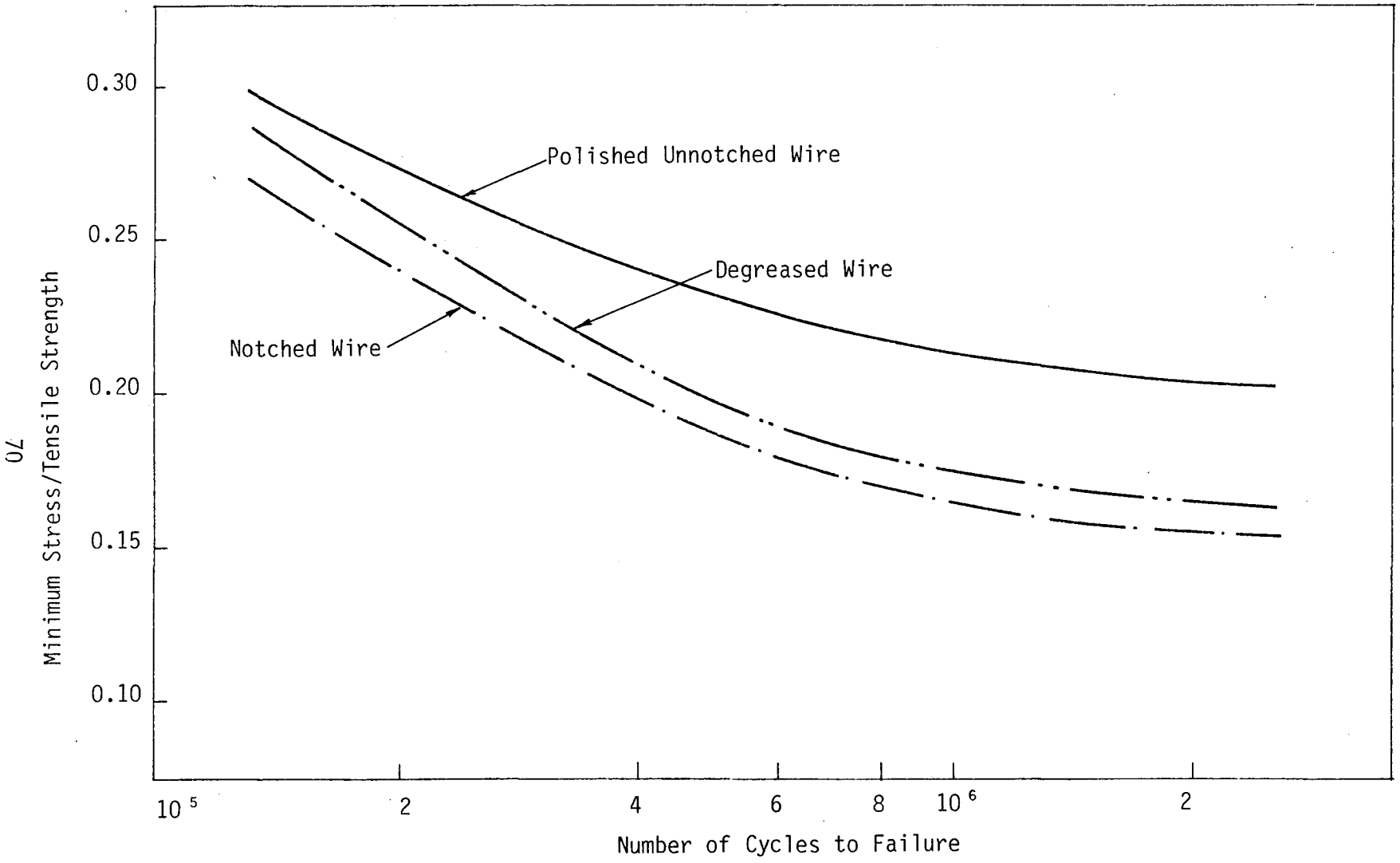

Figure 28. Schematics Showing Fatigue Strength of Polished, Notched and Degreased Wire Specimen

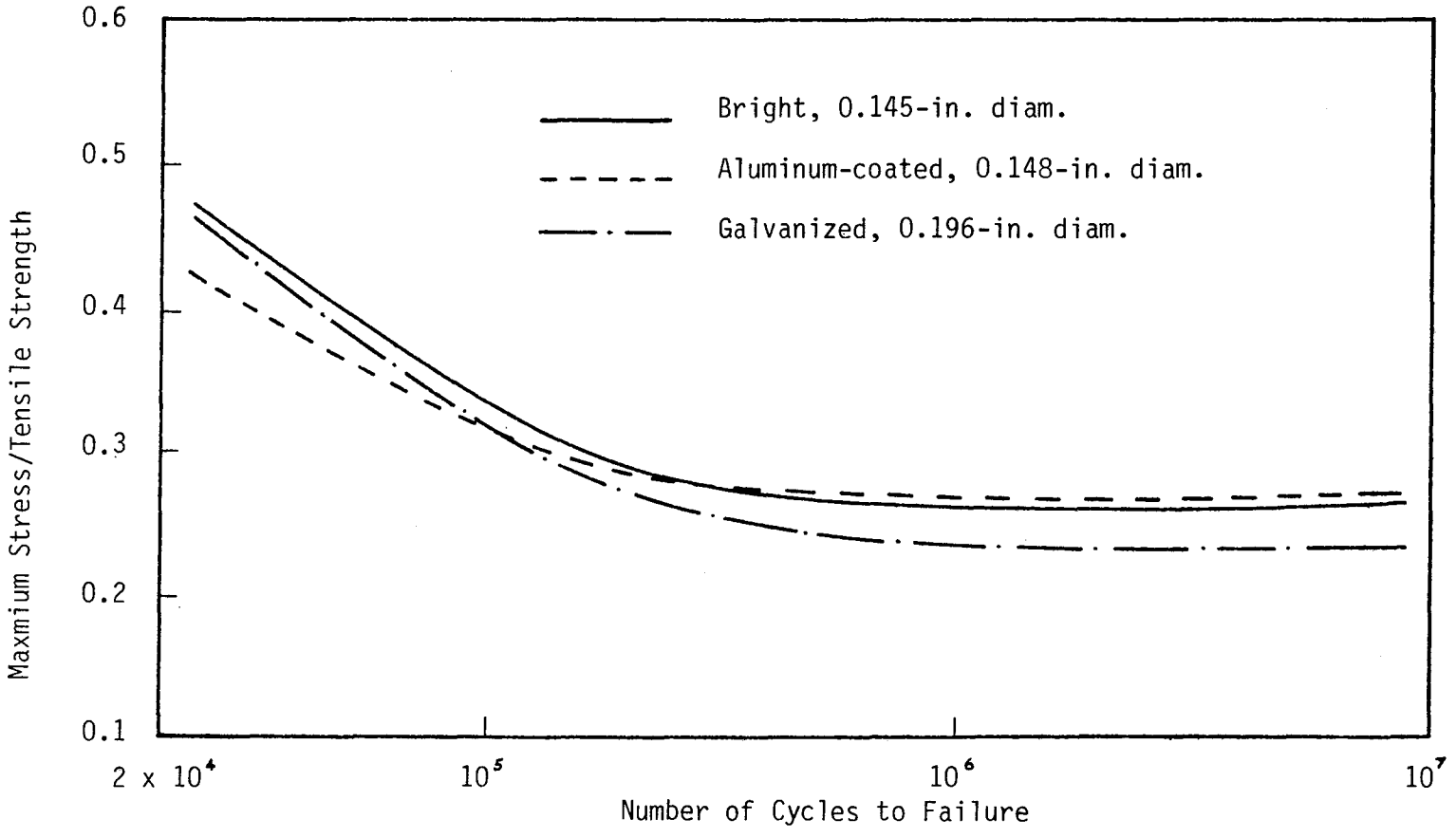

Figure 29. Rotating Strut Fatigue Tests - Single Wires

Improved Plow Steel (Reemsnyder[42])

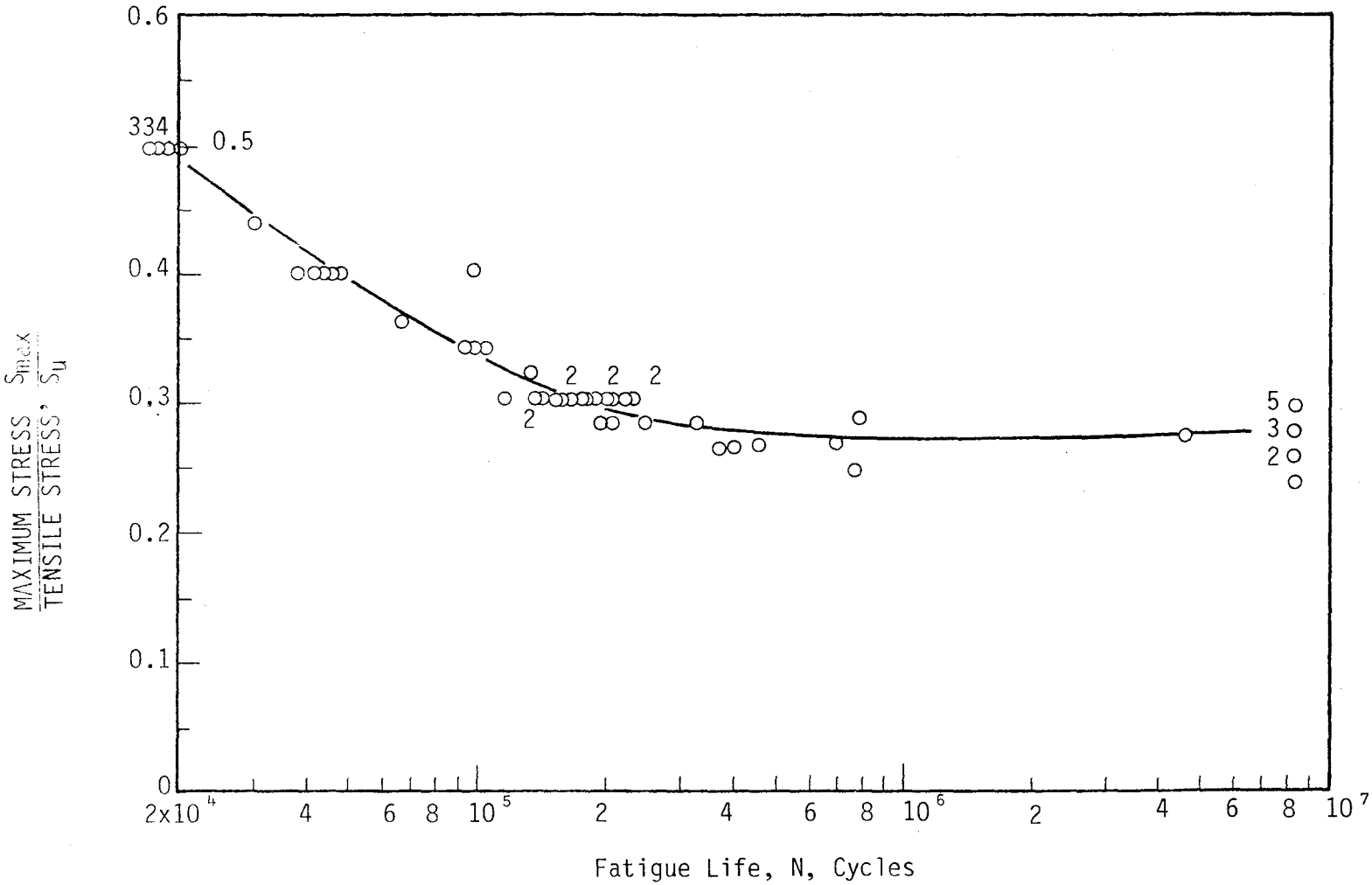

Figure 30. Fatigue Tests on Improved Plow Wire (Reemsnyder[42])

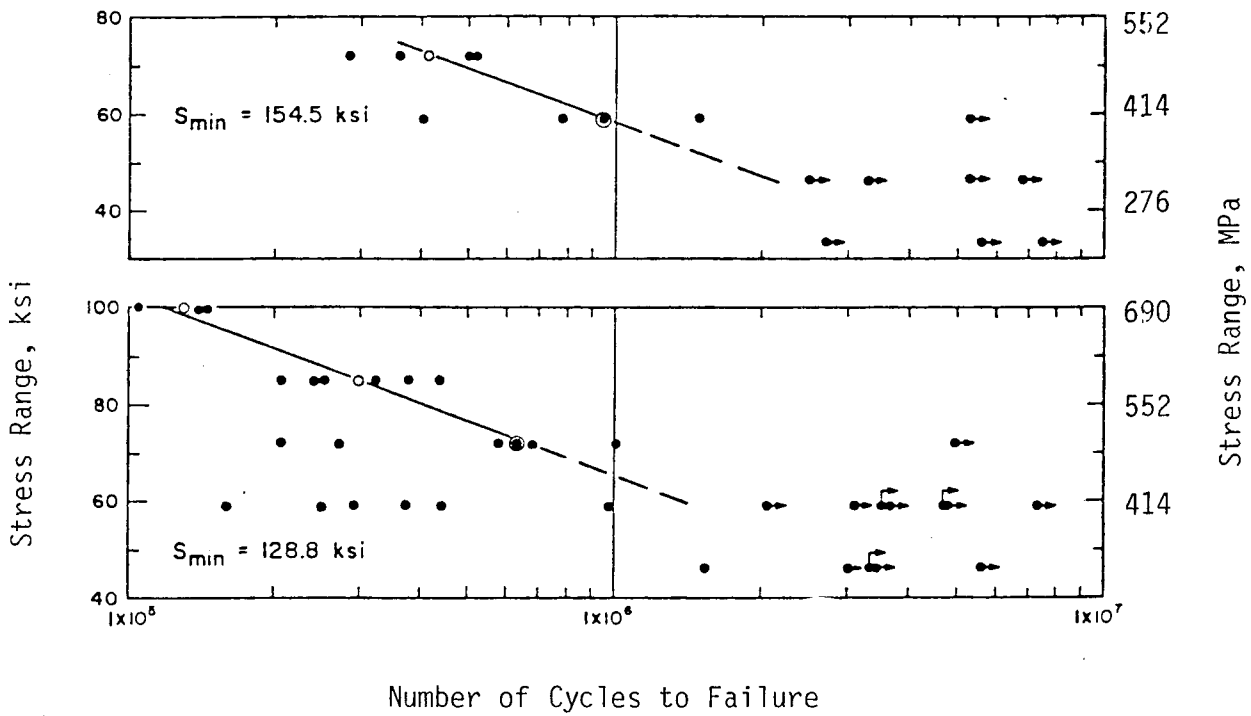

Figure 31. Test Results of Prestressing Wires Showing a Wide Scatter (Fisher and Viest[43])

In yet another direction, Barsom and McNicol [38], Clark [44], and Clausing [45], and others have attempted to correlate various mechanical properties with the crack initiation life. A detailed account of this may be found in Rolfe and Barsom [36].

In summary, it may be pointed out that the analytical framework of the crack initiation in a wire is by no means complete. Furthermore, preliminary conclusions reached at this stage still require substantiation by experimental work. It can be safely assumed, however, that the fatigue limit of a single unnotched and polished wire is fairly high and therefore, the crack initiation, under commonly occurring wind loading during a reasonable span of service life, should not be a grave concern. This statement, of course, requires some qualification when one considers the taut ends of a cable or a wire. It may be evident from the dynamic analysis presented in previous chapters that bending stresses are usually much higher at the ends. As previously discussed, higher stresses considerably reduce the initiation life.

6.4 Fatigue Crack Propagation

Crack initiation life dominates the total fatigue life in the high strength material of which bridge cables and wires are made. Hence, from the service viewpoint, the fatigue problem is practically eliminated if the cables are so designed that commonly occurring wind loading will not produce high bending stresses. However, there is still some probability, small as it may be, that some wires in the cable will contain preexisting cracks, surface discontinuity or voids. In this case it is important to determine the crack propagation life.

It is a conventional practice to divide the fatigue crack propagation behavior into three regions (see Figure 32). Region I in the figure corresponds to non-propagating fatigue cracks. Rolfe and Barsom's [36] experimental results on non-propagating fatigue cracks show that the threshold stress-intensity factor below which a crack will not propagate is given by:

$$\Delta K_{th} = 6.4\ (1-0.85\ R) \quad \text{for } R \geq +0.1$$
$$= 5.5\ \text{ksi}\sqrt{\text{in.}} \quad \text{for } R < +0.1 \qquad (39)$$

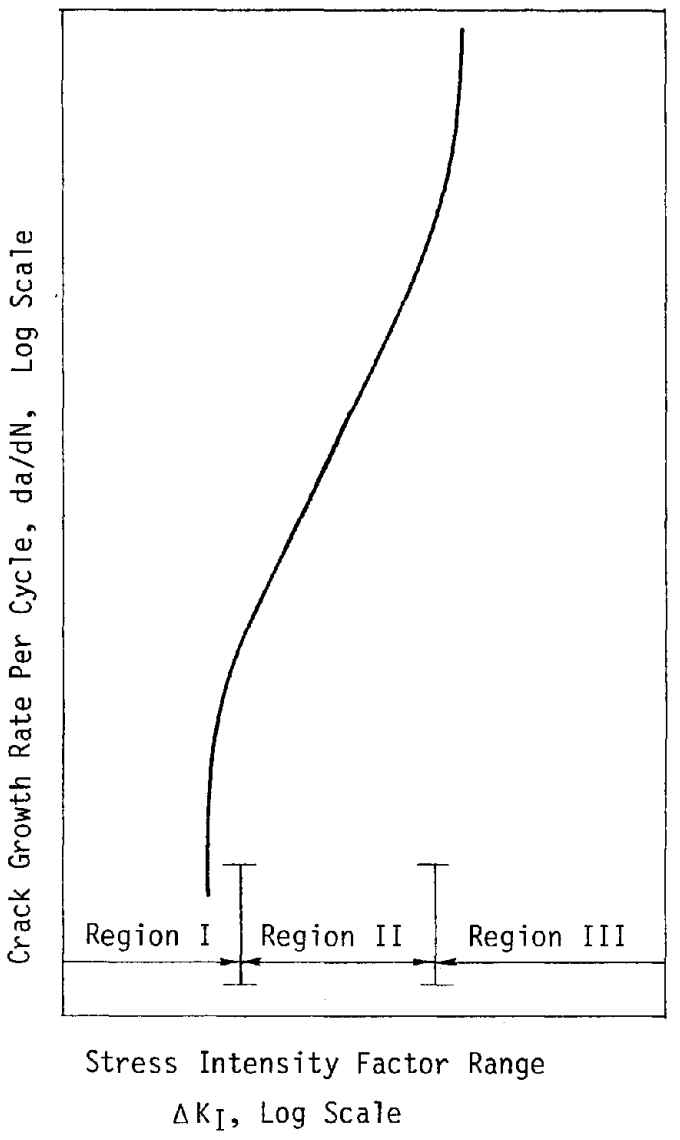

Figure 32. Schematic of Fatigue Crack Growth Regions in Steel (Rolfe and Barsom[36])

For the present case, the value of R is always greater or equal to 0.1 for all possible design stresses and all possible wind loadings. In fact for large value of applied tension, such as 110 ksi (758 MPa), and for low bending stress, such as 10 ksi (59 MPa), the value of R will be as high as 0.8 and consequently, the value of ΔK_{th} will be very low. Hence, for all practical purposes, once a crack is initiated in a wire it will propagate.

Let us now consider Region III which corresponds to accelerating fatigue crack or the unstable crack growth. The usual LEFM description of such phenomenon is given in terms of crack tip opening displacement (CTOD), δ_c. The latter is related to a threshold value of stress intensity factor K_{th} and the elastic properties in the following manner:

$$\delta_c = \frac{K^2_{th}}{E\sigma_y} \tag{40}$$

In fact, it is observed that the accelerating fatigue crack propagates at a constant value of δ_c equal to 1.6×10^{-3} in. (0.04 mm). For the bridge wire ($E = 29 \times 10^3$ ksi, [200 GPa], σ_y = 204 ksi [140.7 MPa]) this gives K_{th} = 97.29 ksi $\sqrt{in.}$ [107 MPa$\sqrt{m}$] approximately. It will be assumed that the fracture toughness of wire, K_{IC} or K_{ID}, falls in the range of 80 ksi $\sqrt{in.}$ (88 MPa$\sqrt{m}$). Therefore, we assume that for most cases of interest with the fatigue design of bridge cables, $K_{th} > K_{IC}$. This means we need not be concerned about the evaluation of accelerating fatigue crack propagation life which will indeed be very small.

The above analysis indicates that the fatigue crack propagation life of a wire, while relatively small in comparison to the initiation life, is limited mainly to steady-state crack propagation Region II. We will describe the latter in terms of some rate equations discussed next.

6.4.1 Steady-State Crack Propagation

In its formulation, a general law of fatigue crack propagation should include, as a minimum, the following factors:

1. Geometry of specimen and crack.

2. Nature of cyclic loading (constant and variable amplitude).

3. Material properties.

4. Growth rate.

In addition, environmental factors such as temperature, humidity, environmental corrosion, etc. may affect the propagation rate. Therefore, ideally, they should be considered in a general propagation law. The existing laws of crack propagation are basically two types:

1. Laws derived from theoretical analysis of strain hardening, fatigue damage, CTOD, interference and other models.

2. Semi-empirical laws based on statistical analysis of experimental data.

From a practical engineering standpoint, the second type seems to be more promising. Therefore, our discussion will concentrate only on this type. The semi-empirical laws can generally be written as:

$$\frac{da}{dN} = C_2(\Delta K)^{\mu} \tag{41}$$

where a is the crack size, and C_2 and μ are two parameters which depend, among other things, on material properties. Determination of the crack propagation life of a wire by the above formula involves knowledge of the following quantities:

1. Values of C and μ

2. Values of critical crack length a_c and fracture toughness K_{IC} or K_{ID}

3. Value of initial crack length

Barsom [46] has tested various high-yield-strength (σ_y > 80 ksi) [55 MPa] martensitic steels for fatigue crack propagation. The results of these experiments show that (see also Figure 33):

$$\mu = 2.25 \text{ and } 0.27 \times 10^{8} \leq C \leq 0.66 \times 10^{-8}$$

Since C and μ are assumed to depend only on the material properties, and since it has been established by Bucci et al. [41], Barsom [46], Imhof and Barsom [48], and Parry et al. [49] that the growth equation:

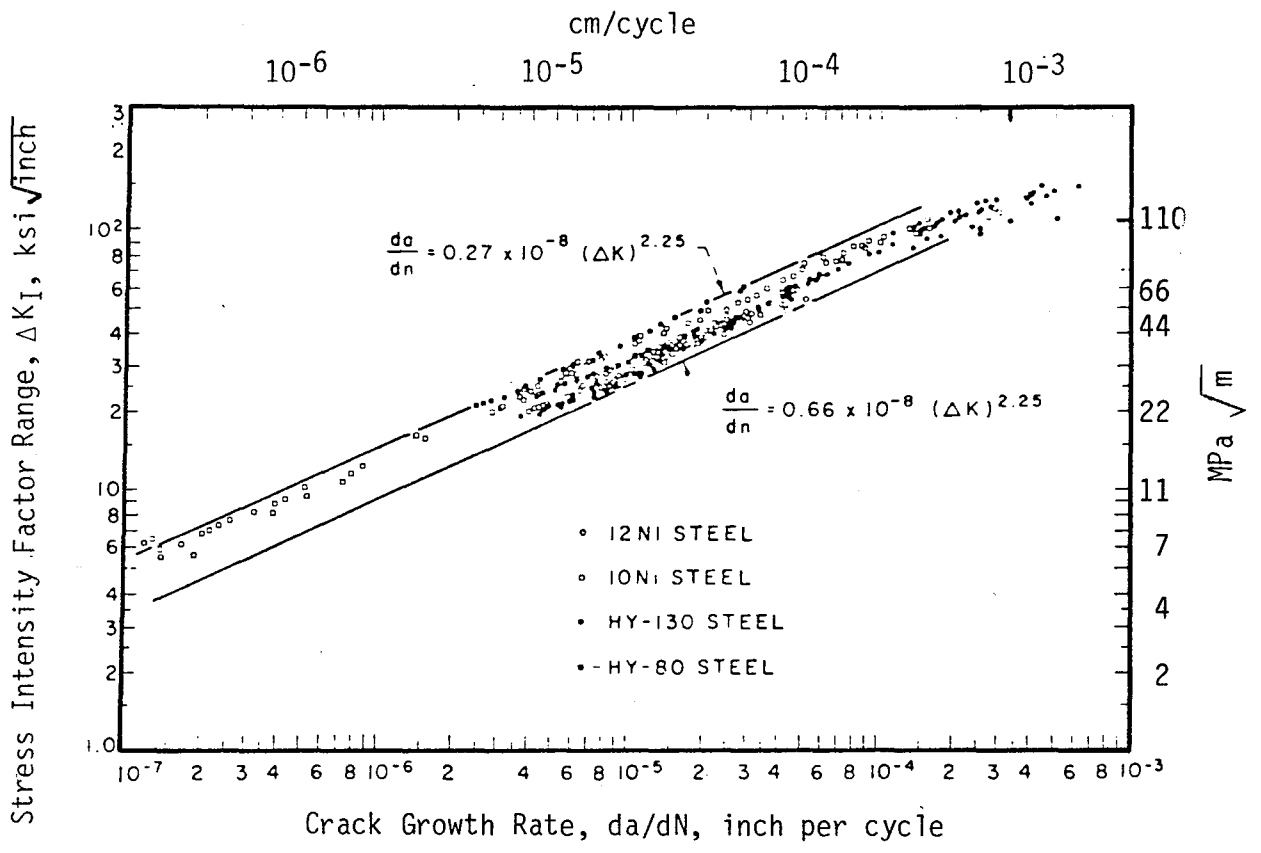

Figure 33. Fatigue Crack Propagation Data in Martensitic Steel (Barsom[46])

$$\frac{da}{dN} = 0.66 \times 10^{-8} (\Delta K)^{2.25} \tag{42}$$

is valid for steels having yield strength ranging from 80 to 300 ksi, (552 to 2068 MPa), we shall consider the above form as representative for fatigue crack propagation in cold-drawn wires.

The determination of fracture toughness, K_{IC} or K_{ID}, and hence the critical crack size, a_c, requires, at this point, some detailed analysis of the stress intensity factor.

6.4.2 Fracture Toughness and Critical Crack Size

It is stated earlier that the fracture toughness of a material represents its inherent ability to resist progressive crack extension. In the case of tensile cracking, the parameter is denoted by K_{IC} and in the case of bending, by K_{ID}. In either case:

$$a_c = f(K_{IC} \text{ or } K_{ID}, \sigma_{max}, g) \tag{43}$$

where g is a function of crack geometry. The above formula determines the critical crack length, a_c, if K_{IC} or K_{ID}, σ_{max}, and g are known.

Fracture toughness K_{IC} or K_{ID} may be theoretically calculated using their relationships with the mechanical properties of the structural component. One such relationship due to Sailor [50] is as follows:

$$\frac{K_{IC}^2}{E} = \sigma_y C H_s \delta_o e^{\bar{\varepsilon}_\rho} \tag{48}$$

where C = constant factor = 1.3

H_s = strain hardening correction term; typically between 1.2 and 1.5

δ_o = mean free ferrite path

$\bar{\varepsilon}_\rho$ = plastic strain at the crack tip (= 0.8 for plane-strain fracture strain)

Although the above equation is strictly valid for ferrite structure, it provides a reasonable estimate of K_{IC} for martensitic steel of which the cable is made. Sailor's theoretical calculation shows that fracture toughness of SAE 4340 steel (steel having a comparable strength value to that of ASTM A586-68 material) is in the range of 70 ksi $\sqrt{in.}$ (77 MPa $\sqrt{m}$) to 85 ksi $\sqrt{in.}$ (93 MPa $\sqrt{m}$). On the other hand, the measured value of K_{IC} [51] (see Figure 34) falls within a much wider range

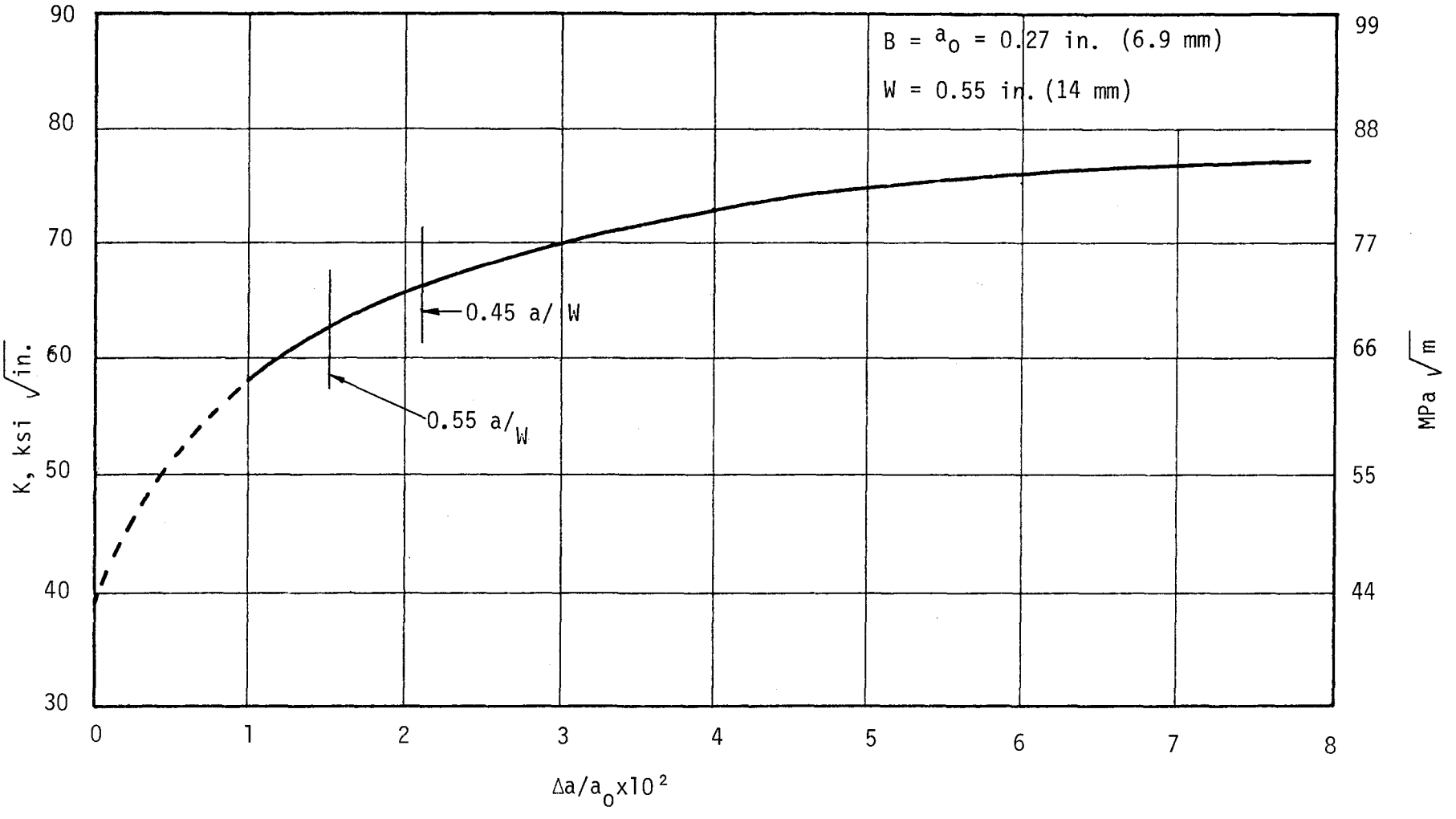

Figure 34. Plane-strain Fracture Toughness of SAE 4340 Steel (Jones and Brown [51])

between 60 ksi $\sqrt{in.}$ (66 MPa$\sqrt{m}$) to 80 ksi $\sqrt{in.}$ (88 MPA$\sqrt{m}$). For the present analysis, we shall assume a set of values of K_{IC}, namely, 60 ksi $\sqrt{in.}$ (66 MPa$\sqrt{m}$), 80 ksi $\sqrt{in.}$ (88 MPa$\sqrt{m}$), and 100 ksi $\sqrt{in.}$ (110 MPa$\sqrt{m}$). We consider that, in the absence of further experimental and analytical evidence, this will provide sufficient useful information about the range of crack propagation life in bridge cables.

Fracture toughness can also be determined experimentally. At present, the standard ASTM method for measuring K_{IC}, called the K_{IC} test method, requires a certain specification of the test specimen dimensions. These specifications are not satisfied by a 0.250 in. (6 mm) diameter wire having yield strength of 204 ksi (1407 MPa). Consequently, this is another area which needs further exploration. In any event, we conclude at present that from the assumed or computed values of K_{IC}, the critical crack size can be determined using the functional relation in equation (43).

In fracture mechanics methodology, several explicit relationships between the stress intensity factor and crack length are derived by various methods. We recall that a knowledge of the stress intensity factor is required to determine the crack propagation life of a wire analytically. Accordingly, we shall consider here some of these relationships which seem to closely represent the situation of crack propagation in a wire.

Let us examine the case of a circumferential crack in a cylindrical shell (see Figure 35). Folias [52] has obtained an approximate analytical expression for the stress intensity factor K_I as follows:

$$K_I = \sigma \sqrt{a}\left\{1 + \frac{\pi\lambda^2}{64}\right\} + \sigma_b \left\{ \frac{(1 + \nu^2)^{\frac{1}{2}} \lambda^2 \sqrt{a}}{\sqrt{3} \quad (3 + \nu)} \right\}$$

$$\left\{\frac{(1 + \nu)}{32(1 - \nu)} + \frac{(1 + \nu)}{16(1 - \nu)} \quad (\lambda + \ln \frac{\lambda}{8})\right\} + O(\lambda^4 \ln \lambda) \quad (49)$$

where λ is given by

$$\lambda = 12 \ (1 - \nu^2)^{\frac{1}{4}} \ (a/R)(R/h)^{\frac{1}{2}} \quad (50)$$

For a solid cylinder approximation, h/R = 1 and substituting $\nu = 0.3$ for steel, we get:

$$\lambda = 1.82 \ (\frac{a}{R}) \quad (51)$$

The stress intensity factor in this case may be approximated by the following expression:

$$K_I = \sigma(1 + 0.163 \ \lambda^2) \ \sqrt{a} \quad (52)$$

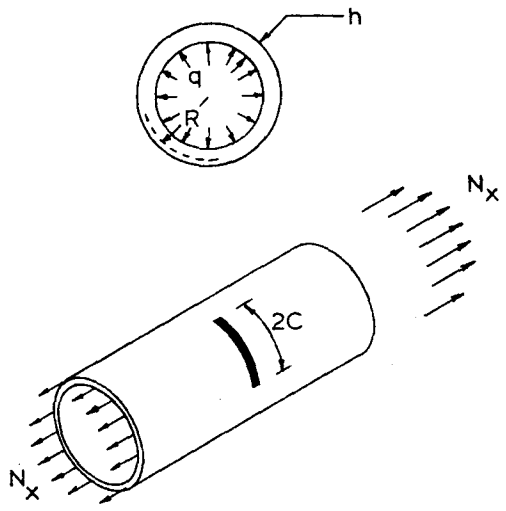

Figure 35. Circumferential Crack in a Cylindrical Shell (Folias[52])

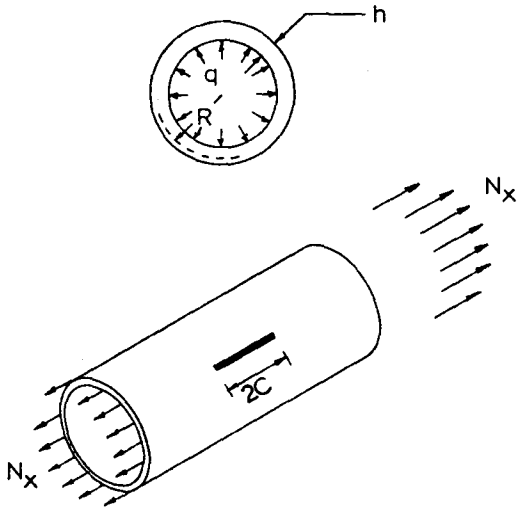

Figure 36a. Axial Crack in a Cylindrical Shell (Folias[52])

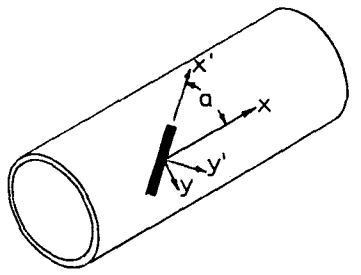

Figure 36b. Oriented Axial Crack in a Cylindrical Shell (Folias[52])

provided the contribution of the term containing the bending stress is negligible. Folias found that this type of approximation results in about a 6% error in K_I for all values of λ. If, in the above case, the crack is axial, (see Figure 36a) the stress intensity factor may be approximated by:

$$K_I = \sigma(1 + 0.815\ \lambda^2)\ \sqrt{a} \tag{53}$$

Finally, for a circumferential crack with arbitrary orientation (see Figure 36b), the approximate stress intensity factor is:

$$K_I = \sigma(1 + 0.163\ \lambda^2)(5\ \cos^2\ \Theta + \sin^2\ \Theta)\ \sqrt{a} \tag{54}$$

Hilton and Sih[53] have calculated the stress intensity factor for a circumferential crack in a solid cylinder by the finite element method and found the following expression:

$$K_I = \sigma\left(\frac{2R}{a}\right)^{\frac{1}{2}} \overline{K}\ \sqrt{a} \tag{55}$$

where $\overline{K}$ is the normalized stress intensity factor. They found that for $2R/a = 1.25$, $\overline{K} = 0.250$.

We have developed an approximate expression for the stress intensity factor using the result of single-edge notch in a plate, i.e.

$$K_I = \sigma\sqrt{\pi a}\ f(A_c/B) \tag{56}$$

where the ratio A/B in our case corresponds to that of the area of cracking to that of the semi-circle. From Figure 37 the area of cracking is given by:

$$A = \frac{\pi R^2}{2} - (R - a)\sqrt{2aR - a^2} - R^2 \tan^{-1}\left(\frac{R-a}{\sqrt{2aR - a^2}}\right) \tag{57}$$

The values of $f(A_c/B)$ for different A_c/B are assumed to be those for the single-edge notched specimen, and are given in Table 7.

Using the above expression for the stress intensity factors, the critical crack size in a 0.250 in. (6 mm) diameter wire has been computed for different values of nominal stress and fracture toughness. The relationship between maximum nominal stress and critical crack size is shown in Figure 38.

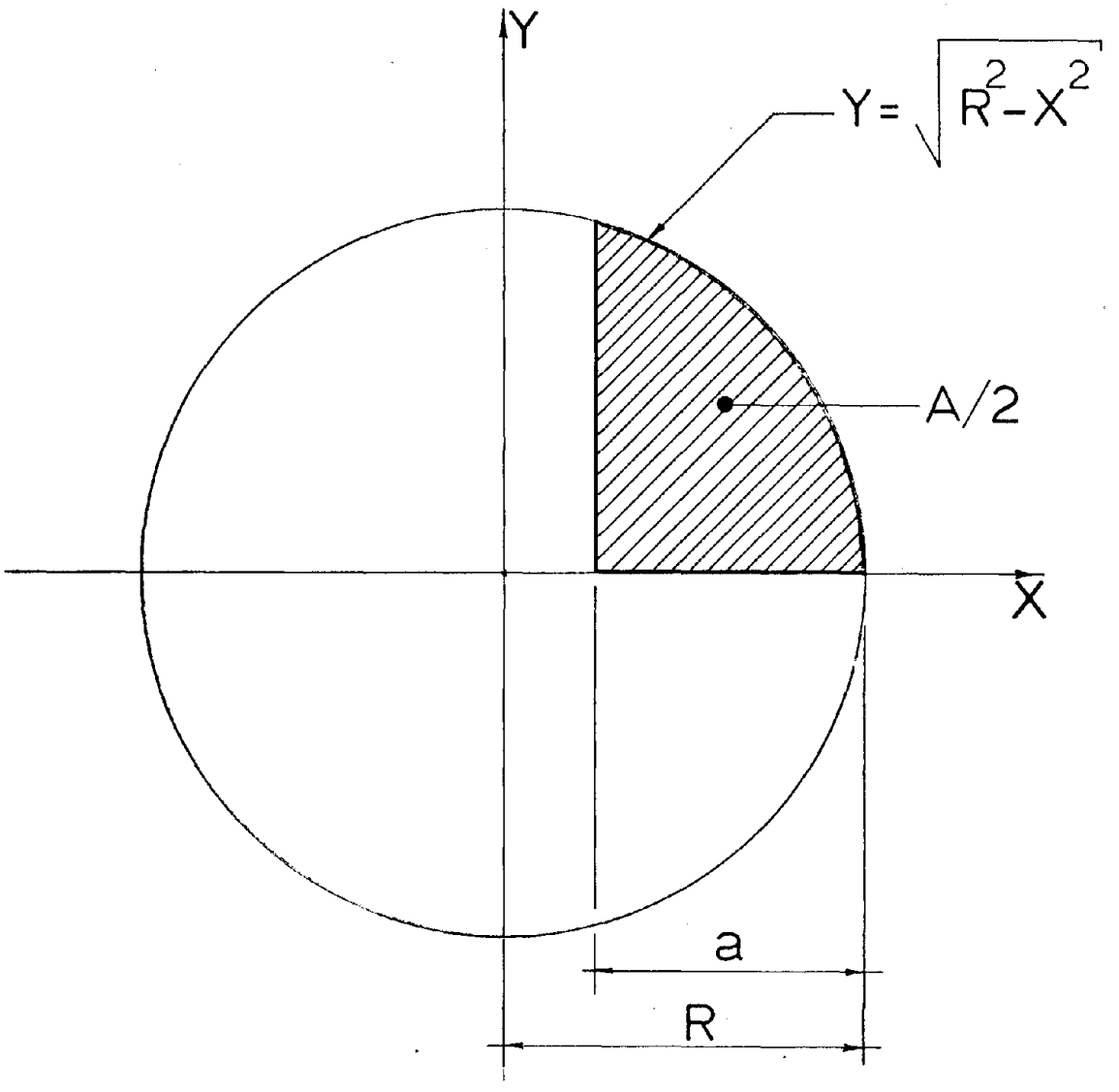

Figure 37. Approximate Representation of Cracking in a Wire

Table 7. Correction Factors for a Single-Edge-Notched Plate

a/b	f(a/b)
0.10	1.15
0.20	1.20
0.30	1.29
0.40	1.37
0.50	1.51
0.60	1.68
0.70	1.89
0.80	2.14
0.90	2.46
1.00	2.86

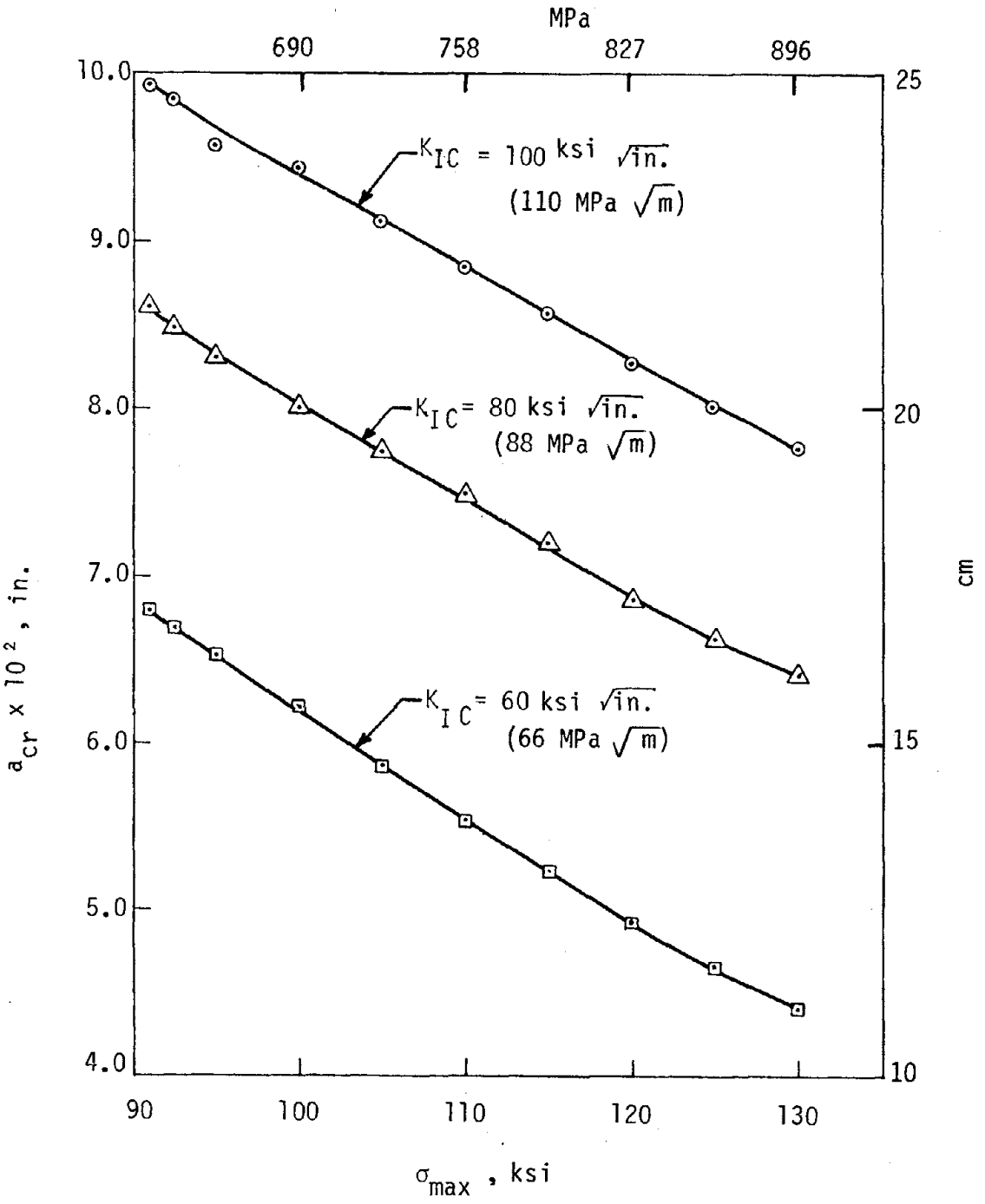

Figure 38. Relationship Between Maximum Nominal Stress and Critical Crack Size for Different Toughness Values.

6.4.3 Propagation Life

It was stated previously that the crack propagation in a wire can be approximated by the growth equation (42). The propagation life is obtained by direct integration of the growth equation. Thus, if N_p denoted the propagation life:

$$N_p = \int_{a_o}^{a_c} \frac{da}{0.66 \times 10^{-8} (\Delta K)^{2.25}} \tag{58}$$

The term ΔK is a function of $\Delta\sigma_{max}$ and a and, therefore, for a given value of $\Delta\sigma_{max}$, the above integral can be numerically evaluated. Figures 39 to 44 show the crack propagation life as a function of stress fluctuation $\Delta\sigma$ for different values of initial and critical crack sizes. In the absence of more specific information, the initial crack size, a_o, has been arbitrarily selected from a range of 0.01 in. (0.25 mm) to 0.05 in. (1.25 mm).

6.5 Total Fatigue Life of Wire and Cable

As mentioned earlier, the total fatigue life of a structural component is composed of two quantities namely, the fatigue crack initiation life and the fatigue crack propagation life. In the particular case of bridge cables, it was also stated that the initiation governs most of the total fatigue life. From the knowledge of crack initiation and crack propagation in a wire, as discussed in the preceding sections, an empirical S-N curve may be drawn. A set of such curves for different propagation lives (Figures 39 to 44) is shown in Figure 45. It can be seen that the S-N curves are very close to each other indiacting that the difference in propagation lives has little significance on the total fatigue life of a wire.

It is now important to comment on the analytical basis for fatigue life predictions. We have noted that the calculation of fatigue life by semi-empirical methods involves some form of curve-fitting through statistical data. Because of our limited knowledge of the parameters which affect fatigue life such as the fracture toughness, exponent of fatigue equation, load spectrum, etc., the statistical data may be widely scattered. In this case the prediction of fatigue life by an empirical law may produce unrealistic results. What is needed, therefore, is a statistical theory of fatigue behavior. According to

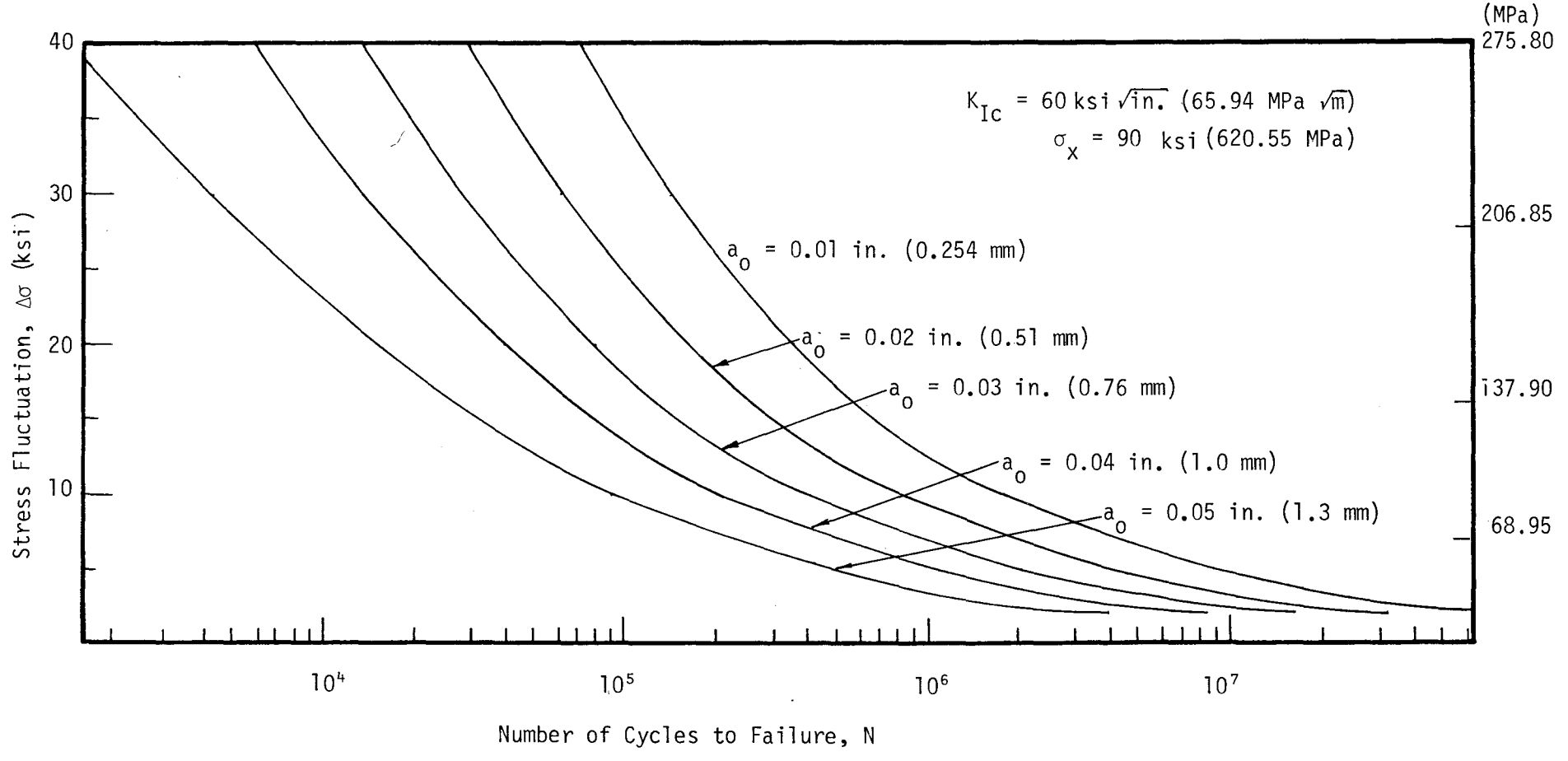

Figure 39. Crack Propagation Life of a Wire

(K_{IC} = 60 ksi $\sqrt{in.}$, σ_x = 90 ksi)

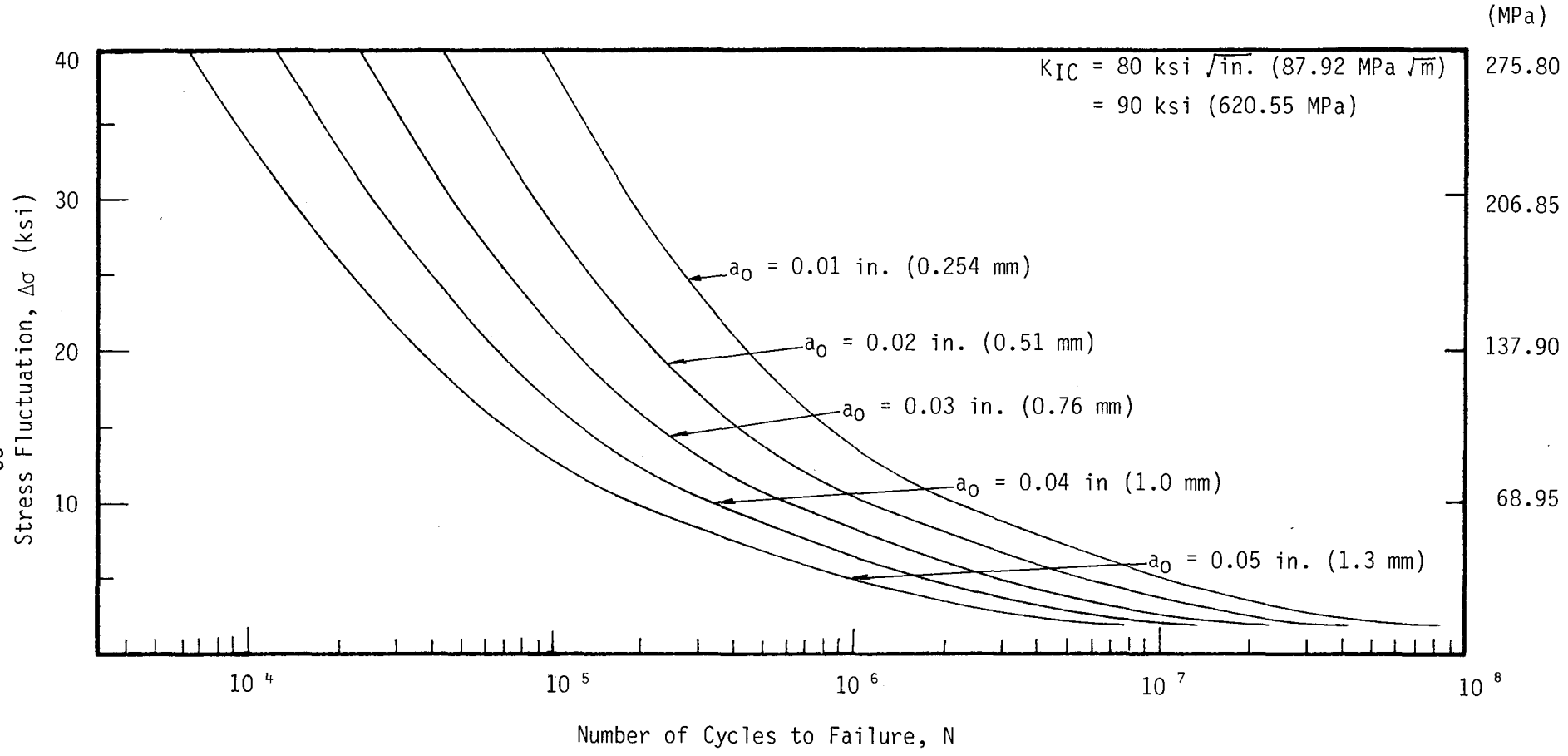

Figure 40. Crack Propagation Life of a Wire
(K_{IC} = 80 ksi $\sqrt{in}$, σ_x = 90 ksi)

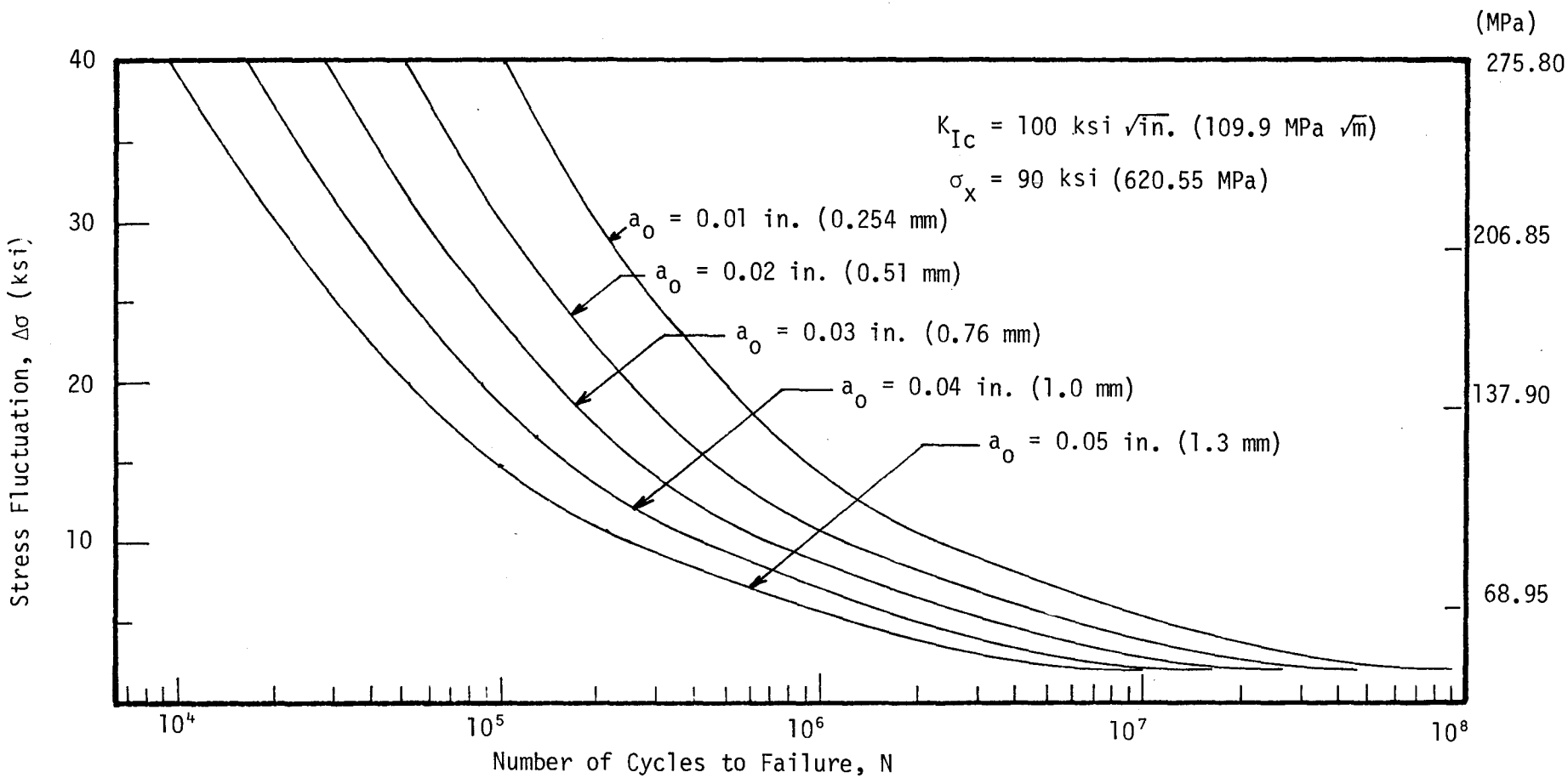

Figure 41. Crack Propagation Life of a Wire

(K_{IC} = 100 ksi $\sqrt{in.}$, σ_x = 90 ksi)

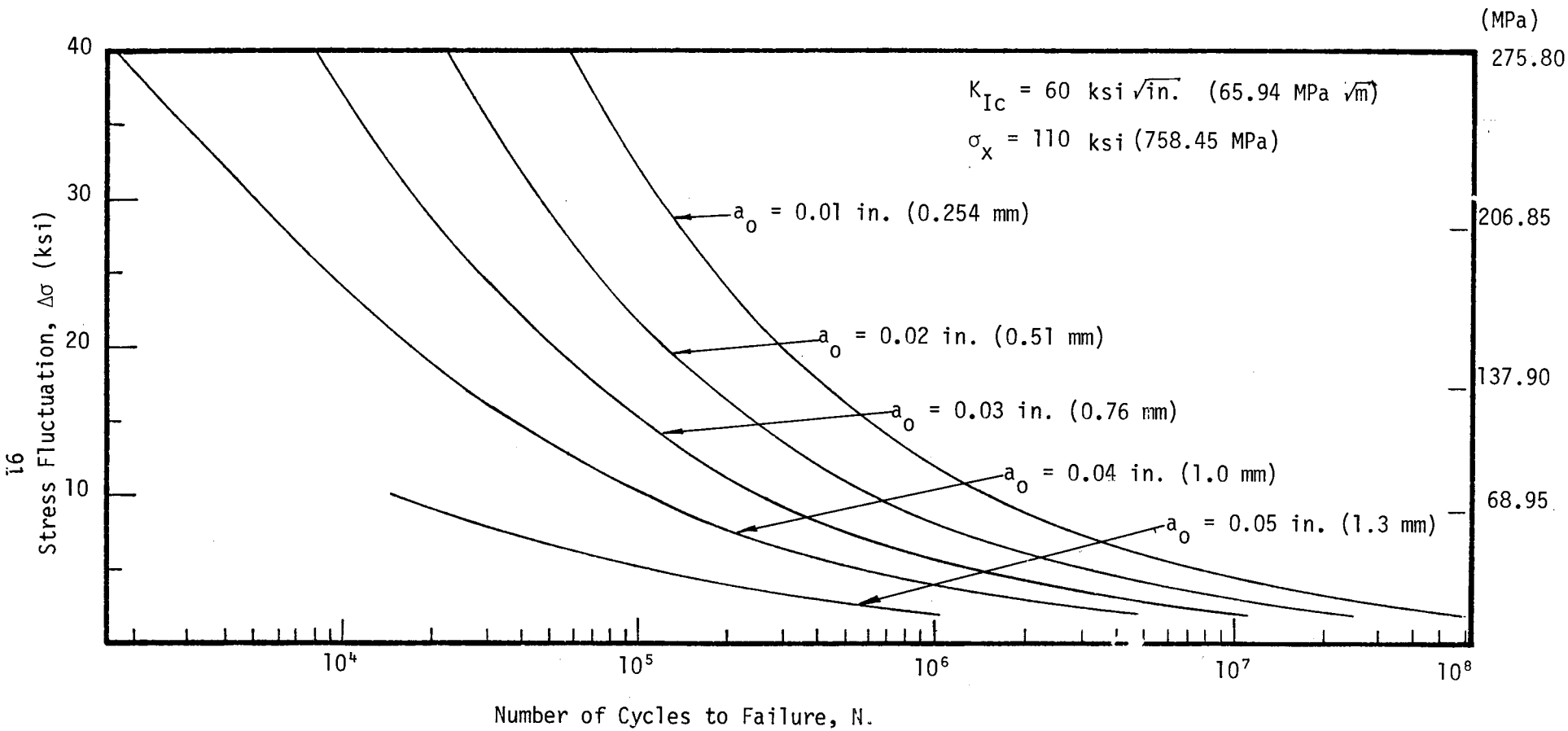

Figure 42. Crack Propagation Life of a Wire

(K_{IC} = 60 ksi $\sqrt{in.}$, σ_x = 110 ksi)

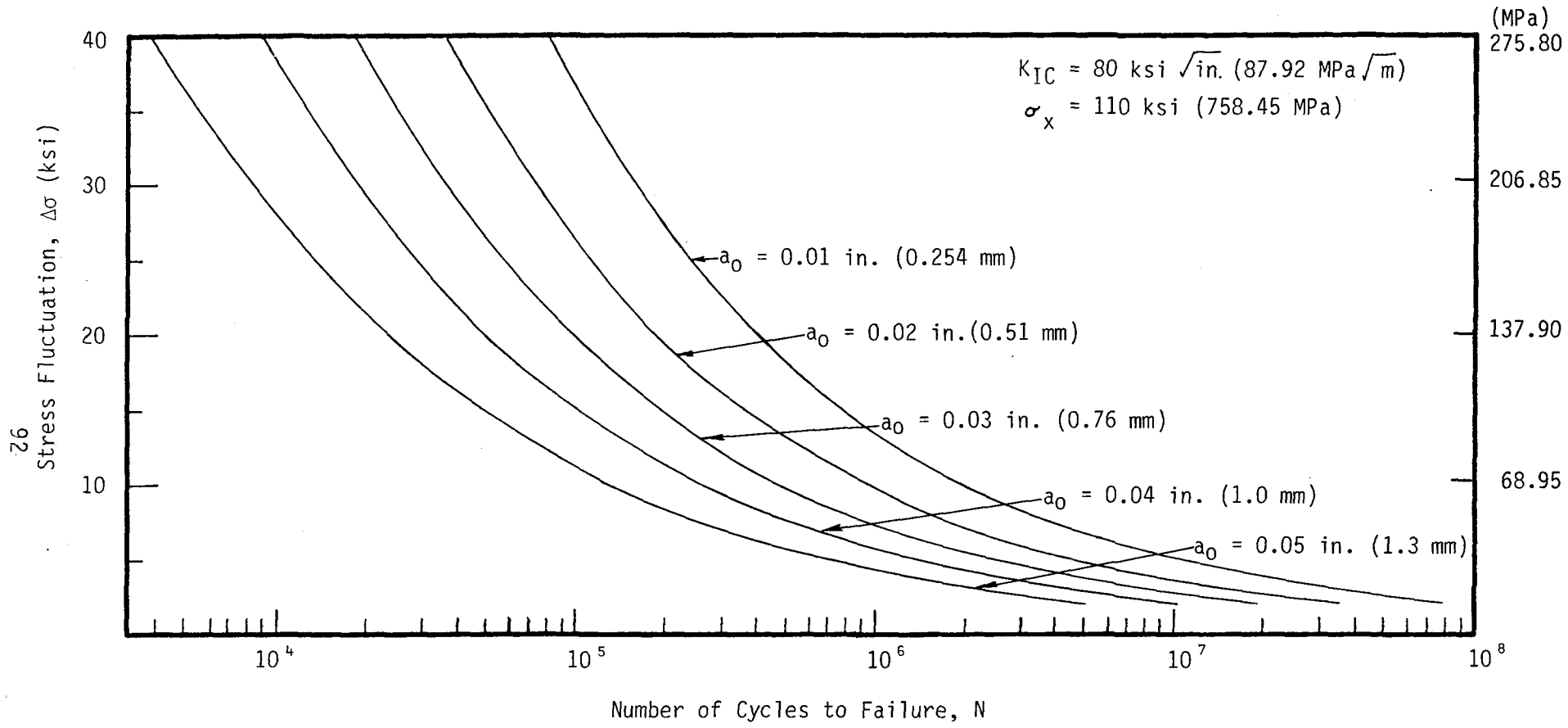

Figure 43. Crack Propagation Life of a Wire

(K_{IC} = 80 ksi $\sqrt{in}$, σ_x = 110 ksi)

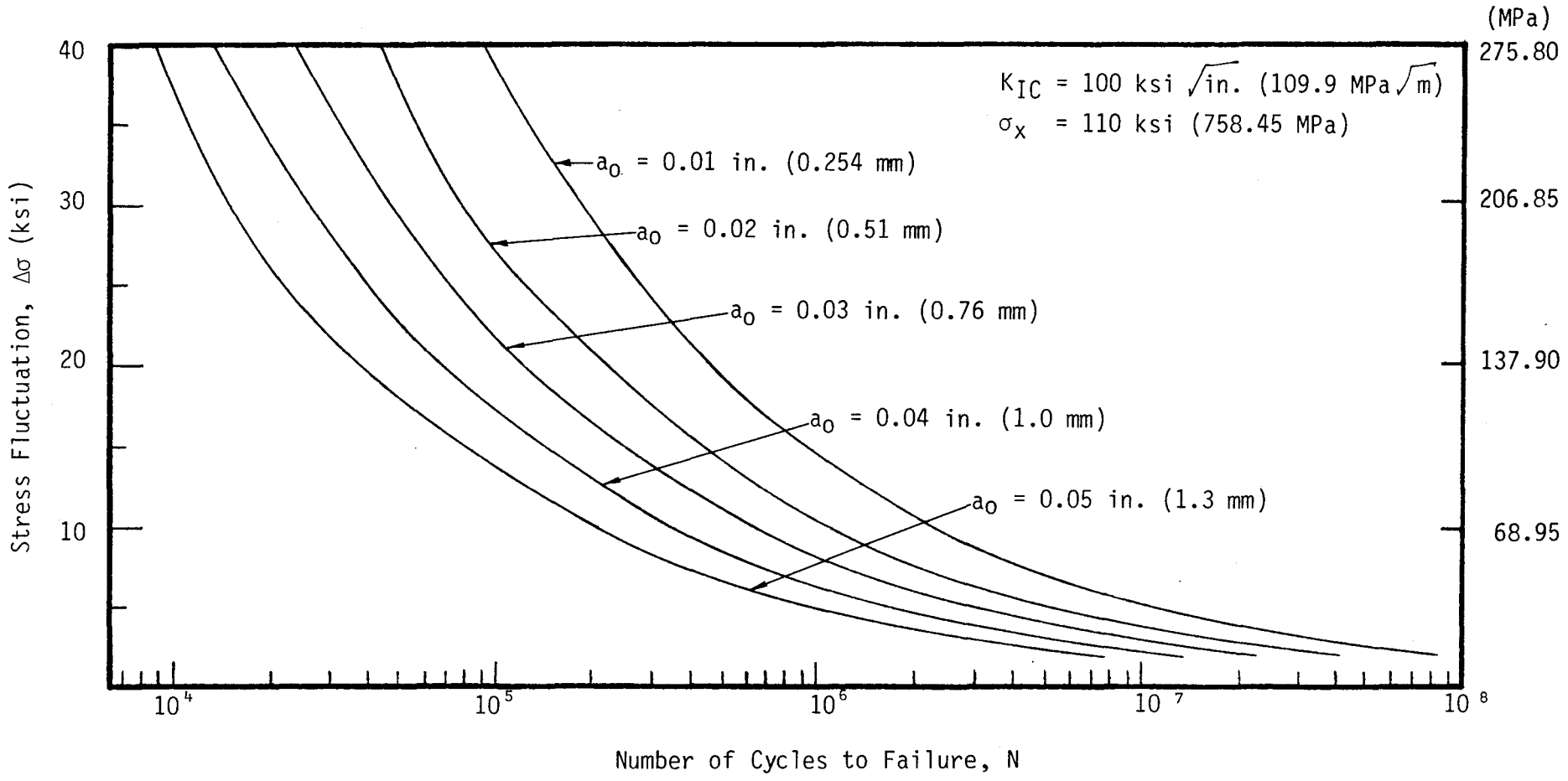

Figure 44. Crack Propagation Life of a Wire
(K_{IC} = 100 ksi $\sqrt{in.}$, σ_x = 110 ksi)

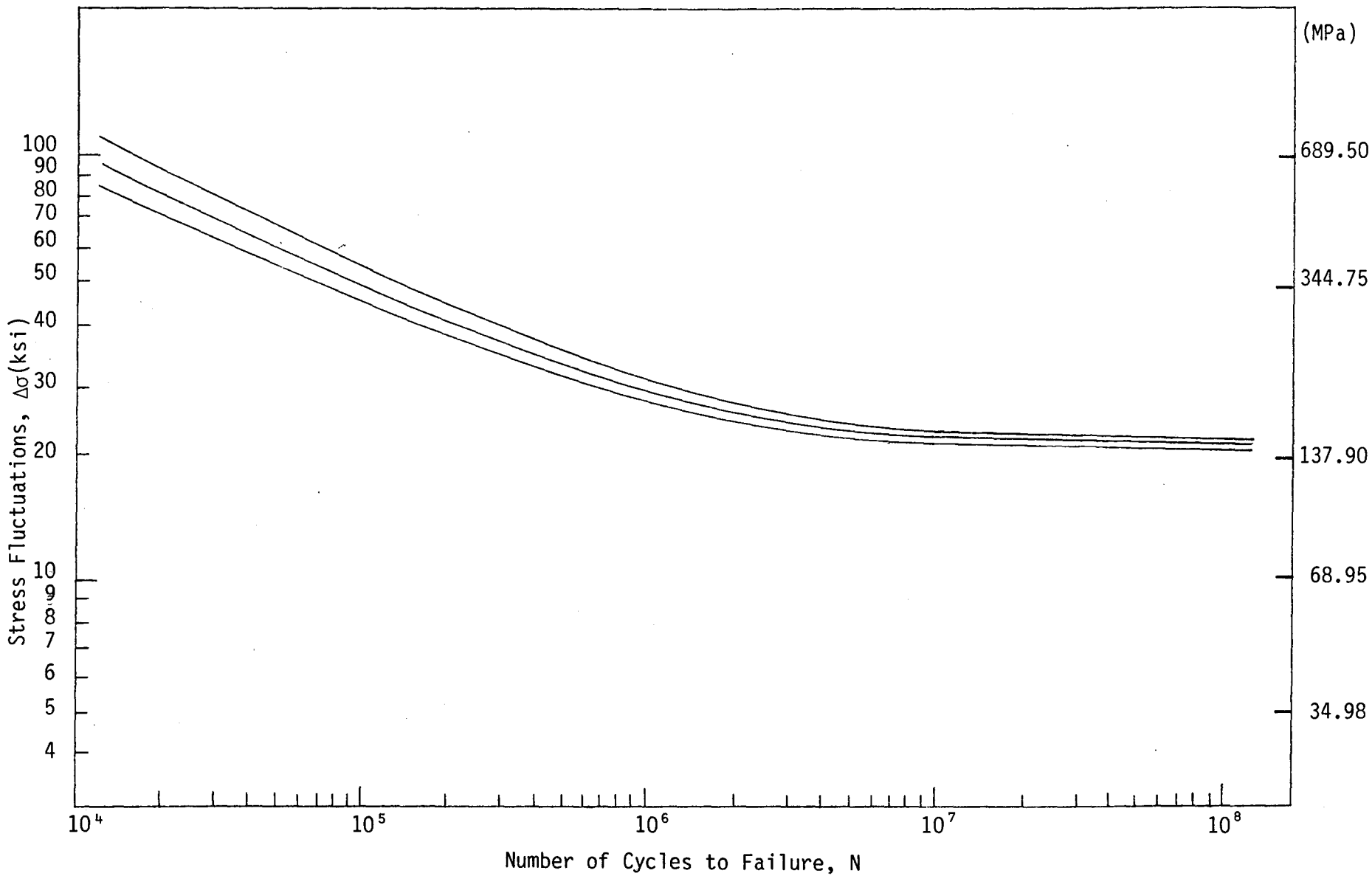

Figure 45. Total Fatigue Life of a Wire Showing the Dominance of Initiation Life (Initiation life is chosen to be more than 10^7 cycles)

this theory, the fatigue life of a wire is described in terms of a probability distirbution involving the ultimate strength of the wire material and the applied nominal stress. This type of analysis has its beginning in the poineering work of Weibull[54]. Much of the later development on the statistical aspects of brittle fracture was carried out along this line by Freudenthal[55] and on the statistical aspects of fatigue by Freudenthal and Gumbel[56]. More recently, Andra and Saul[57] proposed a statistical theory of fatigue of parallel wire cables based on the assumption that the wire failure is distributed binomially.

Following the statistical theory, the ultimate strength of a wire is considered to be distributed normally according to the following formula:

$$P(\sigma_u) = \frac{1}{\sqrt{2\pi}s_{\sigma u}} \exp \frac{-(\sigma_u - \langle\sigma\rangle)^2}{2s_{\sigma u}^2} \tag{59}$$

where $\langle\sigma_u\rangle$ is the mean ultimte strength and $s_{\sigma u}$ is the standard deviation of the ultimate strength. Similarly, applied stress is distributed as follows:

$$P(\sigma) = \frac{1}{\sqrt{2\pi}s_{\sigma}} \exp \frac{-(\sigma - \langle\sigma\rangle)^2}{2s_{\sigma}^2} \tag{60}$$

where $\langle\sigma\rangle$ and s_{σ} bear the similar meaning. The probability of a crack to be initiated in a wire is then given by:

$$P(\sigma \geq \sigma_u) = \frac{1}{\sqrt{2\pi}s_{\xi}} \exp \frac{-(\xi - \langle\xi\rangle)^2}{2s_{\xi}^2} \tag{61}$$

where the new variable ξ is defined by

$$\xi = \sigma - \sigma_u \tag{62}$$

so that

$$\langle\zeta\rangle = \langle\sigma\rangle - \langle\sigma_u\rangle \tag{63}$$

and

$$s_{\zeta}^2 = s_{\sigma u}^2 + s_{\sigma}^2 \tag{64}$$

Thus, the probability of crack initiation can be described in terms of the interference between two distributions $P(\sigma_u)$ and $P(\sigma)$ as shown in Figure 46.

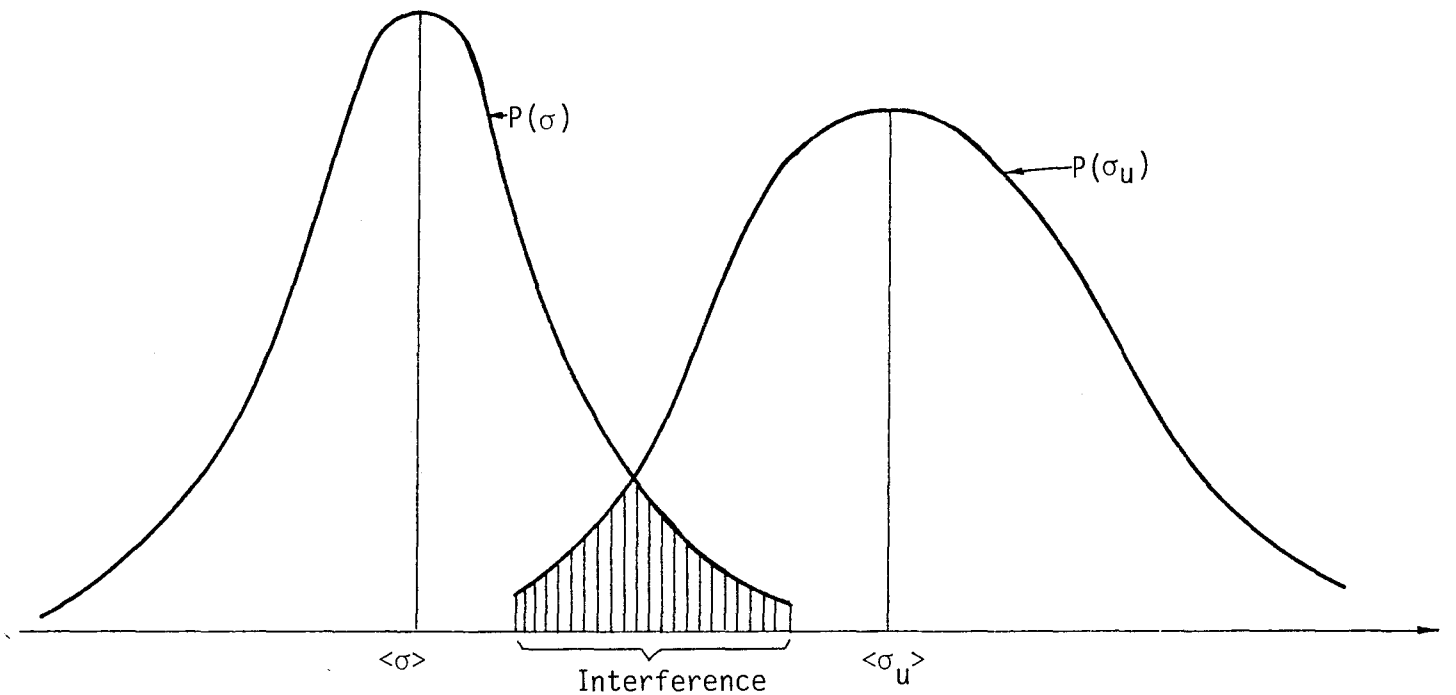

Figure 46. Interference Between Probability Distribution of Applied Nominal Stress and Ultimate Tensile Strength

The shaded area in Figure 46 represents the probability that the crack will initiate in a wire. For practical engineering application of the above concept, it is useful to think in terms of a laboratory test with several identical wire specimens. If such a test is conducted for the determination of crack initiation in a wire and if the two distributions, $P(\sigma)$ and $P(\sigma_u)$, are known, then the shaded area in the figure will indicate the percentage or fraction of the total number of wires in which cracks are initiated.

It should be noted that the above probabilistic description of the fatigue life of a wire inherently takes into account the effect of a spectrum of load range rather than a single load range. The consideration of a spectrum of load range is important in the study of the fatigue of bridge wires and cables from the standpoint of wind loading. The latter varies within a wide range corresponding to the diurnal and seasonal variations of wind speed. Consequently, it is more appropriate to consider several load ranges or a load spectrum and its effect on the fatigue life. A more versatile method of doing this from the standpoint of simplicity and engineering practicality is the use of Miner's Rule[58]. This rule allows the determination of the cumulative fatigue damage of a component if the fatigue damage due to individual loadings are known (see Figure 47). According to this rule, if N_1 is the fatigue life of the wire due to a load σ_1, N_2 due to σ_2, and so on, then the total fatigue life N is given by:

$$N = \frac{\Sigma\sigma_j N_j}{\Sigma\sigma_j} \tag{65}$$

It is interesting to note that the above derivation can be obtained as a special case of the more general probabilistic formulation described earlier. The fatigue life of a wire under a load spectrum ranging from 2 ksi (14 MPa) to 40 ksi (276 MPa) is shown in Figure 48.

While the fatigue behavior and fatigue life of a wire is of fundamental importance to engineers responsible for designing suspension cable and cable-stayed bridges, from a maintenance standpoint it is equally important to know the fatigue life of a cable. We note again that a cable is comprised of a large number of individual wires tied together in some fashion. It, therefore, appears that the fatigue life of a cable is several times larger than the life

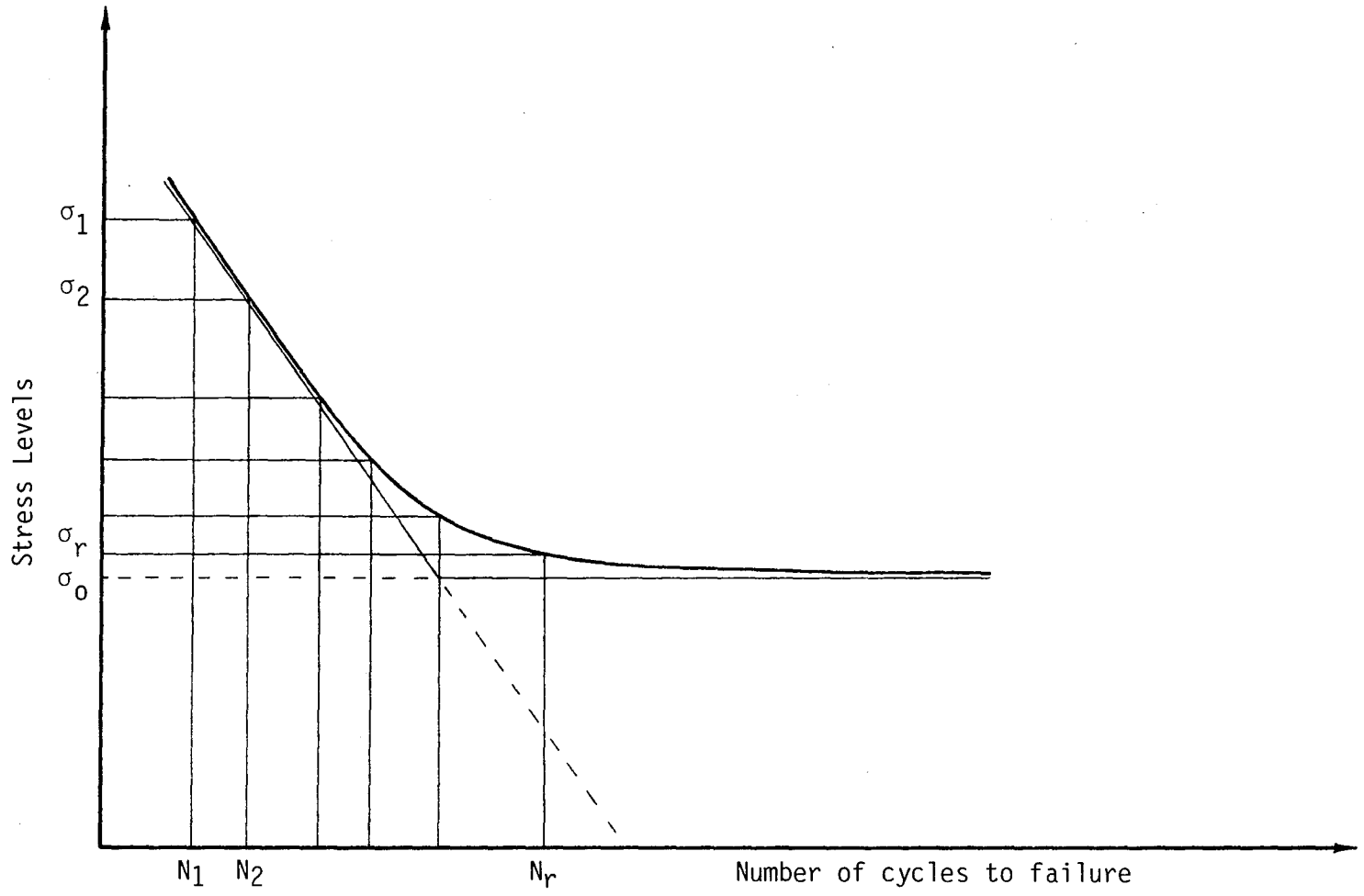

Figure 47. Representation of Cumulative Fatigue Damage of a Component due to Various Stress Levels

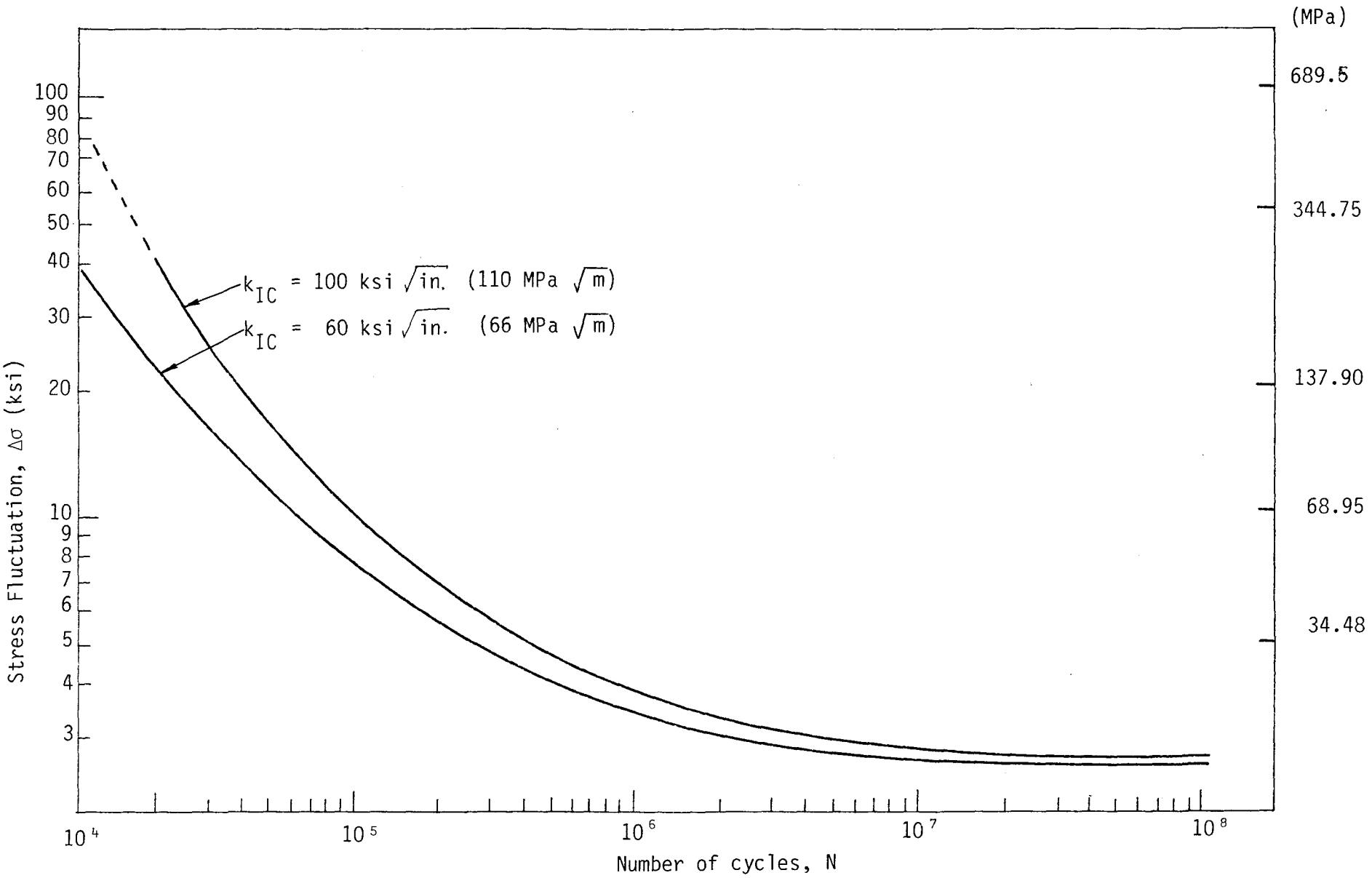

Figure 48. Fatigue Propagation Life of a Wire for Variable Load Range and for Different K_{IC} Values

of a single wire. However, Figure 49 makes it evident that the contrary is true, at least for helical cables. This striking phenomenon raises some interesting questions. For example, is the fatigue life of a cable related to that of a single wire? If so, how is the fatigue life of a cable determined?

Reemsnyder[42] concluded that there is little correlation between rope and single wire fatigue tests (see Figure 49). However, his data from the axial fatigue tests are too few to provide a good statistical fit and the error estimate appears to be too high. Therefore, any correlation, whether good or bad, loses its meaning. On the other hand, it is natural to consider that if an individual wire of a cable failed by fatigue, the load in the cable will be redistributed. If a sufficient number of individual wires have failed, the redistributed load will be large enough to exceed the ultimate strength, thereby rendering the cable to be structurally ineffective. This reasoning, when applied to a 0.250 in. (6 mm) diameter 283-wires cable (Prescon parallel-wire Group I cable for Pasco-Kennewick bridge), means that approximately 20% or about 56 wires may be allowed to fail by fatigue before cable replacement becomes necessary. However, this must be interpreted in terms of the number of loading cycles. To illustrate this, we consider two examples.

Figure 50a shows the section of a helically wound cable under the action of an external load. If the load is cyclic, repeated, and of sufficient magnitude, it will produce high degrees of stress concentration at the contact region giving rise to "strand nicking" as shown in Figure 50b. The nicks act as mechanical notches which considerably reduce the initiation life of a wire. This conjecture had been verified experimentally by Reemsnyder[42] (see Figure 49). In the case of parallel wire cables, there is practically no contact between the wires. However, if one looks at a parallel wire cable cable in bending, it will be apparent that the adjacent surface of two neighboring wires in a cable will have an opposite loading situation. If the external load is sufficiently large, this will create occasional contacts between the wires which again gives rise to stress concentration and mechanical notches. In either case, the life of a wire is greatly reduced. A rigorous estimate of the fatigue life of a cable requires detailed analysis which is beyond the scope of the present effort. Nevertheless, this study offers a rational explanation for Reemsnyder's[42] experimental

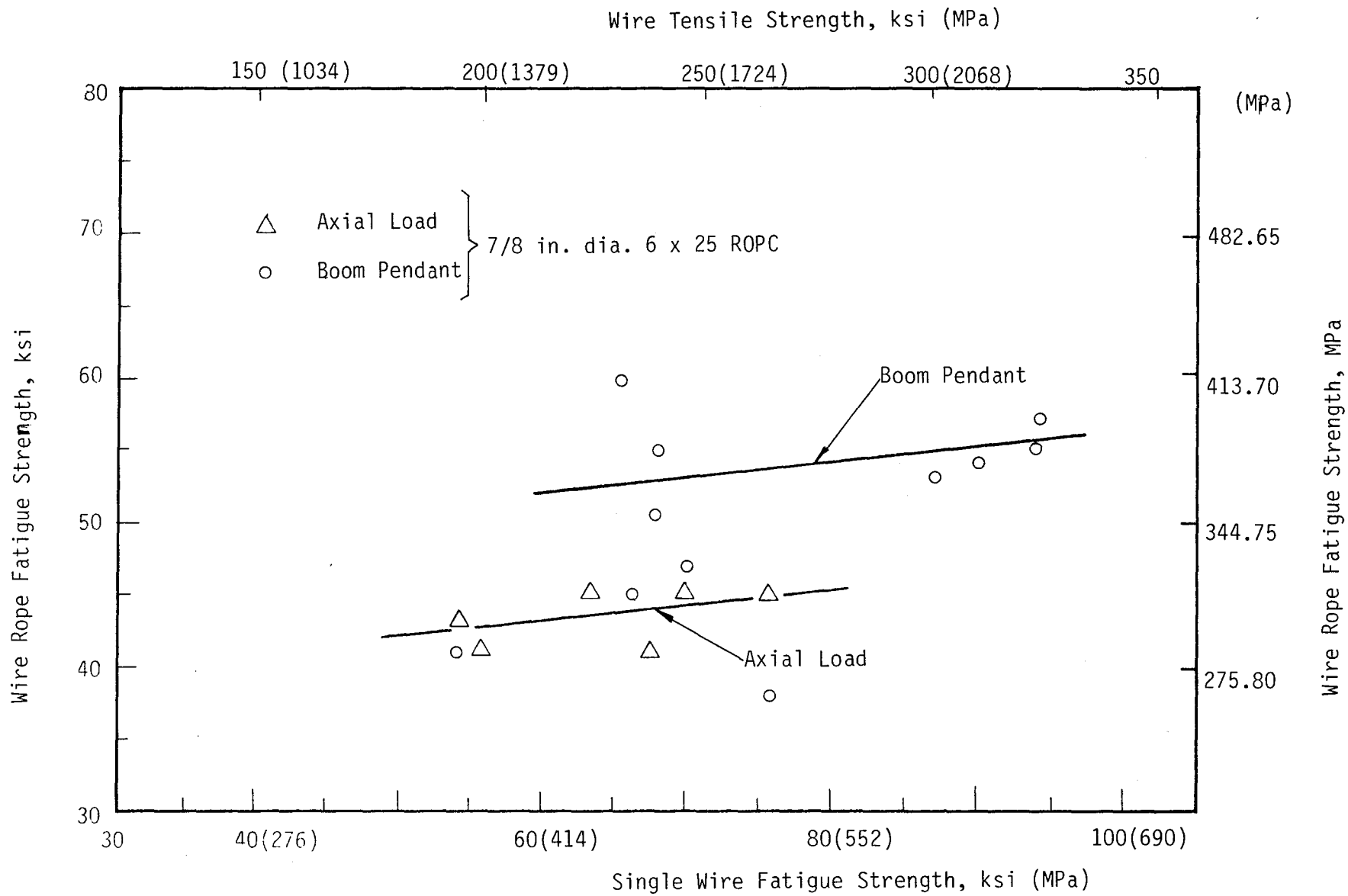

Figure 49. Comparison of Single Wire and Wire Rope Fatigue Strengths (Reemsnyder[42])

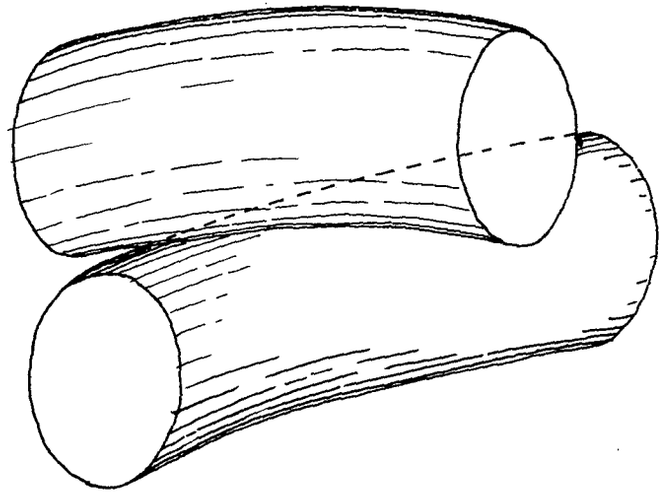

a. Section of a Helically Wound Cable

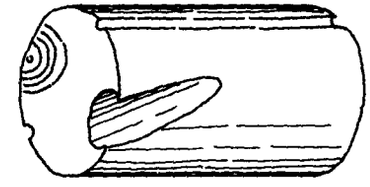

b. Strand Nicking

Figure 50. Strand Nicking in a Helically Wound Cable

results and attempts to find a correlation between the wire fatigue and cable fatigue life.

In concluding this section, we would like to touch upon the subject of fatigue failure of wires and cables at the socket end. In the past, this was a growing concern among the design engineers and users of cables who found that the socket failure in cables is more predominant. It is our understanding that, since the invention of swaged fittings, epoxy groutings, etc., this is no longer a case of grave concern. Our analysis shows that bending stress remains largest at the socket ends. However, due to swaged sockets and epoxy fillers, there is a gradual load transfer mechanism at the socket ends. Our preliminary studies of this mechanism in terms of viscoelastic modeling show that the magnitude of bending stresses in the latter case is about half as much as that in the case of rigid sockets.

6.6 Testing Data of Wires and Cables

The analysis of the fatigue behavior of bridge cables and wires presented above is very much intertwined with the experimental work on the subject. For example, the determination of fatigue crack propagation life requires the knowledge of fracture toughness K_{IC} which is experimentally obtained from fracture testing. Second, the results of fatigue experiments are used to construct S-N curves which, in turn, are used to verify the experimental results. For the sake of completeness of fatigue analysis, it is important to discuss the experimental work on fatigue testing of wires and cables.

Reemsnyder[42] has made a series of tests on wires, strands and ropes. In one of these experiments, the strand specimen was 0.75 in. (19 mm) diameter 1 x 37 wires of ultimate tensile strength 250 ksi (1724 MPa). The results of the experiment (axial fatigue load test) showed that at 50 ksi (345 MPa) stress range, the first wire breakage occurred at 2×10^5 cycles. At a stress range of 75 ksi (517 MPa), however, the first wire breakage occurred at 1.5×10^5 cycles. Other tests that Reemsnyder performed with different structural strands (1 x 19, 1 x 37, 1 x 55, 1 x 59 wires) indicated that for the same stress range, 1 x 19 strand had the lowest fatigue life. Some experiments also showed that bright strands had a higher fatigue life than did galvanized ones.

Fisher and Viest[43] tested prestressing wires and strands for fatigue life. Wires were 0.192 in. (5 mm) diameter made of steel consisting of mean ultimate strength 257.5 ksi (1775 MPa) (range between 250 and 264 ksi [1724 to 1820 MPa])and strands which were made of 0.375 in. (9.5 mm) diameter 7 wires with mean ultimate strength 270.4 ksi (1864 MPa) (range between 248 and 293 ksi [1710 to 2020 MPa]). The strands were tested at different stress levels with stress fluctuation ranging between 38.4 ksi (265 MPa) to 75.7 ksi (522 MPa) and with maximum stress between 197.3 ksi (1360 MPa) to 210.9 ksi (1454 MPa). The results showed that some strands did not fail after as much as 2.5×10^6 cycles at a stress fulctuation of 28.4 ksi (196 MPa). However, at the stress fluctuation of 75.7 ksi (522 MPa),the fatigue life of the same strand was reduced to as low as 3.8×10^4 cycles. The wires were also tested at different stress ranges. The results showed that some wires did not fail even after 7.5×10^6 cycles at a stress fluctuation of 33.5 ksi (231 MPa). At a higher fluctuation of about 97.8 ksi (674 MPa), the fatigue life was sharply reduced to 10.4×10^4 cycles. In either case, the experimental results conclusively showed that the single wire fatigue life is longer than the fatigue life of strands.

Jevtic[59] tested fatigue behavior of 0.1 in (2.5 mm) and 0.2 in. (5 mm) diameter cold-drawn wires at elevated temperatures and found that the rupture strength of wires drops sharply beyond a temperature of 392° F (200° C). The testing was done at zero-to-tension loading and Jevtic derived from the experimental results the limits of fatigue behavior of the cold-drawn wires.

Bennett and Boga[60] tested cold-drawn wires used for prestressed concrete and found that crimped and indented wires have a much lower fatigue limit than the smooth wires. The specimens used by Bennett and Boga consisted of 0.276 in. (7 mm) diameter cold-drawn wires. The specimens were tested between an applied minimum tensile stress level (S_{min}) to a maximum tensile stress level (S_{max}) chosen to be very close to the ultimate strength of the wire (208 ksi [1434 MPa]). The minimum stress level was kept constant during a series of tests but varied between 102.8 ksi (709 MPa) to 142 ksi (979 MPa) during different series of tests. Bennett and Boga found out that fatigue

life of a wire increased for larger values of minimum stress levels. The reason for this is attributed to a smaller value of the range of fluctuating stress.

Cullmore[61] tested the fatigue strength of high tensile steel wire cable subjected to stress fluctuations of small amplitude and found that in all tests, failure occurred in one of the outer helical wires. An explanation of this phenomenon may be found in our analysis of the bending stress (Section 4.2.2) whereby we have concluded that outer wires have a wider range of stress variations than the core wire. Cullmore also noted fretting to be a dominant phenomenon causing the failure of a helical wire cable. His fatigue data on the fatigue life of a wire indicated an endurance limit of 38 ksi (262 MPa) at a mean stress level of 80 ksi (552 MPa) which is double that of the value for a cable (18.8 ksi [130 MPa]). The most important conclusion Cullmore had drawn from his work was that there was no minimum value of the stress fluctuation below which failure of a cable would not occur in less than ten million cycles.

Edwards and Picard[62] carried out fatigue tests on 0.5 in. (12.7 mm) diamater seven-wire prestressing strands. These tests were in connection with the analysis of the fatigue behavior of prestressing strands in both concrete and free air environments. The effect of lateral pressure simulating the environments as well as the effect of test length on the fatigue life were reported by the authors. In arriving at their conclusion, Edward and Picard made a statistical regression analysis of the test data in a manner very similar to that employed by Fisher and Viest[43].

Fleming[63] performed fatigue testing on specimens of one inch (25.4 mm) diameter, 19 wire helically wound galvanized steel strand to establish the effect of the load variables such as load range, mean load and maximum load upon the fatigue life. The results from the test showed that the maximum load and mean load had very little effect upon the fatigue life. During the experiment, it was observed that the wire breakage occurred randomly throughout the length of the specimens and were not concentrated at any specific location.

Castellaw, Frank, and Campbell[64] tested Pasco-Kennewick bridge cables for fatigue failure under axial loading. The specimen was made of 83 - 0.25 in. (6 mm) diameter of 240 ksi (1655 MPa) ultimate strength and the cable had an outer diameter of approximately 4 in. (10 cm). The maximum stress level was 108 ksi (745 MPa) with a fluctuation of 24 ksi (165 MPa) and the specimen was cyclically loaded for 2×10^6 cycles. No fatigue failure of wires was observed. The limited experimental results briefly described here, and an extensive literature search by CHI engineers during the course of the project revealed that few experimental works on the fatigue of bridge cables exists. This is partly due to the fact that suitable fatigue experiments are difficult to conceive and design in the case of a 0.250 in. (6 mm) diameter wire. We shall discuss this issue in more detail in the section dealing with recommendations for future research.

CHAPTER 7
DISCUSSION AND CONCLUSION

7.1 Discussion of Results

In the preceding chapters, we developed analytical formulations for the dynamic response and fatigue behavior of stay cables in bridges. Based on them, we determined the deflection and bending stresses in typical cables in the Pasco-Kennewick bridge. The fatigue analysis was presented in Chapter 6, and with that we have also estimated the approximate fatigue life of wires and cables in a wind-induced vibration environment. In this section we will review the results obtained therein.

From the numerical results of deflections and bending stresses (see Example 2 in Chapter 5), one can notice that the deflection is nearly constant for all wind speeds. This is in apparent contradiction to the intuitive notion that the higher the wind velocity, the higher the excursion should be. To provide an explanation we recall the following observations made elsewhere in the text.

1. The resonance mode contributes primarily to the amplitude of excursion of deflection while the net contribution of all other modes is insignificant. This is so even though modal superposition is considered in the numerical computation of the deflection.

2. The analytical model of vortex excitation considered in this report assumes that the wind force be harmonic and that its magnitude varies quadratically with the wind velocity.

The second item indicates that the deflection is linearly dependent on the critical wind velocity which increases with the mode number. The first item indicates that the nondimensional deflection decreases with the mode number. For this reason, the maximum deflection, being a function of non-dimensional deflection and wind velocity, yields a nearly constant value for all modes.

Despite the fact that deflections remain nearly constant, the bending stresses are higher for higher modes. However, because of inherently low moment of inertia of the cable far enough away from the end-anchorages, the maximum value of bending stress is relatively low. For instance, in Example 2

of Chapter 5, we find that the bending stress in a 506 ft (154.23 m) long, 4.75 in. (12.07 cm) diameter cable is less than 2,685 psi (18.511 MPa).

Near the end-anchorages, one can expect a much higher flexural stress. The magnitude of the stress depends on the cable anchorage system and the end support conditions, among others. The exact value of moment of inertia at the end anchorage is hard to ascertain but, due to the constraint of wires from relative movement with respect to one another, is probably many times higher than that in the middle. Therefore, it is reasonable to expect high bending stress at the ends of a cable. This seems to explain the intuitive notion of earlier design engineers that the end-anchorage is the weak point of a cable.

In regards to determining natural frequencies and critical wind velocities, results from the present analysis indicate that long flexible stay cables are prone to resonant vibration at some wind velocities at a particular site. This is so because, at higher modes, the natural frequencies are densely populated and hence, increment in critical wind velocities corresponding to two consecutive resonance modes is quite small. At many sites the wind data show that the velocity increment may be easily exceeded by the usual fluctuation of wind speeds. This means that, if a particular cable is designed out of resonance with respect to a specific mode, it does not necessarily guarantee that the cable will not vibrate in the next higher or lower mode. Fortunately, at higher modes, the deflection is also small, and the wind-induced bending stress can be easily kept to a reasonably low value by proper selection of cable construction and end anchorages. It should be noted here that it is the fatigue phenomenon caused by reversible or cyclic bending stresses that are damaging, not the high stresses, per se.

In the analytical formulation of the fatigue behavior of wire ropes and cables, we have made use of fracture mechanics methodologies. In other words, we have attempted to describe the fatigue crack initiation and propagation in a wire in terms of such parameters as the threshold stress value, the stress intensity factors, and others. Certain simplifying assumptions are inherently involved in this approach, and it is quite likely that some of these assumptions may not be justifiable on the grounds that the fracture mechanism in a high strength steel wire of small diameter (0.25 in. [6 mm]) is far more complex than that in a plate, beam, or shell of reasonably large dimensions. Moreover,

the validity of the fracture mechanics approach cannot be guaranteed when one tries to explain the fatigue behavior of a whole cable in terms of its constituent wires. Nevertheless, the present approach provides some guidelines in understanding the fatigue behavior of wires and cables.

From the analysis of fatigue initiation in a wire, we have determined the endurance limit and the fatigue initiation life which is consistent with the fracture mechanics methodology. The value of endurance limit for the type of steel wire used in Pasco-Kennewick and Luling bridge construction has been found to be approximately equal to 160 ksi (1103 MPa). The wires used in the cables to construct these bridges has an ultimate tensile strength of 240 ksi (1655 MPa) and maximum working stress (excluding cyclic bending stress) of 108 ksi (745 MPa). This means an unnotched, dislocation-free single wire can sustain a bending stress up to 52 ksi (358 MPa) without exceeding its endurance limit. In the examples provided in Chapter 5, we found that the maximum bending stress in a cable corresponding to a wind velocity as high as 52 mph (83 km/hr) is about 2.6 ksi (17.9 MPa). Even if we assume that the ends of the particular cable in question is 20 times less stiff, no fatigue crack will be initiated in an otherwise fault-free wire. Thus, according to classical fracture mechanics, the fatigue crack in a wire, does not initiate below 10^7 cycles of load applications.

It is an accepted fact that the fatigue life of a high strength steel specimen is largely dominated by its initiation life, as may be evidenced by the order of magnitude comparisons between fatigue initiation life and fatigue propagation life. The fatigue crack propagation curves obtained in Chapter 6 demonstrate that, even at lower ranges of stress fluctuations, the crack-initiation life is at least ten times larger than the crack-propagation life. This indicates that crack-initiation life constitutes more than 90 percent of the total fatigue life.

The computation of the fatigue propagation life of a single wire has been based on empirical crack propagation law for high strength martensitic steel. In a strict sense, the law has not been verified for steels having ultimate tensile strength higher than 212 ksi (1462 MPa), nor for material which was cold-drawn extensively. Fortunately, for high-strength wires we have just

indicated that the propagation life is only a small fraction of the total life. It is hoped that approximation of the fatigue propagation life will not materially affect the total life of a wire.

Finally, in this report we have attempted to correlate the fatigue life of a wire to a cable in terms of a simplistic approach. In this approach, the cable failure is imminent when the effective stress in the unbroken wires in the cable exceeds ultimate tensile strength. For Pasco-Kennewick Group I cable (283 wires of 0.25 in. [6 mm] diameter), this means approximately 20 percent of the wires can suffer fatigue failure before cable replacement becomes necessary. This should in no way be construed to mean that the fatigue life of Pasco-Kennewick Group I cable is 20 times that of the fatigue life of a constituent wire. It has already been stated that the fatigue life of a cable should be lower than that of a wire. We have offered in Chapter 6 a substantive explanation for this apparent paradox. Within the scope of this contract, it has not been possible to derive a rational relationship between fatigue life of wires and cables by simple extension of analytical formalism.

Summarizing pertinent results, we note that the CHI ASSOCIATES, INC.'s investigation on the analytical formulation of the fatigue behavior of highway bridge cables under wind induced vibration, as well as the content of the report, may be used by the designers of cable-stayed and suspension bridges in the following manner:

1. Formulations presented in the analysis of the dynamic response of bridge cables offer a method to compute natural frequency, critical wind velocity, deflection and bending stress.

2. Formulations presented in the fatigue analysis of bridge wires and cables offer some estimate of the initiation, propagation, and total fatigue life of a wire, and provide some guidelines for the determination of the fatigue life of a cable.

7.2 Concluding Remarks

In the foregoing chapters of this report, we have presented a simplified analytical formulation of the fatigue behavior of bridge wires and cables under wind-induced vibration. It is our understanding, as derived from various discussions with the researchers and experts in the field of structural mechanics, that such a study is the first of its kind. While the results from the study

are not in every respect complete, it is our opinion that the study provides some guidelines and motivation for further research on this subject. We shall outline in Chapter 8 a few recommended research programs designed to bring about a more complete understanding of the fatigue behavior of cables and wires.

We note here that the scope of the present investigation, as well as the content of the report, is basically analytical in nature. We have simplified the analysis to the extent that, we believe, is useful to design engineers. For example, within the framework of the assumptions made in the analysis, our results provide bridge designers with a method by which they can compute deflections and stresses in cables. Further, it provides bridge engineers with an estimate of the fatigue life of wires and cables. This knowledge is important from the standpoint of reliability and maintainability. However, we do not wish to suggest that figures, charts and tables derived in this report should be used without discretion. In fact, the bridge designer must first determine if, in a particular cable design, all assumptions and criteria used in the present analytical development can be justifiably incorporated.

In conclusion, we state that much work, both analytical and experimental, is still needed for a complete understanding of the subject. Only then it will be possible to provide bridge designers with rigorous tools to carry out fatigue designs of stay cables.

CHAPTER 8
RECOMMENDED FUTURE RESEARCH

A more complete understanding of the fatigue behavior of bridge cables and wires requires an extensive amount of additional research in several areas. We shall first enumerate these research areas and then outline some recommended research programs in each of these areas.

1. Fatigue initiation in a single wire.
2. Fatigue behavior of wire under variable amplitude and random loading.
3. Correlation between wire fatigue and cable fatigue.
4. Fracture toughness of wire materials.
5. Environmental effects on fatigue life of wires.
6. Fatigue testing of wires and cables.

Fatigue Initiation in a Single Wire

Wires used in bridge cables are made of high strength steel having martensitic structure. During constant amplitude cyclic loading, a wire will undergo strain-softening, thereby producing dislocation slips. The resulting dislocation pile-ups will form microvoid. It is believed that microvoid coalescence is the mechanism which initiates a fatigue crack. However, from the standpoint of design engineering and application, the above metallurgical explanation of a possible fatigue crack initiation mechanism in a single wire is far from being sufficient for understanding the fatigue behavior.

To the best knowledge of the authors of this report, there is no quantitative figure at this point to indicate what should be termed crack initiation in a 0.25 in. (6.35 mm) diameter single wire. This lack of knowledge is largely due to the extreme difficulty of observing microstructural changes due to the fatigue process in a high-strength martensitic steel. In this context, it should be noted that some efforts in the past have been undertaken by Southwest Research Institute to develop an acoustic device for detecting fatigue crack. The adoption of such a device for the detection of fatigue crack initiation in a thin wire deserves careful investigation.

A problem associated with practical engineering interests is concerned with determining the fatigue initiation life of a thin wire. Once again, there is at this point no quantitative figure to indicate exactly what fraction of the total life is due to initiation. However, it can be ascertained that once a crack is sizeable in a wire specimen, hardly any time will elapse before the wire breaks. Therefore, for all practical purposes, a visible crack in a thin wire means the termination of wire life. At the same time, the long service life of a wire under commonly occurring service conditions is indicative of its high resistance to fatigue.

The above remarks are sufficient to establish the importance of further research into the accurate prediction of fatigue initiation life. In this report, we have outlined two possible methods to determine initiation life. The first of these methods relates the fatigue initiation life in a single wire to the applied load or load fluctuation, material properties and strain-hardening exponent. The relationship can be derived semi-empirically using experimental results. We, therefore, recommend that some fatigue crack initiation tests, similar to the one carried out by Barsom for HY-130 steel, be performed.

The second method to determine initiation life is also semi-empirical and is based on experimental results relating the initiation life to the notch radius and notch toughness factor. In the case of a thin wire, it is, however, difficult to conceive an experiment with notched specimen, particularly since a notched wire is likely to exhibit a rapid fatigue failure which is not indicative of its initiation life. We, therefore, consider that some research effort be expended to develop a meaningful experiment along this line.

Fatigue Behavior of Wire Under Variable Amplitude and Random Loading

Bridge cables are subjected to two major loading conditions: (1) impact or dynamic effects due to live load; and (2) wind loads. The live load has variable amplitude and is often random in nature while wind loads are almost always random. It is, therefore, reasonable that the fatigue behavior of wire be studied under the conditions of variable amplitude and random loading.

Within the scope of the present contract, we have studied the fatigue behavior of wires and cables under wind loads considering the latter as having variable amplitude. We have also presented some rudimentary ideas in the report which accounts for the random nature of the wind load. Unlike the conventional root mean square analysis, our approach considered a reliability type analysis in which the fatigue damage of a wire was expressed in terms of the interference of two probability distributions, namely, those of strength and applied stress. This latter approach is more rational, since it not only incorporates the random nature of wind loads, but also considers random response of material. The approach is certainly more promising, and it is strongly recommended that further analytical work be pursued in this area to obtain a better understanding of the fatigue behavior.

Correlation Between Wire Fatigue and Cable Fatigue

Reemsnyder has done some experimental work on both wire and cable (strand) fatigue and has concluded that there is no apparent correlation between the two corresponding fatigue lives. Fisher and Viest have also done some experiments on the fatigue lives of wires and strands, but have not made any attempt to correlate results. Reemsnyder's experimental data were far too sparse and showed a wide scatter. Besides, it is not clear just what methods of fatigue testing were used for wires and ropes and whether the experiments were consistently reproducible. Therefore, the conclusion reached by Reemsnyder is not definitive and this area of research requires further consideration.

We recommend an analytical approach for the correlation study between wire fatigue and cable fatigue. The approach is based on the consideration that when a single wire in a cable fails by fatigue, a gradual load transfer mechanism takes place. The physical model is, therefore, one which reflects the connection between the applied stress distribution in a single wire to that in the cable. Taking into account that the strength distribution in each wire is identical, the approach leads to the relationship between the fatigue life of a cable and that of a wire.

As discussed earlier, the fatigue process in a single wire due to wind loads is random in nature. The same is true for any wire in a cable. In general, one can assume that the fatigue behavior of each wire is statistically

independent. However, it is conceivable that when the wires form a cable, the gradual load transfer mechanism imposes a conditionality on subsequent wire failures based on how and when the first wire fails. This type of rationalization of the fatigue process in a cable gives rise to a stochastic model which can be readily incorporated in the above analytical approach.

Parallel to the analytical study of correlation between wire fatigue and cable fatigue, it is highly recommended that extensive, but carefully designed experiments be performed to generate sufficiently large sets of fatigue data for single wires and cables. In addition to providing a reliable data base for design engineers, such an effort will be useful in verifying the analytical models for cable fatigue.

Fracture Toughness of Wire Materials

The conventional fracture mechanics approach to determine the fracture toughness under static loading is to follow the K_{IC}-test method (ASTM E399-74) developed by the American Society for the Testing of Materials (ref. ASTM STP-463). The test method has stringent requirements on specimen sizes to insure the accurate reproducibility of test results. For this reason, the application of the method to structures like thin wires and cables has not been successful. On the other hand, for fracture and fatigue analysis, it is essential to know the value of K_{IC} either experimentally or analytically. Therefore, this area constitutes another forefront of research.

The analytical method of determining K_{IC} entails the derivation of an expression for the stress intensity factor K_I. In the present report, K_I for a single wire was approximated by several expressions. One expression is a direct extension of the original analytical work by Folias for circumferential cracks on a hollow cylinder to the case of a solid cylinder. The analytical basis of such extension was not investigated within the scope of the present contract. It is, therefore, recommended to pursue this investigation.

Another approximate expression for K_I considered in this report is involved with the finite element analysis of circumferential crack in a solid cylinder.

The original work was due to Hilton and Sih and a numerical solution of axi-symmetric crack problems in a solid cylinder with a circumferential edge crack was given for a crack length to specimen radius ratio of 0.4 and 0.5. It is recommended that this type of finite element analysis for different crack sizes and geometries be pursued.

The analytical expression for stress intensity factor will directly lead to the determination of fracture toughness once the maximum design load is known and the critical crack length is found experimentally or otherwise.

Environmental Effects on Fatigue Life of Wires

In general, fracture toughness of high yield strength (above 140 ksi [965 MPa]) steels is not very sensitive to a change in temperature. However, if a particular bridge site experiences a severe seasonal temperature fluctuation, cables and wires will undergo a thermal stress reversal in addition to stress reversals due to mechanical and wind loading. The magnitude of thermal stress fluctuation may be significant to cause a reduction in the fatigue life.

Corrosion fatigue is another area which requires some attention. Corrosion may not be a severe problem for cable-stayed bridges in the United States primarily because stayed cables are jacketed with PVC cylinders. On the other hand, several suspension type cable bridges have bare cables and some have zinc-coated and galvanized cables. During the lifetime of these cables, corrosive environments affect their fatigue behavior considerably. We, therefore, recommend to look into the problem of environmental effects on fatigue life of wires.

Fatigue Testing of Wires and Cables

An examination of a specimen failed by fatigue generally reveals some qualitative information. For example, if the fracture surface of a specimen is flat, it indicates the absence of an appreciable amount of gross plastic deformation during service life. The flatness of the fracture surface can be ascertained by naked eyes, optical microscopy or electron microscopy depending on specimen and crack size and scale of measurements. In some cases, it may even be possible to obtain a quantitative estimate of the fatigue life

based on an analysis of the characteristic markings on the fracture surface called the "striation lines." However, this does not give a complete understanding of the quantitative aspects of fatigue behavior of a structure. It is still essential to carry out some form of fatigue testing in conjunction with empirical or analytical work described above.

Over the years, a number of fatigue testing has been developed in the laboratory scale. Those tests can be classified broadly in three categories: constant stress-amplitude testing, constant strain-amplitude testing, and constant stress intensity factor testing. At present, most of the testing methods are of the first type.

We have already noted that fracture and fatigue experiments with single wires are too few for the purpose of any meaningful analysis. The lack of extensive experimentation is understandable. The first and foremost difficulty in performing a single wire fatigue test is to design a test rig with allowable load range while insuring the constant stress-amplitude be maintained. Secondly, for a tension-compression type axial fatigue test, it is difficult to design a test rig so that the grips at wire ends do not produce undesirable mechanical notches. The experiments of Fisher and Viest with single wires indicate a significant number of wire failure at the grouts and it is suspected this, in part, is due to mechanical notches.

Even when a proper test set-up is designed, it is not an easy task to devise an efficient method of crack measurements. Considering all these, it is strongly recommended to expend some research effort into an extensive but careful experimental investigation of wire fatigue life. Some experiments in this area are suggested below.

1. Crack Growth Measurement in a Single Wire

This testing program will allow the measurement of crack growth in a single wire notched specimen under the action of repeated tensile loading.

The major equipment for this testing is an MTS machine with specially designed stress rig similar to the one shown in Figure 51. The specimen is

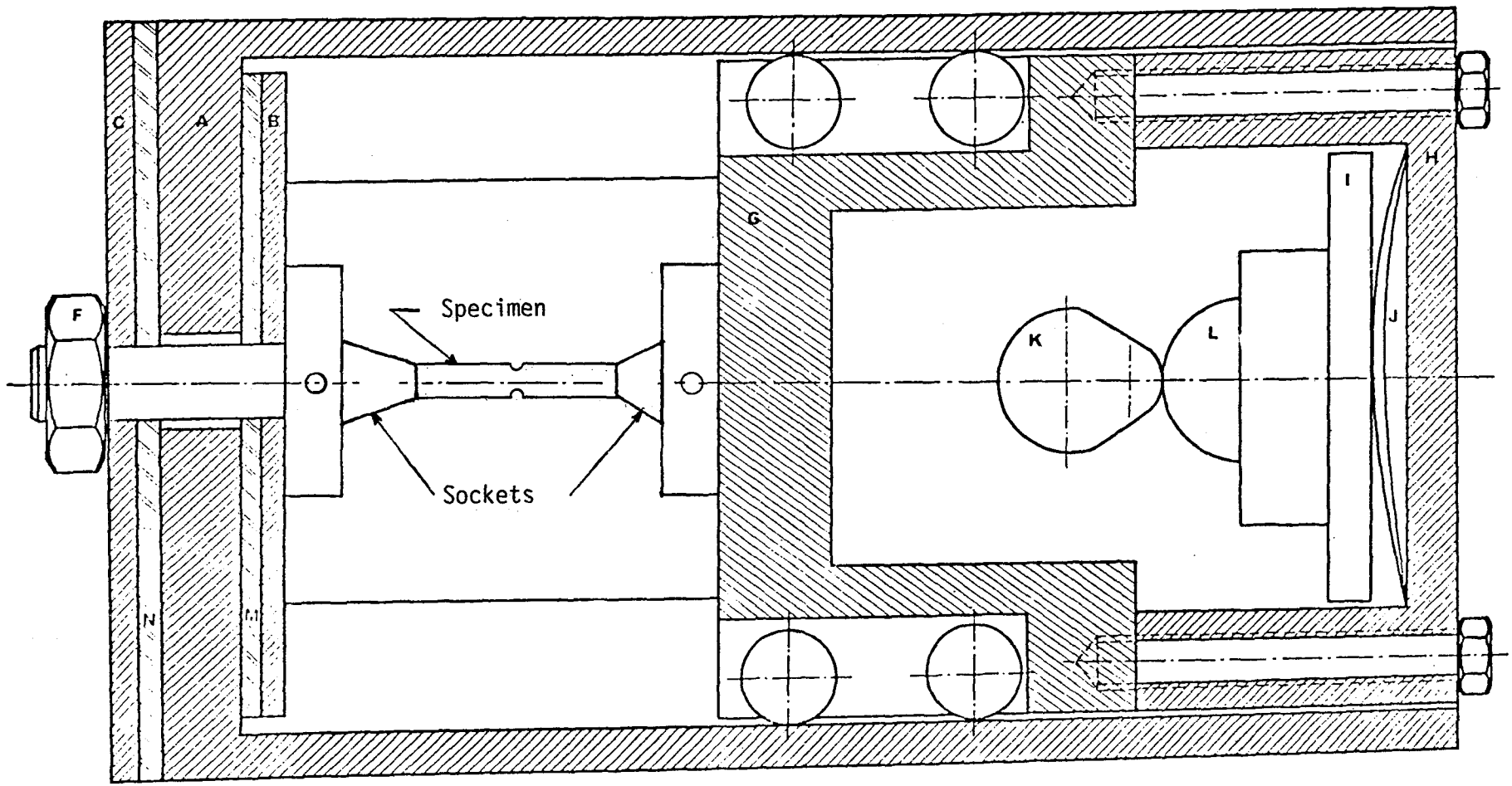

Figure 51. Specially Designed Stress Rig

fixed between fixtures E and D by means of sockets. Fixture D is fixed, and fixture E moves up and down along with block G due to the reciprocal motion produced by the rotation of cam K. The reciprocal motion induces zero-to-tension loading in the specimen. The specimen must be sufficiently long to insure that the premature failure does not occur due to severe stress concentration induced by mechanical notches at the grip or by imperfections along the length.

For the measurement of crack growth under fatigue loading, the specimen may be connected to a potentiometer circuit as shown in Figure 52. A plotter is provided in parallel to the variable resistance R_o to plot the changes of voltage across R_o as a function of the number of fatigue loading cycles. R_o may be calibrated by an ammeter.

When the specimen is cracked or when the crack length is increased, the net cross-section area of the specimen will decrease and hence, R_s will increase. Any change in R_s will change the value of current, I in the circuit. Therefore, the potential difference across R_o will change. If a is the crack length and E_{R_o} is the potential difference across R_o, then it is evident that:

$$\frac{da}{dE_{R_o}} = f\,(R_s,\ R_{sh},\ R_o,\ r_o) \tag{66}$$

For a simple potentiometer circuit such as the one in Figure 52, the function f can be easily determined. Hence, from the measurement of E_{R_o}, a can be found. A typical curve relating E_{R_o} to a is shown in Figure 53. It is also possible, at this stage, to determine a relationship between crack length and the number of cycles of load application, N, as shown schematically in Figure 54.

For better accuracy of experimental results, the basic test program can be modified in various ways. An air cylinder can be used with calibrated gauge to replace the cam-roller mechanical combination. This will not only add accuracy to the tensile stress measurement but also provide the system with a variable loading mechanism. The latter is achieved by changing the air flow to the air cylinder. Similarly, a fiber optic can be used to replace the potentiometer circuit. The optical signals from fiber optic can be translated through photo cells to electrical signals which can then be displayed in a CRT. Finally, acoustic transducer (ultrasonic) can be used to replace the potentiometer circuit. During the crack propagation, the

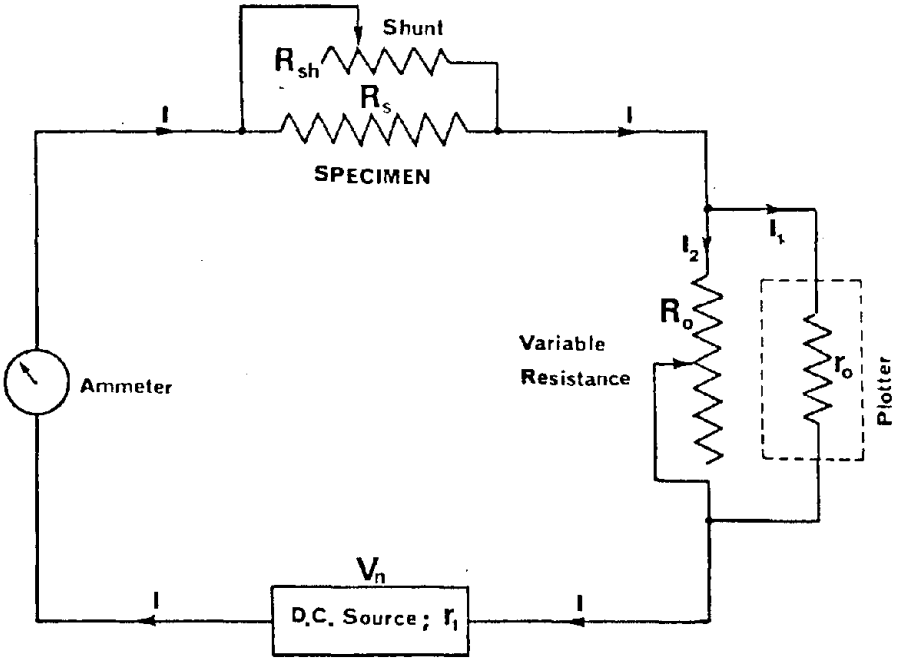

Figure 52. Potentiometer Circuit for Crack Growth Measurement

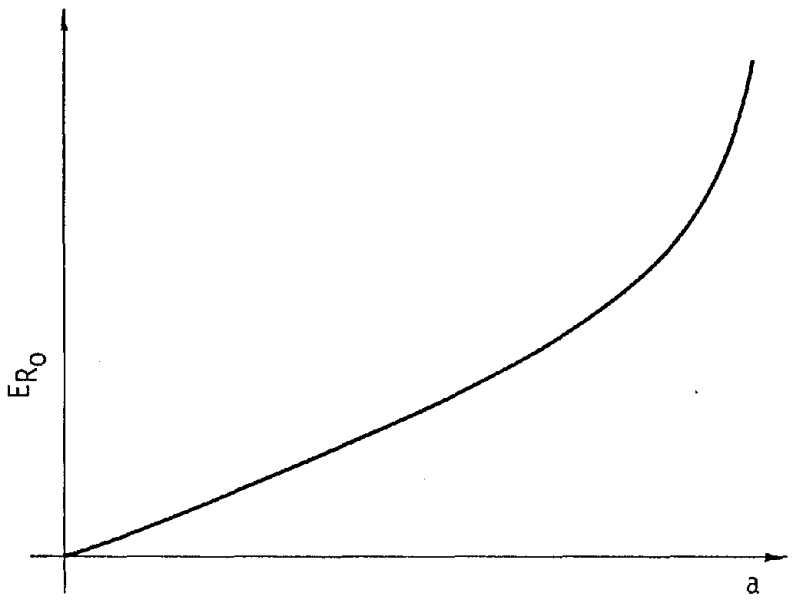

Figure 53. Schematic Relationship Between E_{R_0} and a

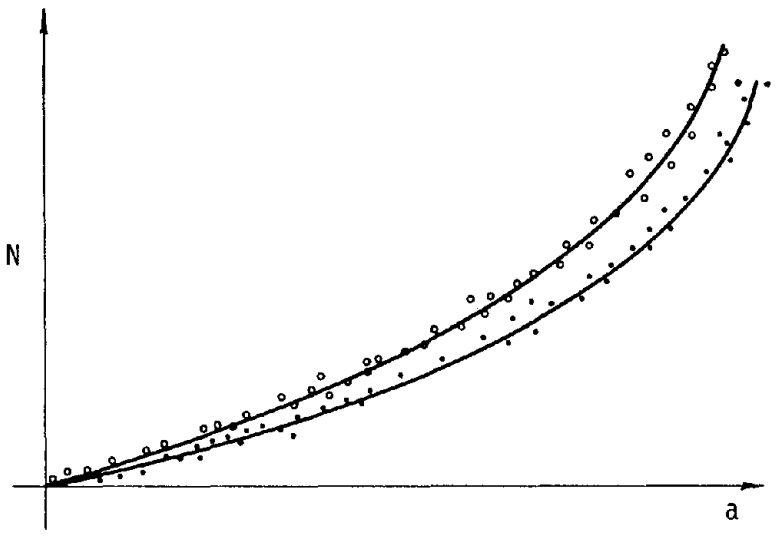

Figure 54. Schematic Relationship Between N and a

ultrasonic transducer will attenuate resulting in acoustic emission. The two latter modifications will give better accuracy in crack growth measurements.

2. Three-Points Bend Test of a Single Wire

Wires used for manufacturing cables and strands are usually 0.25-0.375 in. (6-10 mm) diameter and cold drawn. The conventional ASTM three-points bend test is not suitable for these wires. Fisher and Viest suggested elsewhere another form of three-points bend test which is only applicable for reinforcing wires embedded in PCC slabs. To determine the bending fatigue characteristics of a single wire, it is necessary to subject the wire alone to reverse bending. Reemsnyder designed a test rig with a rotating buckled strut fitted to it to allow completely reverse bending with very small axial load. However, this test rig seems to give torsional rotation in addition to reverse bending. In order to avoid torsional rotation, the reverse bending test of Reemsnyder can be modified in the following manner.

First, the specimen will be fixed between two fixtures similar to D and E of Figure 51. A small tension will be applied at both ends of the specimen to make it straight. It is understood that the specimen for bend test is long enough and is notched at midlength. A small segment of the specimen covering both sides of the notch is embedded in an epoxy mat as shown in Figure 55. A sinusoidal load can be applied across the epoxy resin mat through the use of a cam-roller mechanical combination operated by step motors. Once again, this can be achieved by a specially designed stress rig.

3. Fatigue Testing of a Cable

The experimental set-up for fatigue testing of a cable can be fairly involved depending on the test program. For instance, the bending fatigue test of a cable by a method similar to the one for single wires will require the provision of an equipment to create sinusoidal motion in a cable of diameter 4 in. (10 cm) or more. A simple tensile fatigue testing of cable is, however, feasible using a universal testing machine and an acoustic emission console including audio frequency spectrometer and tape recorder.

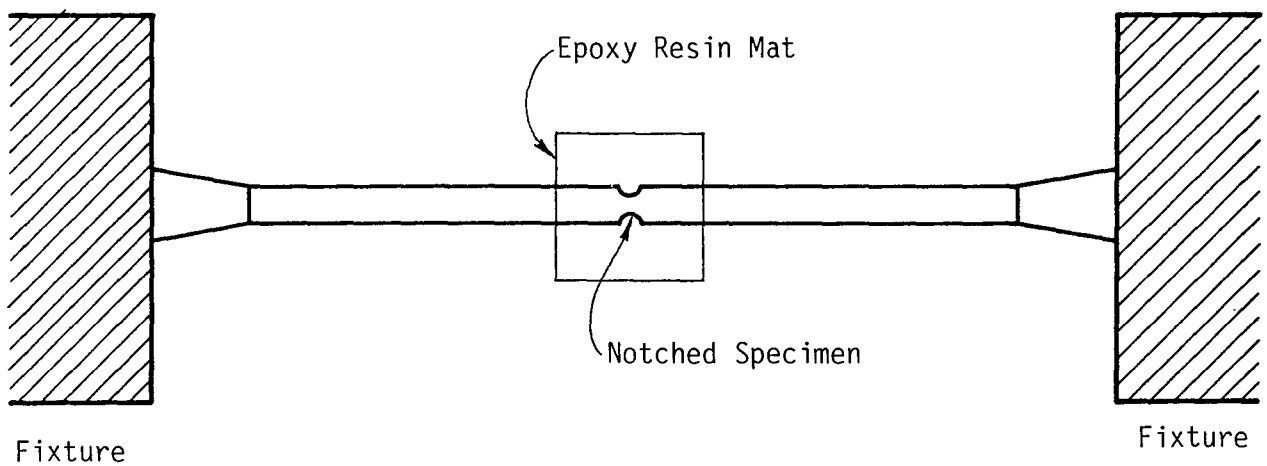

Figure 55. Schematic of Notched Specimen and Fixtures for Three-Points Bend Test

REFERENCES

1. Leonhardt, F., "Latest Developments of Cable-Stayed Bridges for Long Spans," Saertryk af Bygingsstatiske Meddelelser, Vol. 45, No. 4, 1974.

2. Strouhal, V., "Uber Eine Besondere Art der Tonnergung," Annalen der Physik und Chemie, Vol. 5, 1878, pp. 216-251.

3. Feng, C.C., "The Measurement of Vortex-Induced Effects in Flow Past Stationary and Oscillating Circular and D-Section Cylinders," MASc Thesis, University of British Columbia, 1968.

4. Bishop, R.E.D., and Hassan, A.Y., "The Lift and Drag Forces on a Circular Cylinder in a Flowing Fluid," Proc. Royal Society, London, Series A, Vol. 277, 1963, pp. 32-50.

5. Hartlen, R.T., and Currie, I.G., "Lift Oscillator Model of Vortex Induced Vibration," ASCE Journal of Engineering Mechanics, EM-5, Vol. 96, 1970, pp. 577-591.

6. Skop, R.A., and Griffin, O.M., "A Model for the Vortex Excited Resonant Response of Bluff Cylinders," Journal of Sound and Vibration, Vol. 27, 1973, pp. 225-233.

7. Iwan, I.D., and Blevins, R.D., "A Model for Vortex-Induced Oscillation of Structures," ASME Journal of Applied Mechanics, Vol. 41, 1974, pp. 581-586.

8. Birkhoff, G., and Zarantonello, E.H., Jets, Wakes, and Cavities, Academic Press, New York, 1957.

9. Jones, Jr., G.W., "Unsteady Lift Forces Generated by Vortex Shedding About a Large Stationary and Oscillating Cylinder at High Reynolds Number," Symposium on Unsteady Flow, American Society of Mechanical Engineers, Philadelphia, May, 1968.

10. Griffin, O.M., Skop, R.A., and Ramberg, S.E., "The Resonant Vortex Excited Vibrations of Structures and Cable Systems," Proceedings of the Offshore Technology Conference, Paper No. 2319, Houston, Texas, 1975.

11. Landl, R., "Theoretical Model for Vortex-Induced Oscillations," Proceedings of the International Symposium on Vibration Problems in Industry, Keswick, England, 1973.

12. Szechenyi, E., "Modele Mathematique du Mouvement Vibratoire Engendre par un Echappment Tourbillonnaire," La Recherche Aerospatiale, Vol. 1975, No. 5, pp. 301-312.

13. Scanlan, R.H., and Tomko, J.J., "Aerofoil and Bridge Deck Flutter Derivatives," Journal of Engineering Mechanics Division, ASCE, Vol. 97, No. EM6, 1976, pp. 1717-1737.

14. Davenport, A.G., Isyumov, N., and Miyata, T., "The Experimental Determination of the Response of Suspension Bridges to Turbulent Wind," Proc. Third Int. Conf. on Wind Effects on Buildings and Structures, Tokyo, Japan, September 1971.

15. Irwin, H.P.A.H., "Wind Tunnel and Analytical Investigations of the Response of Lions' Gate Bridge to a Turbulent Wind," Report LTR-LA-210, National Aero. Estab., N.R.C., Ottawa, Canada, June, 1977.

16. Scanlan, R.H., and Gade, R.H., "Motion of Suspended Bridge Spans Under Gusty Wind," Journal of Structural Division, ASCE, Vol. 103, No. ST9, 1977, pp. 1867-1883.

17. Chi, M., "Analysis of Operating Characteristics of Strands in Tension Allowing End-Rotation," Paper No. 72, ASME Winter Annual Meeting, November, 1972.

18. Karamchetty, S., "Some Geometrical Characteristics of Wires in Wire Ropes," Proceedings of the Ninth SECTAM, May, 1978, pp. 519-541.

19. Phillips, J.W., and Costello, G.A., "Contact Stresses in Twisted Wire Cables," J. of Eng. Mech. Div., Vol. 99, April, 1973, pp. 331-341.

20. Seely, F.B., and Smith, J.O., Advanced Mechanics of Materials, John Wiley & Sons, Inc., New York, 1966.

21. Hruska, F.H., "Calculation of Stresses in Wire Ropes," Wire and Wire Products, Vol. 26, September, 1951, pp. 766-767, 799-801.

22. Leissa, A., "Contact Stresses in Wire Ropes," Wire and Wire Products, Vol. 34, May, 1959, pp. 307-314, 372-373.

23. Starkey, W.L., and Cress, H.A., "An Analysis of Critical Stresses and Mode of Failure of a Wire Rope," Journal of Engineering for Industry, Trans. ASME, November, 1959, pp. 307-316.

24. Stein, R.A., and Bert, C.W., "Stress Analysis of Wire Rope in Tension and Torsion," Wire and Wire Products, Vol. 37, May, 1962, pp. 621-624, June, 1962, pp. 769-770, 772 and 816.

25. Ernst, J.H., "Der E-Modul von Seilen unter Berücksichtigung des Durchanges," Der Bavingenieur, Col. 40, No. 2, February 1965.

26. Scanlan, R.H., and Swart, R.L.,"Bending Stiffness and Strain in Stranded Cables."

27. Karamchetty, S., "Theoretical Determination of Natural Torsional and Extensional Frequencies of Wire Strands." To be published.

28. Kondo, K., Komatsu, S., Inoue, H., and Matsukawa, A., "Design and Construction of Toyosato-Ohhashi Bridge," Der Stahlbau, No. 6. (1972), pp. 282-189.

29. Andrä, W., and Zellner, W., "Zugglieder aus Paralleldrahtbündeln und ihre Verankerung bei hoher Dauerschwellbelastung," Die Bautechnik, Vol. 46, (1969), No. H8, pp. 263-268, No. H9, pp. 309-315.

30. Andrä, W., and Saul, R., "Versuche mit Bundeln aus Parallelen Drähten und Litzen für die Nordbrücke Mannheim-Ludwigschafen und das Zeldach in München," Die Bautechnik Nos. 9, 10, and 11, (1974), pp. 289-298, 332-340, and 371-373.

31. Podolny, W., and Scalzi, R., "Construction and Design of Cable-Stayed Bridges," John Wiley & Sons, 1976.

32. Birkenmaier, M., "Fatigue Resistant Tendons for Cable-Stayed Construction," IABSE Proceedings P-30/80, May 1980, pp. 65-79.

33. Chi, M., "Response of Bridge Structural Members Under Wind-Induced Vibrations," Report No. FHWA-RD-78, 25, Federal Highway Administration, Office of Research and Development, Washington, D.C., June, 1976.

34. Landgraf, R.W., Morrow, J.D., and Endo, T., Journal of Materials, JMLSA, 4(1), 1969, p. 176.

35. Bullens, D.K., Steel and Its Heat Treatment, 1, 1938, p. 37.

36. Rolfe, S.T., and Barsom, J.M., Fracture and Fatigue Control in Structures, Prentice-Hall, Inc., Englewood Cliffs, N.J., 1977.

37. Yokobori, T., Strength, Fatigue and Fracture of Materials, Noordhoff, 1965.

38. Barsom, J.M., and McNicol, R.C., "Effect of Stress Concentration on Fatigue Crack Initiation in HY-130 Steel," ASTM STP-559, American Society for Testing and Materials, Philadelphia, 1974.

39. Roberts, R., Barsom, J.M., Fisher, J.W., and Rolfe, S.T., "Fracture Mechanics for Bridge Design," Federal Highway Administration Report, July, 1977.

40. Craeger, M., "The Elastic Stress-Field Near the Tip of a Blunt Crack," M. Sc. Thesis, Lehigh University, Bethlehem, PA, 1966.

41. Barsom, J.M., and McNicol, R.C., Unpublished data.

42. Reemsnyder, H.S., "The Mechanical Behavior and Fatigue Resistance of Steel Wire, Strand, and Rope," Report of the Ad Hoc Committee on Mechanical Rope and Cable, National Materials Advisory Board, National Research Council, Washington, D.C., 1972.

43. Fisher, J.W., and Viest, I.M., "Fatigue Tests of Bridge Materials of the AASHO Road Test," Highway Research Board Report No. HRB: OR-463, Special Report No. 66, 1961.

44. Clark, W.G., Jr., "How Fatigue Crack Initiation and Growth Properties Affect Material Selection and Design Criteria," Metals Engineering Quarterly, August, 1974.

45. Clausing, D.P., "Tensile Properties of Eight Constructional Steels Between 70° and 320° F.," Journal of Materials, 4, 2, June, 1969.

46. Barsom, J.M., "Fatigue Behavior of Pressure Vessel Steels," WRC Bulletin 194, Welding Research Council, New York, May, 1974.

47. Bucci, R.J., Clark, W.G., Jr., and Paris, P.C., "Fatigue Crack Propagation Growth Rates Under a Wide Variation of ΔK for an ASTM A517 Grade F (T-1) Steel," ASTM STP513, American Society for Testing and Materials, Philadelphia, 1972.

48. Imhof, E.J., and Barsom, J.M., "Fatigue and Corrosion-Fatigue Crack Growth of 4340 Steel at Various Yield Strengths," ASTM STP 536, American Society for Testing and Materials, Philadelphia, 1973.

49. Parry, M., Nordberg, H., and Hertzberg, R.W., "Fatigue Crack Propagation in A514 Base Plate and Welded Joints," Welding Journal, 51, 10, October, 1972.

50. Sailors, R.H., "Relationship Between Tensile Properties and Microscopically Ductile Plane-strain Fracture Toughness," ASTM STP-605, American Society for Testing and Materials, Philadelphia.

51. Jones, M.H., and Brown, W.F., Jr., "Review of Developments in Plane Strain Fracture Toughness Testing," ASTM STP-463, American Society for Testing and Materials, Philadelphia.

52. Folias, E.S., "Asymptotic Approximations to Crack Problems in Shells," in Fracture, ed. H. Leibowitz, Academic Press, 1971.

53. Hilton, P.D., and Sih, G.C., "Applications of the Finite Element Method to the Calculations of Stress Intensity Factors," in Fracture, ed. H. Leibowitz, Academic Press, 1971.

54. Weibull, W., "Ingeniors Vetenshaps Akadamein, Handlinger, 151, (1939).

55. Freudenthal, A.M., "Statistical Aspects of Brittle Fracture," Fracture, Vol. 2, H. Liebowitz, ed., Academic Press, New York (1968).

56. Freudenthal, A.M., and Gumbel, E.J., "Physical and Statistical Aspects of Fatigue," Advances in Mechanics, Vol. 4, pp. 111-138.

57. Andrä, W., and Saul, R., "Die Festigkeit, insbesondere Dauerfestigkeit langer Paralleldrahtbündel," Die Bautechnik, 56 (1979), H4, pp. 128-130.

58. Miner, M.A., Journal of Applied Mechanics, 12, 1954, p. A-159.

59. Jevtic, D., "Essais de Relaxation, de Fluage, de Fatigue et de Comportement aux Températures Élevées des Fils d'Acier pour Béton Précontraint," pp. 66-74.

60. Bennett, E.W., and Boga, R.K., "Some Fatigue Tests of Large Diameter Deformed Hard Drawn Wire Used for Prestressed Concrete," Engineering and Public Works Review, January 1967, pp. 58-61.

61. Cullmore, M.S.G., "The Fatigue Strength of High Tensile Steel Wire Cable Subjected to Stress Fluctuations of Small Amplitude."

62. Edwards, A.D., and Picard, A., "Fatigue Characteristics of Prestressing Strands."

63. Fleming, J.F., "Fatigue of Cables," A Report to American Iron and Steel Institute under Project No. 1201-311, SETEC CE 74-079, June 1974.

64. Castellaw, T., Frank, K., and Campbell, M., "Fatigue Design Characteristics and Fatigue Testing of Prescon Stay Cable Anchorages." in Cable Stayed Bridges, ed. E. Podolny, Jr., Federal Highway Administration, Washington, D.C. 1977.

APPENDIX A

DYNAMICS OF STAY CABLES

I. Free Vibration Analysis of Stay Cables

The governing differential equation of the motion of a stay cable has the following general form (see equation (9) also):

$$\rho A \frac{\partial^2 y}{\partial t^2} + c \frac{\partial y}{\partial t} + \frac{\partial^2}{\partial x^2} \left(EI \frac{\partial^2 y}{\partial x^2} - T\right) = F(x,t) \qquad \text{(A-1)}$$

where all terms in the above equation have been explained previously in Chapter 4.

The natural frequencies and mode shapes of a stay cable are obtained from the complementary solution of equation (A-1). The following assumptions are made in solving the complementary part of equation (A-1).

a) The natural frequencies of a stay cable are widely separated from one another;
b) The damping is small and hence, can be neglected;
c) The stay cable has fixed ends; and finally,
d) The stiffness of the cable is constant along its axis and the axial force, T, is independent of time.

Under the above assumptions, the equation of free vibration of a stay cable is given by:

$$EI \frac{\partial^4 y}{\partial x^4} - T \frac{\partial^2 y}{\partial x^2} + \rho A \frac{\partial^2 y}{\partial t^2} = 0 \qquad \text{(A-2)}$$

By a separation of variable technique, and considering a solution of equation (A-2) of the form,

$$y(x,t) = y(x)e^{i\omega t} \qquad \text{(A-3)}$$

the small amplitude, free, transverse vibration of a cable can be written as follows:

$$EI \frac{d^4 y}{dx^4} - T \frac{d^2 y}{dx^2} - \rho A \omega^2 y = 0 \qquad \text{(A-4)}$$

Equation (A-4) is nondimensionalized by setting:

$$Y = \frac{y}{L} \quad , \; X = \frac{x}{L} \tag{A-5}$$

thus yielding:

$$\frac{d^4Y}{dX^4} - P\frac{d^2Y}{dX^2} - QY = 0 \tag{A-6}$$

where

$$P = \frac{TL^2}{EI} = \text{nondimensional force} \tag{A-7}$$

$$Q = \frac{\rho A\omega^2}{EI} = \text{nondimensional frequency}$$

The most general solution of equation (A-6) is given by:

$$Y(x) = \sum_{n=1}^{\infty} \Phi_n(X) = \sum_{n=1}^{\infty} A_n \sin\alpha_n X + B_n \cos\alpha_n X + C_n \sinh\beta_n X + D_n \cosh\beta_n X \tag{A-8}$$

where A_n, B_n, C_n, and D_n are coefficients to be determined from the boundary conditions, and where α_n and β_n are given by the following expressions:

$$\alpha_n^2 = \frac{P}{2}\left(-1 + \sqrt{1 + \frac{4Q}{P^2}}\right) \tag{A-9}$$

$$\beta_n^2 = \frac{P}{2}\left(1 + \sqrt{1 + \frac{4Q}{P^2}}\right)$$

The boundary conditions are those corresponding to the fixed ends and these are:

$$\Phi_n = 0 \quad , \; \frac{d\Phi_n}{dX} = 0 \quad \text{at } X = 0$$

$$\Phi_n = 0 \quad , \; \frac{d\Phi_n}{dX} = 0 \quad \text{at } X = 1 \tag{A - 10}$$

By applying the four boundary conditions in equation (A-10) to the expression for $\Phi_n(X)$ (equation A-8) , one obtains a set of four homogeneous equations in A_n, B_n, C_n, and D_n. For nontrivial solution, the determinant of the coefficient matrix must be zero and this yields:

$$\cosh\beta_n \cos\alpha_n + \frac{\alpha_n^2 - \beta_n^2}{2\alpha_n\beta_n} \sinh\beta_n \sin\alpha_n = 1 \tag{A-11}$$

Equation (A-11) is the most general frequency equation for small amplitude transverse vibration of a stay cable. The solution of this equation satisfying

expressions in (A-9) gives the natural frequency, ω_n. In practice, it is more convenient to express the relationship between P and Q, or between P and Z^2 where $Z^2 = 4Q/P^2$ as has been shown in Figures 10 through 14.

The solution of the transcendental equation (A-11) can be substituted back into expression (A-8), and the coefficients A_n, B_n, C_n, and D_n can be determined by usual eigenvalue analysis procedure. In particular, choosing $A_n = 1$ arbitrarily and assuming $B_n = -D_n$, one finds that:

$$A_n = 1$$

$$B_n = \frac{\alpha_n \sinh\beta_n - \beta_n \sin\alpha_n}{\beta_n(\cos\alpha_n - \cosh\beta_n)}$$

$$C_n = -\frac{\alpha_n}{\beta_n} \qquad \text{(A-12)}$$

$$D_n = \frac{\beta_n \sin\alpha_n - \alpha_n \sinh\beta_n}{\beta_n(\cos\alpha_n - \cosh\beta_n)}$$

The term, Φ_n, more commonly called the nth mode shape, can now be given by:

$$\Phi_n = \sin\alpha_n X + \frac{\beta_n \sin\alpha_n - \alpha_n \sinh\beta_n}{\beta_n(\cos\alpha_n - \cosh\beta_n)} (\cosh\beta_n X - \cos\alpha_n X) - \frac{\alpha_n}{\beta_n} \sinh\beta_n X \qquad \text{(A-13)}$$

II. Response of Cables to Harmonic Loading

Consider again the governing differential equation of motion given by equation (A-1). The solution of (A-1) is sought in the following form:

$$y(x,t) = \sum_n \phi_n(x)\psi_n(t) \qquad \text{(A-14)}$$

where $\phi_n(x)$ is the nth natural mode of the cable, and $\psi_n(t)$ is the generalized coordinate of the cable. Substituting (A-14) into (A-1), one obtains:

$$\rho A \sum_n \phi_n(x)\ddot{\psi}_n(t) + EI\sum_n \phi_n^{IV}(x)\psi_n(t) - T\sum_n \phi_n''(x)\psi_n(t) + c\sum_n \phi_n(x)\dot{\psi}_n(t) = F(t) \qquad \text{(A-15)}$$

where it is assumed that F(x,t) is simply a harmonic function, F(t), of time.

An important property of the normal modes, $\phi_n(x)$, is their orthogonality with respect to mass density. This gives:

$$\int_0^L \rho A \phi_m(x) \phi_n(x) dx = \delta_{mn} \tag{A-16}$$

where δ_{mn} is Kronecker delta. The latter is equal to 1 when m=n, and is equal to zero when $m \neq n$.

It is also known that $\phi_n(x)$ is the complementary solution of (A-1) and hence,

$$EI\sum_n \phi_n^{IV}(x) - T\sum_n \phi_n''(x) - \rho A \sum_n \omega_n^2 \phi_n(x) = 0 \tag{A-17}$$

The above two equations, (A-16) and (A-17), can be utilized to reduce equation (A-15) to a set of second order uncoupled differential equations of the form:

$$\psi_n(t) + \frac{c}{\rho A} \psi_n(t) + \omega_n^2 \psi_n(t) = \frac{T_n(t)}{M_n} \tag{A-18}$$

$$n = 1, 2, 3, \ldots$$

where

$$T_n(t) = \int_0^L F(t) \phi_n(x) dx \tag{A-19}$$

is the generalized force vector, and

$$M_n = \int_0^L \rho A \phi_n^2(x)\, dx \tag{A-20}$$

is the generalized mass.

Considering that the harmonic function, F(t), has the form:

$$F(t) = F_o \cos\omega_s t = \frac{1}{2} \rho_a d V_{cr}^2 C_L \cos\omega_s t \tag{A-21}$$

where all terms in the expression have been explained in Chapter 4 of the text, the expression for $T_n(t)$ and M_n are given by:

$$T_n(t) = F_o \left(\frac{1-\cos\alpha_n L}{\alpha_n} - \frac{D_n}{\alpha_n} \sin\alpha_n L + \frac{D_n}{\beta_n} \sinh\beta_n L + \frac{C_n}{\beta_n} \cosh\beta_n L - 1 \right) \cos\omega_s t \tag{A-22}$$

$$= T_{on} \cos\omega_s t$$

$$
\begin{aligned}
M_n = \rho A \Big\{ & \frac{L}{2}\left(1+2D_n^2-C_n^2\right) + \frac{2D_n}{\alpha_n^2+\beta_n^2}\left(\alpha_n+C_n\beta_n\right) \\
& + D_n\left(-\frac{1}{2\alpha_n} + \frac{2C_n}{4\beta_n} + \left(\frac{D_n^2-1}{4\alpha_n}\right)\right. \sin 2\alpha_n L \\
& + \frac{D_n}{2\alpha_n}\cos 2\alpha_n L + \left(\frac{D_n^2+C_n^2}{4\beta_n}\right) \sinh 2\beta_n L \\
& + \frac{2D_nC_n}{4\beta_n}\cosh 2\beta_n L \\
& + \frac{\left(2D_n\beta_n-2D_nC_n\alpha_n\right)}{\alpha_n^2+\beta_n^2} \sin\beta_n L \sin\alpha_n L \\
& + \frac{\left(-2D_n\alpha_n-2D_nC_n\beta_n\right)}{\alpha_n^2+\beta_n^2} \cosh\beta_n L \cos\alpha_n L \\
& + \frac{\left(2C_n\beta_n-2C_n\alpha_n\right)}{\alpha_n^2+\beta_n^2} \sinh\beta_n L \cos\alpha_n L \Big] \\
& + \frac{\left(-2D_n^2\beta_n-2C_n\alpha_n\right)}{\alpha_n^2+\beta_n^2} \sinh\beta_n L \cos\alpha_n L \Big\}
\end{aligned}
\tag{A-23}
$$

Returning to equation (A-18), we assume that the damping coefficient is proportional to mass density, and is given by:

$$c = 2\zeta_n\omega_n\rho A \tag{A-24}$$

Equation (A-18) can then be rewritten as:

$$\psi_n(t) + 2\zeta_n\omega_n\psi_n(t) + \omega_n^2\psi_n(t) = \frac{T_n(t)}{M_n} \tag{A-25}$$

The steady state solution of equation (A-25) is obtained as follows:

$$\psi_n(t) = G_{1n}\sin\omega t + G_{2n}\cos\omega t \tag{A-26}$$

where the coefficients G_{1n} and G_{2n} are given by:

$$
\begin{aligned}
G_{1n} &= \frac{2\zeta_n\,\omega_n\omega_s\,T_{on}}{M_n\left[(\omega_n^2-\omega_s^2)^2+(2\zeta_n\omega_n\omega_s)^2\right]} \\
G_{2n} &= \frac{T_{on}\,(\omega_n^2-\omega_s^2}{M_n\left[(\omega_n^2-\omega_s^2)^2+(2\zeta_n\omega_n\omega_s)^2\right]}
\end{aligned}
\tag{A-27}
$$

The general solution of the governing differential equation can now be written as:

$$y(x,t) = \sum_n y_n(x,t) = F_o \sum_n \phi_n(x) \; [G_{1n}\sin\omega_s t + G_{2n}\cos\omega_s t] \qquad \text{(A-28)}$$

The solution can be nondimensionalized by setting

$$Y_n = \frac{y_n(x,t)}{L} \quad , \quad \chi_n = Ly_n''(x,t) \qquad \text{(A-29)}$$

The expressions for Y_n and χ_n obtained in this manner are given in terms of nondimensional force, P, and nondimensional frequency, Q, or more appropriately, in terms of Z^2 as follows:

$$Y_n = \frac{C_L}{2\pi St} \; f(P,Z) \qquad \text{(A-30)}$$

$$\chi_n = \frac{C_L}{2\pi St} \; g(P,Z) \qquad \text{(A-31)}$$

$$f(P,Z) = \frac{\sqrt{1}+\sqrt{1+Z^2}\;\left[1 - \frac{1+\sqrt{1+Z^2}}{2\sqrt{1+Z^2}}\cos\alpha_n - \frac{Z}{2\sqrt{1+Z^2}}\sin\alpha_n\right]}{\sqrt{-1}+\sqrt{1+Z^2}\;\left[\sqrt{P}(1+\sqrt{1+Z^2}) + 1 - \frac{3}{2}\,\frac{1+\sqrt{1+Z^2}}{\sqrt{1+Z^2}}\right.} \qquad \text{(A-32)}$$

and

$$g(P,Z) = \frac{2(1+Z^2)-[1+Z^2+\sqrt{1+Z^2}]\cos\alpha_n - Z\sqrt{1+Z^2}\sin\alpha_n}{-3-\sqrt{1+Z^2}+2\sqrt{1+Z^2}\sqrt{P}(1+\sqrt{1+Z^2})} \qquad \text{(A-33)}$$

APPENDIX B

NATURAL FREQUENCIES OF PASCO-KENNEWICK AND LULING BRIDGE CABLES

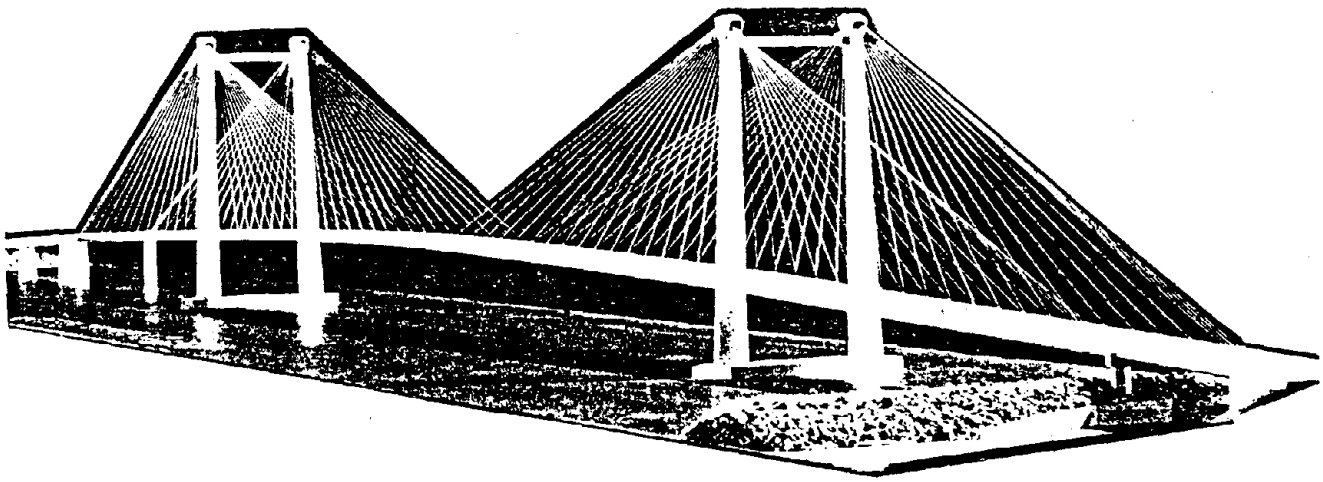

Figure B-1. Model of Intercity Bridge on Columbia River in Pasco-Kennewick, Washington.

Description

Overall length - 2503 ft. (763 m)

Main span - 981 ft. (299 m)

Cable-stayed girder length - 1794 ft. (547 m)

Total number of cables - 144

Special Features of Stay-Cables

Number of wires in a cable - 73 (Group IV) to 283 (Group I)

Wire diameter - 0.25 in. (6 mm) BBR type

Cable length - 180 ft. (55 m) to 506 ft. (154 m)

Outer diameter of cable - 6 in. (15 cm)

Wire stress range - 59 ksi (407 MPa) to 108 ksi (745 MPa)

Pasco-Kennewick Group I Cables

_____ NORMAL FORCE= 800 (KIPS)_____

FREQ.OF BEAM (CYCLE.P.S)	FREQ.OF STRING (CYCLE.P.S)
MODE= 1 ____ .736171	____ .729486
MODE= 2 ____ 1.47279	____ 1.45897
MODE= 3 ____ 2.21028	____ 2.18846
MODE= 4 ____ 2.9491	____ 2.91794
MODE= 5 ____ 3.68968	____ 3.64743
MODE= 6 ____ 4.43246	____ 4.37691
MODE= 7 ____ 5.17786	____ 5.1064
MODE= 8 ____ 5.92633	____ 5.83588
MODE= 9 ____ 6.67828	____ 6.56537
MODE= 10 ____ 7.43416	____ 7.29486
MODE= 11 ____ 8.19437	____ 8.02434
MODE= 12 ____ 8.95934	____ 8.75383
MODE= 13 ____ 9.72947	____ 9.48331
MODE= 14 ____ 10.5052	____ 10.2128
MODE= 15 ____ 11.2869	____ 10.9423
MODE= 16 ____ 12.0749	____ 11.6718
MODE= 17 ____ 12.8697	____ 12.4013
MODE= 18 ____ 13.6717	____ 13.1307
MODE= 19 ____ 14.4812	____ 13.8602
MODE= 20 ____ 15.2986	____ 14.5897
MODE= 21 ____ 16.1242	____ 15.3192
MODE= 22 ____ 16.9585	____ 16.0487
MODE= 23 ____ 17.8017	____ 16.7782
MODE= 24 ____ 18.6543	____ 17.5077
MODE= 25 ____ 19.5165	____ 18.2371
MODE= 26 ____ 20.3887	____ 18.9666
MODE= 27 ____ 21.2712	____ 19.6961
MODE= 28 ____ 22.1643	____ 20.4256
MODE= 29 ____ 23.0683	____ 21.1551
MODE= 30 ____ 23.9836	____ 21.8846

_____ NORMAL FORCE= 900 (KIPS)_____

	FREQ.OF BEAM (CYCLE.P.S)	FREQ.OF STRING (CYCLE.P.S)
MODE= 1	.780419	.773737
MODE= 2	1.56125	1.54747
MODE= 3	2.34291	2.32121
MODE= 4	3.12582	3.09495
MODE= 5	3.91038	3.86869
MODE= 6	4.69702	4.64242
MODE= 7	5.48614	5.41616
MODE= 8	6.27815	6.1899
MODE= 9	7.07345	6.96364
MODE= 10	7.87244	7.73737
MODE= 11	8.67553	8.51111
MODE= 12	9.48311	9.28485
MODE= 13	10.2956	10.0586
MODE= 14	11.1133	10.8323
MODE= 15	11.9367	11.6061
MODE= 16	12.7661	12.3798
MODE= 17	13.6019	13.1535
MODE= 18	14.4445	13.9273
MODE= 19	15.2942	14.701
MODE= 20	16.1514	15.4747
MODE= 21	17.0164	16.2485
MODE= 22	17.8896	17.0222
MODE= 23	18.7714	17.796
MODE= 24	19.662	18.5697
MODE= 25	20.5618	19.3434
MODE= 26	21.4711	20.1172
MODE= 27	22.3902	20.8909
MODE= 28	23.3194	21.6646
MODE= 29	24.2591	22.4384
MODE= 30	25.2095	23.2121

_____ NORMAL FORCE= 1000 (KIPS)_____

	FREQ.OF BEAM (CYCLE.P.S)	FREQ.OF STRING (CYCLE.P.S)
MODE= 1	.822262	.815589
MODE= 2	1.64492	1.63118
MODE= 3	2.46836	2.44677
MODE= 4	3.29299	3.26236
MODE= 5	4.11919	4.07795
MODE= 6	4.94735	4.89353
MODE= 7	5.77787	5.70912
MODE= 8	6.61112	6.52471
MODE= 9	7.44751	7.3403
MODE= 10	8.2874	8.15589
MODE= 11	9.13118	8.97148
MODE= 12	9.97922	9.78707
MODE= 13	10.8319	10.6027
MODE= 14	11.6896	11.4182
MODE= 15	12.5527	12.2338
MODE= 16	13.4215	13.0494
MODE= 17	14.2963	13.865
MODE= 18	15.1777	14.6806
MODE= 19	16.0658	15.4962
MODE= 20	16.9611	16.3118
MODE= 21	17.8638	17.1274
MODE= 22	18.7744	17.943
MODE= 23	19.6931	18.7585
MODE= 24	20.6202	19.5741
MODE= 25	21.5562	20.3897
MODE= 26	22.5012	21.2053
MODE= 27	23.4556	22.0209
MODE= 28	24.4197	22.8365
MODE= 29	25.3938	23.6521
MODE= 30	26.3781	24.4677

_____ NORMAL FORCE= 1100 (KIPS)_____

	FREQ.OF BEAM (CYCLE.P.S)	FREQ.OF STRING (CYCLE.P.S)
MODE= 1	.862065	.855397
MODE= 2	1.72451	1.71079
MODE= 3	2.5877	2.56619
MODE= 4	3.45202	3.42159
MODE= 5	4.31783	4.27699
MODE= 6	5.18552	5.13239
MODE= 7	6.05545	5.98778
MODE= 8	6.928	6.84318
MODE= 9	7.80353	7.69858
MODE= 10	8.6824	8.55397
MODE= 11	9.56499	9.40937
MODE= 12	10.4516	10.2648
MODE= 13	11.3427	11.1202
MODE= 14	12.2386	11.9756
MODE= 15	13.1396	12.831
MODE= 16	14.0461	13.6864
MODE= 17	14.9584	14.5418
MODE= 18	15.8768	15.3972
MODE= 19	16.8018	16.2526
MODE= 20	17.7336	17.1079
MODE= 21	18.6726	17.9633
MODE= 22	19.619	18.8187
MODE= 23	20.5732	19.6741
MODE= 24	21.5356	20.5295
MODE= 25	22.5064	21.3849
MODE= 26	23.4858	22.2403
MODE= 27	24.4744	23.0957
MODE= 28	25.4722	23.9511
MODE= 29	26.4796	24.8065
MODE= 30	27.4969	25.6619

_____ NORMAL FORCE= 1200 (KIPS)_____

	FREQ.OF BEAM (CYCLE.P.S)	FREQ.OF STRING (CYCLE.P.S)
MODE= 1	.900096	.893434
MODE= 2	1.80055	1.78687
MODE= 3	2.70173	2.6803
MODE= 4	3.60398	3.57374
MODE= 5	4.50767	4.46717
MODE= 6	5.41315	5.36061
MODE= 7	6.32077	6.25404
MODE= 8	7.23091	7.14747
MODE= 9	8.14389	8.04091
MODE= 10	9.06008	8.93434
MODE= 11	9.97982	9.82778
MODE= 12	10.9035	10.7212
MODE= 13	11.8314	11.6146
MODE= 14	12.7638	12.5081
MODE= 15	13.7012	13.4015
MODE= 16	14.6439	14.2949
MODE= 17	15.5921	15.1884
MODE= 18	16.5463	16.0818
MODE= 19	17.5067	16.9753
MODE= 20	18.4736	17.8687
MODE= 21	19.4475	18.7621
MODE= 22	20.4285	19.6556
MODE= 23	21.417	20.549
MODE= 24	22.4134	21.4424
MODE= 25	23.4178	22.3359
MODE= 26	24.4306	23.2293
MODE= 27	25.4521	24.1227
MODE= 28	26.4826	25.0162
MODE= 29	27.5224	25.9096
MODE= 30	28.5717	26.803

_____ NORMAL FORCE= 1300 (KIPS)_____

FREQ.OF BEAM (CYCLE.P.S)	FREQ.OF STRING (CYCLE.P.S)
MODE= 1 ____ .936572	____ .929915
MODE= 2 ____ 1.87349	____ 1.85983
MODE= 3 ____ 2.8111	____ 2.78975
MODE= 4 ____ 3.74975	____ 3.71966
MODE= 5 ____ 4.68977	____ 4.64958
MODE= 6 ____ 5.63151	____ 5.57949
MODE= 7 ____ 6.57532	____ 6.50941
MODE= 8 ____ 7.52153	____ 7.43932
MODE= 9 ____ 8.47049	____ 8.36924
MODE= 10 ____ 9.42253	____ 9.29915
MODE= 11 ____ 10.378	____ 10.2291
MODE= 12 ____ 11.3372	____ 11.159
MODE= 13 ____ 12.3005	____ 12.0889
MODE= 14 ____ 13.2682	____ 13.0188
MODE= 15 ____ 14.2406	____ 13.9487
MODE= 16 ____ 15.2181	____ 14.8786
MODE= 17 ____ 16.2009	____ 15.8086
MODE= 18 ____ 17.1895	____ 16.7385
MODE= 19 ____ 18.1841	____ 17.6684
MODE= 20 ____ 19.185	____ 18.5983
MODE= 21 ____ 20.1925	____ 19.5282
MODE= 22 ____ 21.207	____ 20.4581
MODE= 23 ____ 22.2286	____ 21.3881
MODE= 24 ____ 23.2579	____ 22.318
MODE= 25 ____ 24.2949	____ 23.2479
MODE= 26 ____ 25.34	____ 24.1778
MODE= 27 ____ 26.3935	____ 25.1077
MODE= 28 ____ 27.4557	____ 26.0376
MODE= 29 ____ 28.5269	____ 26.9675
MODE= 30 ____ 29.6072	____ 27.8975

_____ NORMAL FORCE= 1400 (KIPS)_____

FREQ.OF BEAM (CYCLE.P.S)	FREQ.OF STRING (CYCLE.P.S)
MODE= 1 ____ .971674	____ .965018
MODE= 2 ____ 1.94368	____ 1.93004
MODE= 3 ____ 2.91635	____ 2.89505
MODE= 4 ____ 3.89002	____ 3.86007
MODE= 5 ____ 4.86502	____ 4.82509
MODE= 6 ____ 5.84167	____ 5.79011
MODE= 7 ____ 6.82031	____ 6.75513
MODE= 8 ____ 7.80128	____ 7.72015
MODE= 9 ____ 8.78488	____ 8.68516
MODE= 10 ____ 9.77145	____ 9.65018
MODE= 11 ____ 10.7613	____ 10.6152
MODE= 12 ____ 11.7548	____ 11.5802
MODE= 13 ____ 12.7522	____ 12.5452
MODE= 14 ____ 13.7539	____ 13.5103
MODE= 15 ____ 14.7601	____ 14.4753
MODE= 16 ____ 15.7713	____ 15.4403
MODE= 17 ____ 16.7876	____ 16.4053
MODE= 18 ____ 17.8094	____ 17.3703
MODE= 19 ____ 18.837	____ 18.3353
MODE= 20 ____ 19.8707	____ 19.3004
MODE= 21 ____ 20.9108	____ 20.2654
MODE= 22 ____ 21.9577	____ 21.2304
MODE= 23 ____ 23.0115	____ 22.1954
MODE= 24 ____ 24.0726	____ 23.1604
MODE= 25 ____ 25.1412	____ 24.1255
MODE= 26 ____ 26.2177	____ 25.0905
MODE= 27 ____ 27.3023	____ 26.0555
MODE= 28 ____ 28.3953	____ 27.0205
MODE= 29 ____ 29.497	____ 27.9855
MODE= 30 ____ 30.6076	____ 28.9506

_____ NORMAL FORCE= 1500 (KIPS)_____

	FREQ.OF BEAM (CYCLE.P.S)	FREQ.OF STRING (CYCLE.P.S)
MODE= 1	1.00554	.998889
MODE= 2	2.0114	1.99778
MODE= 3	3.01791	2.99667
MODE= 4	4.02537	3.99556
MODE= 5	5.03412	4.99445
MODE= 6	6.04448	5.99334
MODE= 7	7.05675	6.99223
MODE= 8	8.07126	7.99111
MODE= 9	9.08833	8.99
MODE= 10	10.1083	9.98889
MODE= 11	11.1314	10.9878
MODE= 12	12.158	11.9867
MODE= 13	13.1884	12.9856
MODE= 14	14.2229	13.9845
MODE= 15	15.2619	14.9833
MODE= 16	16.3056	15.9822
MODE= 17	17.3543	16.9811
MODE= 18	18.4083	17.98
MODE= 19	19.4679	18.9789
MODE= 20	20.5334	19.9778
MODE= 21	21.6052	20.9767
MODE= 22	22.6834	21.9756
MODE= 23	23.7684	22.9745
MODE= 24	24.8604	23.9733
MODE= 25	25.9598	24.9722
MODE= 26	27.0668	25.9711
MODE= 27	28.1816	26.97
MODE= 28	29.3046	27.9689
MODE= 29	30.436	28.9678
MODE= 30	31.5761	29.9667

_____ NORMAL FORCE= 1600 (KIPS)_____

	FREQ.OF BEAM (CYCLE.P.S)	FREQ.OF STRING (CYCLE.P.S)
MODE= 1	____ 1.0383	____ 1.03165
MODE= 2	____ 2.0769	____ 2.06329
MODE= 3	____ 3.11614	____ 3.09494
MODE= 4	____ 4.15629	____ 4.12659
MODE= 5	____ 5.1977	____ 5.15824
MODE= 6	____ 6.24065	____ 6.18988
MODE= 7	____ 7.28547	____ 7.22153
MODE= 8	____ 8.33245	____ 8.25318
MODE= 9	____ 9.3819	____ 9.28482
MODE= 10	____ 10.4341	____ 10.3165
MODE= 11	____ 11.4895	____ 11.3481
MODE= 12	____ 12.5482	____ 12.3798
MODE= 13	____ 13.6105	____ 13.4114
MODE= 14	____ 14.6769	____ 14.4431
MODE= 15	____ 15.7476	____ 15.4747
MODE= 16	____ 16.8228	____ 16.5064
MODE= 17	____ 17.9029	____ 17.538
MODE= 18	____ 18.9882	____ 18.5696
MODE= 19	____ 20.0789	____ 19.6013
MODE= 20	____ 21.1753	____ 20.6329
MODE= 21	____ 22.2777	____ 21.6646
MODE= 22	____ 23.3865	____ 22.6962
MODE= 23	____ 24.5018	____ 23.7279
MODE= 24	____ 25.624	____ 24.7595
MODE= 25	____ 26.7532	____ 25.7912
MODE= 26	____ 27.8899	____ 26.8228
MODE= 27	____ 29.0342	____ 27.8545
MODE= 28	____ 30.1864	____ 28.8861
MODE= 29	____ 31.3468	____ 29.9178
MODE= 30	____ 32.5156	____ 30.9494

Pasco-Kennewick Group I Cables

_____ NORMAL FORCE= 600 (KIPS)_____

FREQ.OF BEAM (CYCLE.P.S)	FREQ.OF STRING (CYCLE.P.S)
MODE= 1 ____ 3.06447	____ 3.03341
MODE= 2 ____ 6.13124	____ 6.06682
MODE= 3 ____ 9.20255	____ 9.10023
MODE= 4 ____ 12.2807	____ 12.1336
MODE= 5 ____ 15.368	____ 15.167
MODE= 6 ____ 18.4665	____ 18.2005
MODE= 7 ____ 21.5787	____ 21.2339
MODE= 8 ____ 24.7067	____ 24.2673
MODE= 9 ____ 27.8527	____ 27.3007
MODE= 10 ____ 31.0189	____ 30.3341
MODE= 11 ____ 34.2074	____ 33.3675
MODE= 12 ____ 37.4204	____ 36.4009
MODE= 13 ____ 40.66	____ 39.4343
MODE= 14 ____ 43.9282	____ 42.4677
MODE= 15 ____ 47.227	____ 45.5011
MODE= 16 ____ 50.5585	____ 48.5345
MODE= 17 ____ 53.9247	____ 51.5679
MODE= 18 ____ 57.3274	____ 54.6013
MODE= 19 ____ 60.7685	____ 57.6348
MODE= 20 ____ 64.2499	____ 60.6682

_____ NORMAL FORCE= 500 (KIPS)_____

	FREQ.OF BEAM (CYCLE.P.S)	FREQ.OF STRING (CYCLE.P.S)
MODE= 1	____ 2.80024	____ 2.76911
MODE= 2	____ 5.60299	____ 5.53823
MODE= 3	____ 8.41074	____ 8.30734
MODE= 4	____ 11.226	____ 11.0765
MODE= 5	____ 14.0512	____ 13.8456
MODE= 6	____ 16.8888	____ 16.6147
MODE= 7	____ 19.7414	____ 19.3838
MODE= 8	____ 22.6112	____ 22.1529
MODE= 9	____ 25.5007	____ 24.922
MODE= 10	____ 28.4123	____ 27.6911
MODE= 11	____ 31.3483	____ 30.4603
MODE= 12	____ 34.3109	____ 33.2294
MODE= 13	____ 37.3026	____ 35.9985
MODE= 14	____ 40.3254	____ 38.7676
MODE= 15	____ 43.3816	____ 41.5367
MODE= 16	____ 46.4732	____ 44.3058
MODE= 17	____ 49.6025	____ 47.0749
MODE= 18	____ 52.7714	____ 49.844
MODE= 19	____ 55.9819	____ 52.6132
MODE= 20	____ 59.2359	____ 55.3823

_____ NORMAL FORCE= 400 (KIPS)_____

FREQ.OF BEAM (CYCLE.P.S)	FREQ.OF STRING (CYCLE.P.S)
MODE= 1 ____ 2.508	____ 2.47677
MODE= 2 ____ 5.01879	____ 4.95354
MODE= 3 ____ 7.53519	____ 7.43031
MODE= 4 ____ 10.06	____ 9.90708
MODE= 5 ____ 12.5959	____ 12.3838
MODE= 6 ____ 15.1457	____ 14.8606
MODE= 7 ____ 17.7122	____ 17.3374
MODE= 8 ____ 20.2979	____ 19.8142
MODE= 9 ____ 22.9057	____ 22.2909
MODE= 10 ____ 25.538	____ 24.7677
MODE= 11 ____ 28.1974	____ 27.2445
MODE= 12 ____ 30.8866	____ 29.7212
MODE= 13 ____ 33.6078	____ 32.198
MODE= 14 ____ 36.3636	____ 34.6748
MODE= 15 ____ 39.1564	____ 37.1515
MODE= 16 ____ 41.9883	____ 39.6283
MODE= 17 ____ 44.8617	____ 42.1051
MODE= 18 ____ 47.7787	____ 44.5818
MODE= 19 ____ 50.7415	____ 47.0586
MODE= 20 ____ 53.752	____ 49.5354

_____ NORMAL FORCE= 300 (KIPS)_____

	FREQ.OF BEAM (CYCLE.P.S)	FREQ.OF STRING (CYCLE.P.S)
MODE= 1	2.1763	2.14495
MODE= 2	4.35585	4.28989
MODE= 3	6.54187	6.43484
MODE= 4	8.73759	8.57978
MODE= 5	10.9462	10.7247
MODE= 6	13.1708	12.8697
MODE= 7	15.4147	15.0146
MODE= 8	17.6807	17.1596
MODE= 9	19.972	19.3045
MODE= 10	22.2915	21.4495
MODE= 11	24.6421	23.5944
MODE= 12	27.0266	25.7394
MODE= 13	29.4477	27.8843
MODE= 14	31.9081	30.0292
MODE= 15	34.4105	32.1742
MODE= 16	36.9572	34.3191
MODE= 17	39.5507	36.4641
MODE= 18	42.1933	38.609
MODE= 19	44.8873	40.754
MODE= 20	47.6348	42.8989
MODE= 21	50.4379	45.0439
MODE= 22	53.2985	47.1888
MODE= 23	56.2186	49.3338
MODE= 24	59.1999	51.4787
MODE= 25	62.2442	53.6237
MODE= 26	65.353	55.7686
MODE= 27	68.5281	57.9135
MODE= 28	71.7708	60.0585
MODE= 29	75.0827	62.2034
MODE= 30	78.4649	64.3484

_____ NORMAL FORCE= 200 (KIPS)_____

	FREQ.OF BEAM (CYCLE.P.S)	FREQ.OF STRING (CYCLE.P.S)
MODE= 1	1.78292	1.75134
MODE= 2	3.56983	3.50268
MODE= 3	5.3647	5.25403
MODE= 4	7.17145	7.00537
MODE= 5	8.994	8.75671
MODE= 6	10.8362	10.5081
MODE= 7	12.7017	12.2594
MODE= 8	14.5943	14.0107
MODE= 9	16.5175	15.7621
MODE= 10	18.4748	17.5134
MODE= 11	20.4695	19.2648
MODE= 12	22.5049	21.0161
MODE= 13	24.584	22.7674
MODE= 14	26.7099	24.5188
MODE= 15	28.8853	26.2701
MODE= 16	31.1131	28.0215
MODE= 17	33.3957	29.7728
MODE= 18	35.7356	31.5242
MODE= 19	38.1352	33.2755
MODE= 20	40.5966	35.0268
MODE= 21	43.1219	36.7782
MODE= 22	45.7131	38.5295
MODE= 23	48.3719	40.2809
MODE= 24	51.1002	42.0322
MODE= 25	53.8995	43.7836
MODE= 26	56.7714	45.5349
MODE= 27	59.7172	47.2862
MODE= 28	62.7384	49.0376
MODE= 29	65.8362	50.7889
MODE= 30	69.0117	52.5403

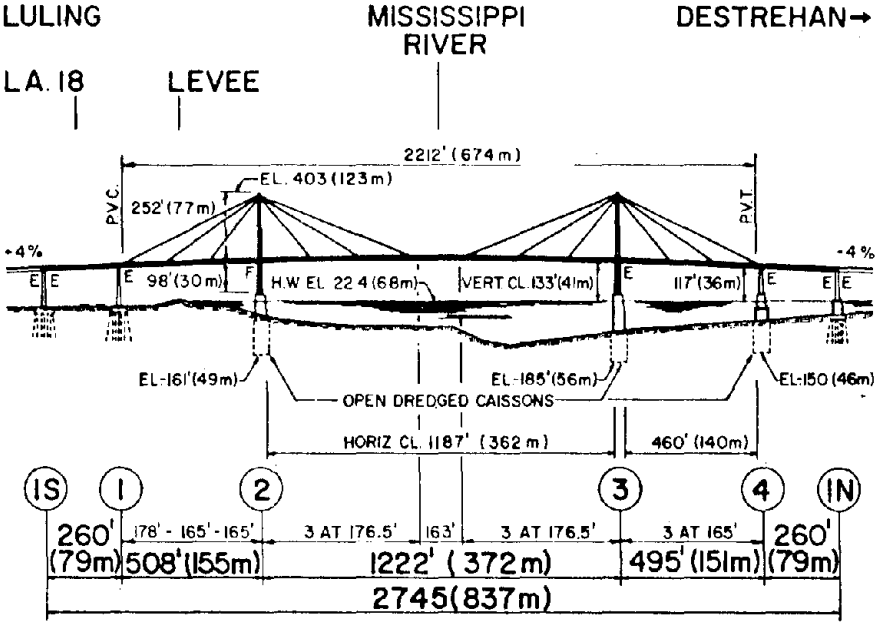

Figure B-2. Cable Stayed Span of Luling Bridge on Mississippi River, Louisiana

Description

Overall length - 11080 ft. (3377 m)

Main span - 1222 ft. (372 m)

Cable-stayed girder length - 2212 ft. (674 m)

Total number of cables - Not available.

Special Features of Stay-Cables*

Number of wires in a cable - 108 (Group IV) to 307 (Group I)

Wire diameter - 0.25 in. (6 mm) ASTMA421 type

Cable Length - 200 ft. (61 m) to 580 ft. (177 m)

Outer diameter of cable - 6 in. (15 cm)

Wire stress range - 108 ksi (745 MPa)

---

* Information obtained in consultation with Prescon. Corp. The figures are approximate.

Luling Bridge Group I Cables

_____ NORMAL FORCE= 1700 (KIPS) _____

FREQ.OF BEAM (CYCLE.P.S)	FREQ.OF STRING (CYCLE.P.S)
MODE= 1 ____ .895991	____ .890723
MODE= 2 ____ 1.79221	____ 1.78145
MODE= 3 ____ 2.68889	____ 2.67217
MODE= 4 ____ 3.58624	____ 3.56289
MODE= 5 ____ 4.4845	____ 4.45361
MODE= 6 ____ 5.38389	____ 5.34434
MODE= 7 ____ 6.28463	____ 6.23506
MODE= 8 ____ 7.18696	____ 7.12578
MODE= 9 ____ 8.09109	____ 8.0165
MODE= 10 ____ 8.99725	____ 8.90723
MODE= 11 ____ 9.90566	____ 9.79795
MODE= 12 ____ 10.8165	____ 10.6887
MODE= 13 ____ 11.7301	____ 11.5794
MODE= 14 ____ 12.6466	____ 12.4701
MODE= 15 ____ 13.5662	____ 13.3608
MODE= 16 ____ 14.4892	____ 14.2516
MODE= 17 ____ 15.4157	____ 15.1423
MODE= 18 ____ 16.346	____ 16.033
MODE= 19 ____ 17.2803	____ 16.9237
MODE= 20 ____ 18.2188	____ 17.8145
MODE= 21 ____ 19.1617	____ 18.7052
MODE= 22 ____ 20.1092	____ 19.5959
MODE= 23 ____ 21.0615	____ 20.4866
MODE= 24 ____ 22.0188	____ 21.3773
MODE= 25 ____ 22.9814	____ 22.2681
MODE= 26 ____ 23.9494	____ 23.1588
MODE= 27 ____ 24.923	____ 24.0495
MODE= 28 ____ 25.9025	____ 24.9402
MODE= 29 ____ 26.8879	____ 25.831
MODE= 30 ____ 27.8796	____ 26.7217

_____ NORMAL FORCE= 1600 (KIPS)_____

FREQ.OF BEAM (CYCLE.P.S)	FREQ.OF STRING (CYCLE.P.S)
MODE= 1 ____ .869399	____ .864129
MODE= 2 ____ 1.73903	____ 1.72826
MODE= 3 ____ 2.60914	____ 2.59239
MODE= 4 ____ 3.47994	____ 3.45651
MODE= 5 ____ 4.35167	____ 4.32064
MODE= 6 ____ 5.22458	____ 5.18477
MODE= 7 ____ 6.09888	____ 6.0489
MODE= 8 ____ 6.97481	____ 6.91303
MODE= 9 ____ 7.8526	____ 7.77716
MODE= 10 ____ 8.73248	____ 8.64129
MODE= 11 ____ 9.61468	____ 9.50542
MODE= 12 ____ 10.4994	____ 10.3695
MODE= 13 ____ 11.3869	____ 11.2337
MODE= 14 ____ 12.2775	____ 12.0978
MODE= 15 ____ 13.1712	____ 12.9619
MODE= 16 ____ 14.0684	____ 13.8261
MODE= 17 ____ 14.9693	____ 14.6902
MODE= 18 ____ 15.874	____ 15.5543
MODE= 19 ____ 16.7829	____ 16.4184
MODE= 20 ____ 17.696	____ 17.2826
MODE= 21 ____ 18.6137	____ 18.1467
MODE= 22 ____ 19.5362	____ 19.0108
MODE= 23 ____ 20.4636	____ 19.875
MODE= 24 ____ 21.3962	____ 20.7391
MODE= 25 ____ 22.3341	____ 21.6032
MODE= 26 ____ 23.2777	____ 22.4673
MODE= 27 ____ 24.227	____ 23.3315
MODE= 28 ____ 25.1823	____ 24.1956
MODE= 29 ____ 26.1438	____ 25.0597
MODE= 30 ____ 27.1116	____ 25.9239

_____ NORMAL FORCE= 1500 (KIPS)_____

	FREQ.OF BEAM (CYCLE.P.S)	FREQ.OF STRING (CYCLE.P.S)
MODE= 1	.841962	.836688
MODE= 2	1.68417	1.67338
MODE= 3	2.52686	2.51006
MODE= 4	3.37026	3.34675
MODE= 5	4.21464	4.18344
MODE= 6	5.06022	5.02013
MODE= 7	5.90725	5.85682
MODE= 8	6.75595	6.69351
MODE= 9	7.60659	7.53019
MODE= 10	8.45937	8.36688
MODE= 11	9.31455	9.20357
MODE= 12	10.1724	10.0403
MODE= 13	11.033	10.8769
MODE= 14	11.8968	11.7136
MODE= 15	12.7639	12.5503
MODE= 16	13.6346	13.387
MODE= 17	14.509	14.2237
MODE= 18	15.3874	15.0604
MODE= 19	16.2701	15.8971
MODE= 20	17.1573	16.7338
MODE= 21	18.0491	17.5705
MODE= 22	18.9458	18.4071
MODE= 23	19.8476	19.2438
MODE= 24	20.7548	20.0805
MODE= 25	21.6674	20.9172
MODE= 26	22.5859	21.7539
MODE= 27	23.5103	22.5906
MODE= 28	24.4408	23.4273
MODE= 29	25.3777	24.264
MODE= 30	26.3211	25.1006

_____ NORMAL FORCE= 1400 (KIPS)_____

FREQ.OF BEAM (CYCLE.P.S)	FREQ.OF STRING (CYCLE.P.S)
MODE= 1 ____ .813597	____ .808317
MODE= 2 ____ 1.62744	____ 1.61663
MODE= 3 ____ 2.44179	____ 2.42495
MODE= 4 ____ 3.25688	____ 3.23327
MODE= 5 ____ 4.07297	____ 4.04158
MODE= 6 ____ 4.89031	____ 4.8499
MODE= 7 ____ 5.70915	____ 5.65822
MODE= 8 ____ 6.52973	____ 6.46654
MODE= 9 ____ 7.35229	____ 7.27485
MODE= 10 ____ 8.17709	____ 8.08317
MODE= 11 ____ 9.00437	____ 8.89149
MODE= 12 ____ 9.83437	____ 9.6998
MODE= 13 ____ 10.6673	____ 10.5081
MODE= 14 ____ 11.5035	____ 11.3164
MODE= 15 ____ 12.3431	____ 12.1248
MODE= 16 ____ 13.1864	____ 12.9331
MODE= 17 ____ 14.0336	____ 13.7414
MODE= 18 ____ 14.8849	____ 14.5497
MODE= 19 ____ 15.7406	____ 15.358
MODE= 20 ____ 16.6009	____ 16.1663
MODE= 21 ____ 17.4661	____ 16.9747
MODE= 22 ____ 18.3363	____ 17.783
MODE= 23 ____ 19.2118	____ 18.5913
MODE= 24 ____ 20.0928	____ 19.3996
MODE= 25 ____ 20.9795	____ 20.2079
MODE= 26 ____ 21.8721	____ 21.0162
MODE= 27 ____ 22.7708	____ 21.8246
MODE= 28 ____ 23.6759	____ 22.6329
MODE= 29 ____ 24.5876	____ 23.4412
MODE= 30 ____ 25.506	____ 24.2495

_____ NORMAL FORCE= 1300 (KIPS)_____

FREQ.OF BEAM (CYCLE.P.S)	FREQ.OF STRING (CYCLE.P.S)
MODE= 1 ____ .784193	____ .778914
MODE= 2 ____ 1.56865	____ 1.55783
MODE= 3 ____ 2.35362	____ 2.33674
MODE= 4 ____ 3.13937	____ 3.11566
MODE= 5 ____ 3.92616	____ 3.89457
MODE= 6 ____ 4.71424	____ 4.67348
MODE= 7 ____ 5.50388	____ 5.4524
MODE= 8 ____ 6.29532	____ 6.23131
MODE= 9 ____ 7.08882	____ 7.01023
MODE= 10 ____ 7.88464	____ 7.78914
MODE= 11 ____ 8.68304	____ 8.56805
MODE= 12 ____ 9.48425	____ 9.34697
MODE= 13 ____ 10.2885	____ 10.1259
MODE= 14 ____ 11.0961	____ 10.9048
MODE= 15 ____ 11.9073	____ 11.6837
MODE= 16 ____ 12.7223	____ 12.4626
MODE= 17 ____ 13.5413	____ 13.2415
MODE= 18 ____ 14.3647	____ 14.0205
MODE= 19 ____ 15.1925	____ 14.7994
MODE= 20 ____ 16.0252	____ 15.5783
MODE= 21 ____ 16.8628	____ 16.3572
MODE= 22 ____ 17.7057	____ 17.1361
MODE= 23 ____ 18.554	____ 17.915
MODE= 24 ____ 19.4081	____ 18.6939
MODE= 25 ____ 20.268	____ 19.4729
MODE= 26 ____ 21.134	____ 20.2518
MODE= 27 ____ 22.0064	____ 21.0307
MODE= 28 ____ 22.8854	____ 21.8096
MODE= 29 ____ 23.7712	____ 22.5885
MODE= 30 ____ 24.6639	____ 23.3674

_____ NORMAL FORCE= 1200 (KIPS) _____

	FREQ.OF BEAM (CYCLE.P.S)	FREQ.OF STRING (CYCLE.P.S)
MODE= 1	.753642	.748357
MODE= 2	1.50755	1.49671
MODE= 3	2.262	2.24507
MODE= 4	3.01726	2.99343
MODE= 5	3.7736	3.74178
MODE= 6	4.53129	4.49014
MODE= 7	5.29059	5.2385
MODE= 8	6.05178	5.98686
MODE= 9	6.81511	6.73521
MODE= 10	7.58085	7.48357
MODE= 11	8.34927	8.23193
MODE= 12	9.12062	8.98028
MODE= 13	9.89517	9.72864
MODE= 14	10.6732	10.477
MODE= 15	11.4549	11.2254
MODE= 16	12.2405	11.9737
MODE= 17	13.0304	12.7221
MODE= 18	13.8248	13.4704
MODE= 19	14.6238	14.2188
MODE= 20	15.4278	14.9671
MODE= 21	16.237	15.7155
MODE= 22	17.0517	16.4639
MODE= 23	17.872	17.2122
MODE= 24	18.6981	17.9606
MODE= 25	19.5305	18.7089
MODE= 26	20.3691	19.4573
MODE= 27	21.2144	20.2056
MODE= 28	22.0664	20.954
MODE= 29	22.9255	21.7024
MODE= 30	23.7918	22.4507

_____ NORMAL FORCE= 1100 (KIPS)_____

FREQ.OF BEAM (CYCLE.P.S)	FREQ.OF STRING (CYCLE.P.S)
MODE= 1 ____ .721785	____ .716497
MODE= 2 ____ 1.44385	____ 1.43299
MODE= 3 ____ 2.16648	____ 2.14949
MODE= 4 ____ 2.88996	____ 2.86599
MODE= 5 ____ 3.61456	____ 3.58249
MODE= 6 ____ 4.34058	____ 4.29898
MODE= 7 ____ 5.06827	____ 5.01548
MODE= 8 ____ 5.79794	____ 5.73198
MODE= 9 ____ 6.52985	____ 6.44848
MODE= 10 ____ 7.26427	____ 7.16497
MODE= 11 ____ 8.00149	____ 7.88147
MODE= 12 ____ 8.74177	____ 8.59797
MODE= 13 ____ 9.48538	____ 9.31447
MODE= 14 ____ 10.2326	____ 10.031
MODE= 15 ____ 10.9837	____ 10.7475
MODE= 16 ____ 11.7389	____ 11.464
MODE= 17 ____ 12.4985	____ 12.1805
MODE= 18 ____ 13.2628	____ 12.897
MODE= 19 ____ 14.0319	____ 13.6135
MODE= 20 ____ 14.8062	____ 14.3299
MODE= 21 ____ 15.586	____ 15.0464
MODE= 22 ____ 16.3713	____ 15.7629
MODE= 23 ____ 17.1626	____ 16.4794
MODE= 24 ____ 17.96	____ 17.1959
MODE= 25 ____ 18.7638	____ 17.9124
MODE= 26 ____ 19.5742	____ 18.6289
MODE= 27 ____ 20.3914	____ 19.3454
MODE= 28 ____ 21.2157	____ 20.0619
MODE= 29 ____ 22.0472	____ 20.7784
MODE= 30 ____ 22.8862	____ 21.4949

_____ NORMAL FORCE= 1000 (KIPS)_____

	FREQ.OF BEAM (CYCLE.P.S)	FREQ.OF STRING (CYCLE.P.S)
MODE= 1	.688446	.683153
MODE= 2	1.37719	1.36631
MODE= 3	2.06652	2.04946
MODE= 4	2.75674	2.73261
MODE= 5	3.44814	3.41577
MODE= 6	4.14102	4.09892
MODE= 7	4.83567	4.78207
MODE= 8	5.53238	5.46523
MODE= 9	6.23144	6.14838
MODE= 10	6.93315	6.83153
MODE= 11	7.63777	7.51468
MODE= 12	8.34561	8.19784
MODE= 13	9.05694	8.88099
MODE= 14	9.77205	9.56414
MODE= 15	10.4912	10.2473
MODE= 16	11.2147	10.9305
MODE= 17	11.9427	11.6136
MODE= 18	12.6757	12.2968
MODE= 19	13.4137	12.9799
MODE= 20	14.1572	13.6631
MODE= 21	14.9063	14.3462
MODE= 22	15.6613	15.0294
MODE= 23	16.4225	15.7125
MODE= 24	17.19	16.3957
MODE= 25	17.9642	17.0788
MODE= 26	18.7453	17.762
MODE= 27	19.5335	18.4451
MODE= 28	20.3291	19.1283
MODE= 29	21.1322	19.8114
MODE= 30	21.9432	20.4946

Reproduced from
best available copy

_____ NORMAL FORCE= 900 (KIPS)_____

FREQ.OF BEAM (CYCLE.P.S)	FREQ.OF STRING (CYCLE.P.S)
MODE= 1 ____ .653393	____ .648097
MODE= 2 ____ 1.3071	____ 1.29619
MODE= 3 ____ 1.96143	____ 1.94429
MODE= 4 ____ 2.61669	____ 2.59239
MODE= 5 ____ 3.27321	____ 3.24048
MODE= 6 ____ 3.93127	____ 3.88858
MODE= 7 ____ 4.59121	____ 4.53668
MODE= 8 ____ 5.25331	____ 5.18477
MODE= 9 ____ 5.9179	____ 5.83287
MODE= 10 ____ 6.58526	____ 6.48097
MODE= 11 ____ 7.25571	____ 7.12906
MODE= 12 ____ 7.92953	____ 7.77716
MODE= 13 ____ 8.60704	____ 8.42526
MODE= 14 ____ 9.28851	____ 9.07335
MODE= 15 ____ 9.97424	____ 9.72145
MODE= 16 ____ 10.6645	____ 10.3695
MODE= 17 ____ 11.3596	____ 11.0176
MODE= 18 ____ 12.0599	____ 11.6657
MODE= 19 ____ 12.7655	____ 12.3138
MODE= 20 ____ 13.4767	____ 12.9619
MODE= 21 ____ 14.1939	____ 13.61
MODE= 22 ____ 14.9173	____ 14.2581
MODE= 23 ____ 15.6471	____ 14.9062
MODE= 24 ____ 16.3837	____ 15.5543
MODE= 25 ____ 17.1272	____ 16.2024
MODE= 26 ____ 17.8779	____ 16.8505
MODE= 27 ____ 18.636	____ 17.4986
MODE= 28 ____ 19.4018	____ 18.1467
MODE= 29 ____ 20.1756	____ 18.7948
MODE= 30 ____ 20.9575	____ 19.4429

_____ NORMAL FORCE= 800 (KIPS)_____

FREQ.OF BEAM (CYCLE.P.S)	FREQ.OF STRING (CYCLE.P.S)
MODE= 1 ____ .616334	____ .611031
MODE= 2 ____ 1.233	____ 1.22206
MODE= 3 ____ 1.85032	____ 1.83309
MODE= 4 ____ 2.46865	____ 2.44412
MODE= 5 ____ 3.08829	____ 3.05516
MODE= 6 ____ 3.70959	____ 3.66619
MODE= 7 ____ 4.33286	____ 4.27722
MODE= 8 ____ 4.95843	____ 4.88825
MODE= 9 ____ 5.58664	____ 5.49928
MODE= 10 ____ 6.21779	____ 6.11031
MODE= 11 ____ 6.8522	____ 6.72134
MODE= 12 ____ 7.4902	____ 7.33237
MODE= 13 ____ 8.13209	____ 7.94341
MODE= 14 ____ 8.77818	____ 8.55444
MODE= 15 ____ 9.42878	____ 9.16547
MODE= 16 ____ 10.0842	____ 9.7765
MODE= 17 ____ 10.7447	____ 10.3875
MODE= 18 ____ 11.4106	____ 10.9986
MODE= 19 ____ 12.0822	____ 11.6096
MODE= 20 ____ 12.7597	____ 12.2206
MODE= 21 ____ 13.4435	____ 12.8317
MODE= 22 ____ 14.1339	____ 13.4427
MODE= 23 ____ 14.831	____ 14.0537
MODE= 24 ____ 15.5352	____ 14.6647
MODE= 25 ____ 16.2467	____ 15.2758
MODE= 26 ____ 16.9658	____ 15.8868
MODE= 27 ____ 17.6927	____ 16.4978
MODE= 28 ____ 18.4277	____ 17.1089
MODE= 29 ____ 19.171	____ 17.7199
MODE= 30 ____ 19.9228	____ 18.3309

Luling Bridge Group IV Cable

_____ NORMAL FORCE= 600 (KIPS)_____

	FREQ.OF BEAM (CYCLE.P.S)	FREQ.OF STRING (CYCLE.P.S)
MODE= 1	____ 2.614	____ 2.58732
MODE= 2	____ 5.22999	____ 5.17465
MODE= 3	____ 7.84991	____ 7.76197
MODE= 4	____ 10.4758	____ 10.3493
MODE= 5	____ 13.1095	____ 12.9366
MODE= 6	____ 15.753	____ 15.5239
MODE= 7	____ 18.4082	____ 18.1113
MODE= 8	____ 21.0772	____ 20.6986
MODE= 9	____ 23.7617	____ 23.2859
MODE= 10	____ 26.4637	____ 25.8732
MODE= 11	____ 29.1849	____ 28.4606
MODE= 12	____ 31.9274	____ 31.0479
MODE= 13	____ 34.6928	____ 33.6352
MODE= 14	____ 37.4829	____ 36.2225
MODE= 15	____ 40.2996	____ 38.8098
MODE= 16	____ 43.1445	____ 41.3972
MODE= 17	____ 46.0193	____ 43.9845
MODE= 18	____ 48.9257	____ 46.5718
MODE= 19	____ 51.8654	____ 49.1591
MODE= 20	____ 54.8398	____ 51.7465

_____ NORMAL FORCE= 500 (KIPS)_____

FREQ.OF BEAM (CYCLE.P.S)	FREQ.OF STRING (CYCLE.P.S)
MODE= 1 ____ 2.38864	____ 2.36189
MODE= 2 ____ 4.77944	____ 4.72378
MODE= 3 ____ 7.17456	____ 7.08568
MODE= 4 ____ 9.57616	____ 9.44757
MODE= 5 ____ 11.9864	____ 11.8095
MODE= 6 ____ 14.4074	____ 14.1714
MODE= 7 ____ 16.8412	____ 16.5332
MODE= 8 ____ 19.29	____ 18.8951
MODE= 9 ____ 21.7559	____ 21.257
MODE= 10 ____ 24.2408	____ 23.6189
MODE= 11 ____ 26.7468	____ 25.9808
MODE= 12 ____ 29.2759	____ 28.3427
MODE= 13 ____ 31.83	____ 30.7046
MODE= 14 ____ 34.4111	____ 33.0665
MODE= 15 ____ 37.021	____ 35.4284
MODE= 16 ____ 39.6616	____ 37.7903
MODE= 17 ____ 42.3347	____ 40.1522
MODE= 18 ____ 45.042	____ 42.5141
MODE= 19 ____ 47.7853	____ 44.8759
MODE= 20 ____ 50.5662	____ 47.2378

_____ NORMAL FORCE= 400 (KIPS)_____

FREQ.OF BEAM (CYCLE.P.S)	FREQ.OF STRING (CYCLE.P.S)
MODE= 1 ____ 2.13936	____ 2.11254
MODE= 2 ____ 4.28115	____ 4.22508
MODE= 3 ____ 6.42778	____ 6.33762
MODE= 4 ____ 8.58165	____ 8.45016
MODE= 5 ____ 10.7452	____ 10.5627
MODE= 6 ____ 12.9207	____ 12.6752
MODE= 7 ____ 15.1107	____ 14.7878
MODE= 8 ____ 17.3173	____ 16.9003
MODE= 9 ____ 19.5429	____ 19.0128
MODE= 10 ____ 21.7898	____ 21.1254
MODE= 11 ____ 24.0601	____ 23.2379
MODE= 12 ____ 26.3561	____ 25.3505
MODE= 13 ____ 28.6799	____ 27.463
MODE= 14 ____ 31.0335	____ 29.5755
MODE= 15 ____ 33.419	____ 31.6881
MODE= 16 ____ 35.8384	____ 33.8006
MODE= 17 ____ 38.2937	____ 35.9132
MODE= 18 ____ 40.7866	____ 38.0257
MODE= 19 ____ 43.319	____ 40.1382
MODE= 20 ____ 45.8927	____ 42.2508

_____ NORMAL FORCE= 300 (KIPS)_____

FREQ.OF BEAM (CYCLE.P.S)	FREQ.OF STRING (CYCLE.P.S)
MODE= 1 ____ 1.85645	____ 1.82951
MODE= 2 ____ 3.7157	____ 3.65903
MODE= 3 ____ 5.58057	____ 5.48854
MODE= 4 ____ 7.4538	____ 7.31806
MODE= 5 ____ 9.33819	____ 9.14757
MODE= 6 ____ 11.2365	____ 10.9771
MODE= 7 ____ 13.1513	____ 12.8066
MODE= 8 ____ 15.0854	____ 14.6361
MODE= 9 ____ 17.0412	____ 16.4656
MODE= 10 ____ 19.0215	____ 18.2951
MODE= 11 ____ 21.0287	____ 20.1247
MODE= 12 ____ 23.0651	____ 21.9542
MODE= 13 ____ 25.1332	____ 23.7837
MODE= 14 ____ 27.2353	____ 25.6132
MODE= 15 ____ 29.3736	____ 27.4427
MODE= 16 ____ 31.5503	____ 29.2722
MODE= 17 ____ 33.7673	____ 31.1017
MODE= 18 ____ 36.0268	____ 32.9313
MODE= 19 ____ 38.3306	____ 34.7608
MODE= 20 40.6807	36.5903

_____ NORMAL FORCE= 200 (KIPS)_____

	FREQ.OF BEAM (CYCLE.P.S)	FREQ.OF STRING (CYCLE.P.S)
MODE= 1	1.52092	1.49379
MODE= 2	3.04529	2.98758
MODE= 3	4.57655	4.48138
MODE= 4	6.11809	5.97517
MODE= 5	7.67328	7.46896
MODE= 6	9.24545	8.96275
MODE= 7	10.8378	10.4565
MODE= 8	12.4536	11.9503
MODE= 9	14.0958	13.4441
MODE= 10	15.7675	14.9379
MODE= 11	17.4715	16.4317
MODE= 12	19.2107	17.9255
MODE= 13	20.9876	19.4193
MODE= 14	22.805	20.9131
MODE= 15	24.6652	22.4069
MODE= 16	26.5705	23.9007
MODE= 17	28.5232	25.3945
MODE= 18	30.5253	26.8883
MODE= 19	32.5789	28.3821
MODE= 20	34.6859	29.8758

*U.S. GOVERNMENT PRINTING OFFICE: 1981-0-729-470/2079